ISAS - INTERNATIONAL SCHOOL
FOR ADVANCED STUDIES

October 1991

Feige 86
a Halo Blue star with chemical peculiarities
perspectives for a spectroscopic study

Thesis submitted for the degree of
"Magister Philosophiae"

Candidate
Piercarlo Bonifacio

Supervisors
Prof. George F.R. Ellis
Prof. Margherita Hack
Dr. Fiorella Castelli

TRIESTE

SISSA - SCUOLA
INTERNAZIONALE
SUPERIORE
DI STUDI AVANZATI
TRIESTE
Strada Costiera 11

Introduction

By looking at the astronomical literature of the recent years one may notice that the study of single stars has become rather uncommon, if we exclude special classes of objects such as novae and supernovae. The reason for this is readily understood: a detailed study of a single star may require large amount of work and expensive resources (telescope time, computer time, etc...), but the results usually concern only that single object and people often feel that this does not contribute much to the progress of science. On th other hand more superficial studies on a large number of stars may yield, at the same cost, results which concern entire classes or sets of stars, thus givin a considerable contribution to our knowledge of the world surrounding us.

Although I agree with the general conclusions of such a line of thought I feel that there is a danger in it: one may draw conclusions from superficial studies of a large number of objects, however these conclusions may be affected by large systematic errors. In this respect the detailed study of a single object will never be surpassed. On the other hand, by looking carefully at a single object one may discover interesting phenomena which may have unexpected implications in other contexts.

Among the classes of stars which, in the recent years, suffered of a decrease of interest by the astronomical community, are the Chemically Peculiar (CP) stars. The reasons for this loss of popularity are similar to those which caused a loss of popularity of the studies on binary star evolution: the more closely one looks at the indivivuals the less they resemble the other members of their own class. Each has a story of its own which may be very complicated indeed. Moreover, in spite of over fifty years of strenuous research we have no really satisfactory theory for expalining CP stars. The best theory available, diffusion theory, suffers of so many drawbacks and apparent inconsistencies that it may not be regarded as entirely satisfactory. One of the main puzzles is that often pairs of

stars which should be similar (because they have almost the same temperature, gravity and rotational velocity) often show different peculiarities, or else one is peculiar, while the other is not.

The bulk of the literature on CP stars is about Main Sequence stars. Indeed the notion of CP star is often associate with MS stars (Faraggiana, 1987). However there are Population II objects which show anomalous abundances:the sdO, sdB and HBB stars, discussed in chapter 2. It is generally believed that such anomalies are due to diffusion (Heber, 1987). This draws a connection between the two classes of stars. There is, however, a more direct and immediate connection : star Feige 86 (BD +302431), which is believed to be an HBB star on kinematical grounds (Sargent and Searle, 1967) has a Pop I analogue in the B peculiar star 3 Cen A. It seems therefore that the phenomena of chemical peculiarity affects exactly in the same way Pop I and Pop II objects.

It seems therefore very interesting to make a detailed analysis of such a unique object. Such a study has been made for the visible spectrum by Baschek and Sargent (1976); for the UV spectrum, however, only preliminary results have been published (Hack, 1980; Morossi *et al.* 1981 ; Castelli and Singh, 1990 ; Bonifacio *et al.* 1991). We plan to accomplish this and also to make a comparison with new high S/N visible spectra.

Chapter one is devoted to CP stars and the theories proposed to explain the phenomenon. Chapter 2 deals with Field Blue stars. Chapter 3 is a quick survey of the existing literature on Feige 86. Chapter 4 describes the instruments which shall be used in the future work and how data (both theoretical and observational) is handled. Chapter 5 explains the basic physics which is behind the computation of a synthetic spectrum. Chapter 6, finally, adresses the problem of how atmospheric parameters (temperature and gravity) should be determined for B type stars.

Chapter 1

Chemically peculiar stars, observations and theories

Abundance anomalies, which, as we shall see in the next chapter, characterize halo HB stars are a common feature in upper main sequence stars. The stars affected by such anomalies range from type F to type O (if we include sdO's among these). The peculiarities are very different and include:

^{3}He excess

^{4}He excess (Osmer and Peterson, 1974)

He deficiency

O deficiency

Mn-Si excess

Fe-peak element excess

Fe-peak element defect (λ Boo, Cowley *et al.* 1982)

rare earths excess

All these stars are called Chemically Peculiar (CP) stars. Some stars show presence of strong magnetic fields. In general the peculiarities of magnetic stars are markedly different from those of non-magnetic stars (Alecian, 1985), although some classes of stars have magnetic and non-magnetic members (e.g. He-weak or He-rich stars, Faraggiana, 1987).

Before tackling the problem of the classification of CP stars and were field HB stars fit into this classification, if at all, we shall briefly outline the observational picture of CP stars.

MASSES

Popper (1980) studied 9 Am stars of 5 binary systems, he found their masses to be between 1.6 and 2.5 $M_\odot$. Such masses are expected for normal Main Sequence stars of the same spectral types.

RADII

On a sample of 9 CP stars Shallis *et al.* (1985) find

$$R/R_{\odot} = 2.4 \pm 1.3$$

With a different method Babu and Shylaja (1985) find that for the stars of the Shallis *et al.* sample their radii scatter around the Shallis *et al.* values with a standard deviation of 17%. By computing the average of their sample (23 Am stars and 69 CP2 ; for the definition of cp star classes see further on) they find the average values

$$\langle R/R_{\odot} \rangle = 2.2 \pm 0.6 \qquad (Am)$$

$$\langle R/R_{\odot} \rangle = 2.9 \pm 0.8 \qquad (CP2)$$

these data suggest that CP stars have, on average, slightly larger radii than normal stars of the same spectral type (Hensenberge and Van Resenbrink, 1985).

FREQUENCY

Klochkova and Kopylov (1985), studied the freequency of CP stars in open clusters and found this to be extreemly variable from cluster to cluster, ranging from 0% to 33% . Workers in the field assume an average frequency of the order of 10% Oetken (1985).

BINARITY

The results of Abt and Snowden (1973) tell us that the frequency of CP stars members of binary systems is normal (i.e. similar to that of Jaschek and Gomez, 1970) for Hg-Mn stars, whereas it is considerably lower for magnetic stars. For Am stars instead the frequency of binarity is thought to be close to 100% .

ROTATIONAL VELOCITIES

It has been known for over 30 years that CP stars are slow rotators (Slettebak 1954 and 1955), although some individuals are observed with $v \sin i$ up to

100 km/s (Slettebak, 1955). A systematic study looking for correlation between age and peculiarities allows us to conclude that the evolution of CP stars takes place at constant angular momentum (North, 1985 ; Klochkova and Kopylov, 1985) . Hence any braking mechanism which might have been effective before the star shows up a CP character must be inhibited soon after.

INFRARED EXCESS

Some A and B stars were found to have an excess of infrared flux in the bands M (4.9 μm) and J (1.25 μm) (Groote *et al.* , 1980; Groote and Kaufmann, 1981).

Chemical peculiarities mean different things to different people, this is one of the reasons of the many classification schemes so far proposed. Each scheme focuses on certain classes of stars, neglecting others. Personally I feel that no classification I have met is really satisfactory, the main reason is that at the present level of knowledge we are uncapable of discerning the physically relevant characteristics from those which are not. Only when the CP phenomenon will be fully understood a satisfactory classification will be possible.

I shall mention only three classification schemes, since they are the most widely used: that of Preston (1974), that of Cowley (1979) and that which Jaschek and Egret (1982) used in their Stellar Group Catalogue.

Preston classification

CP1 – (Am) strong metallic lines and weak SiII and/or ScII ; weak CaII

CP2 – (Ap) magnetic with strong Si, Cr, Sr, Eu

CP3 – Hg, Mn enhanced (MnII 398.4 nm)

CP4 – He deficient

It is immediately seen that He rich stars don't find a place in Preston's classes, nor is it true that all Si stars are magnetic (in the sense that they posses a measurable magnetic field).

Cowley classification

A – rare earths enhanced

B – stars with Nd-Sm anomaly

C1 – enhanced Fe, CeII $-0.8 < (b-y) < 0.6$

C2 – enhanced Fe $0.0 < (b-y) < 0.5$

D – normal rare earths

Cowley's D class is a sort of waste paper basket where all the stars which don't fit anywhere else are collected, it turns out that many of the objects in the same class differ markedly, spectroscopically.

Jaschek-Egret classification

He-abnormal stars

A He strong

B He weak

C He variable

Ap stars

A Si and Si 420 nm

B Hg,Mn and Hg-Mn

C Si combined with Cr, Eu, Sr

D Cr, Eu, Sr and combinations of the same

Am stars

λ Boo stars

The Jaschek-Egret classification is the most satisfactory in my opinion,since any known CP star will fall in one of these categories and each category is fairly homogeneus, except perhaps for the λ Boo stars. One may dispute that there are too many classes and subclasses and that some classes contain really few objects. Yet this is the best classification we have, based on purely observational data.

In the Jaschek-Egret scheme HBB, sdB and sdOB stars fall in the He abnormal B group, although some may fall in the He abnormal C group. SdO's and PG1159's fall mainly in the He-abnormal A group, although some may fall in the He abnormal C group.

The reader should be warned that these classifications are tentative. In the sense that the bulk of the literature on CP stars assumes that they are Main Sequence unevolved stars, whereas HBB, sdB sdOB sdO and PG1159 stars are comonly interpreted as evolved objects. Many workers in the field would not accept them to be called CP stars, yet they do show chemical peculiarity. It is natural to suppose that the same physics applies to the two kinds of objects, which in some cases show striking spectral similarities (e.g. Feige 86 and 3 Cen A, see further on).The matter is complicated by two facts:

1) observationally it is difficult if not impossible to distinguish spectroscopically an HBB star with chemical peculiarities from a MS B peculiar star;

2) theoretically it is not clear how the different structure of an HBB star could show up in the abundance pattern.

In what follows we shall make the working hypothesis that chemical peculiarities are phenomena which affect the atmosphere of the star and not the star as a whole and that the same basic physics applies to all CP stars in spite of their evolutionary status. This hypothesis will be verified *a posteriori* if we are able to construct from it a model which explaines the observation. *A priori* justifications for making this hypothesis are the following:

1) there are CP stars which have the same fundamental parameters M, L, R as other non-peculiar stars of the same spectral type. Moreover they obey the same Mass-Luminosity relation;

2) if the peculiarities are referred to the star as a whole, a number of cosmological problems would arise, such as: how could large amounts of heavy elements be formed at early times? Or, alternatively, how could large amounts of heavy ele-

ments concentrate in the protostellar nebula from which a CP star was formed?

3) The hypothesis that the chemical composition of a CP star reflects that of the nebula which originated it cannot possibly explain the existence of binary systems of which one component is peculiar and the other is not.

4) If the peculiarity pertains to the whole star there is no reason for the CP phenomena to be confined to the spectral types from F to O. M type peculiar stars should be detected as well, which is not the case.

Other justifications could be found, but I feel that these are enough, we must bare in mind that no matter how many *a priori* justifications for introducing the hypothesis we find, this will still have to be verified *a posteriori*; so adding more justifications would not put our hypothesis on firmer grounds.

CP stars: an overview of theoretical scenarios.

In what follows we shall briefly outline the main theories proposed to explain the CP phenomena. We shall especially dwell on diffusion theory because it is the most promising and widely accepted although not entirely satisfactory.

1. Nucleosynthesis theory

One of the first ideas was that the overabundant elements were formed by nuclear reactions in the star's atmosphere or at least in superficial enough layers to allow convection to carry the reaction products in the observable zone of the star (Fowler *et al.* 1955). Since particle energies at the temperatures which are typical of stellar atmospheres are too low for nuclear reactions to occur, it is necessary to find a mechanism capable of accelerating the particles up to the required energies. Burbidge and Burbidge (1955) proposed this to be Swann's betatron mechanism (Swann 1933; Riddiford and Butler 1952) which may take place on the border of a spot which is moving. Stellar plasma is an excellent conductor, hence the magnetic field lines are 'frozen-in' the fluid; thereford if

the border of the spot moves, the field lines follow this motion, we thus have a varying magnetic field $\frac{\partial \vec{H}}{\partial t} \neq 0$ (see for example Jackson 1975 pp.474).

Currently nucleosynthesis theory has been abandoned for the following reasons:

- the odd-even effect ough to be observed
- s-r effect ought to be observed.

Observations show several deviations from the odd-even effect and the effect s-r is not observed at all (see for example Hardrop and Shore 1977: the abundances of Ce, Pr, Sn, which are tipical s- elements are not systematically different from those of Eu, Gd, which are typical r-elements).

2. Accretion theory

One shoud really talk about accretion theories, since there isn't a single theory which explains all the complex phenomenology of CP stars. The central point of accretion theories is that abundances of some elements may differ from the solar value due to contamination from the circumstellar environment. We shall examine 3 possible mechanisms:

1. Gas accretion (Havnes and Conti 1971)
2. Dust accretion (Havnes 1979)
3. Solid macroscopic body accretion (Drobyshevsky, 1985)

1. Gas accretion

The theory of Havnes and Conti for gas accretion rests upon three fundamental hypothesis:

a. presence of a magnetic field

b. absence of stellar wind

c. a density of the circumstellar medium of the order of 1 particle cm^{-3}

We notice immediately that such a model is uncapable of explaining anomalies in non-magnetic stars.

Hypothesis (b) is *ad hoc* and seems unrealistic, however it is necessary to build a zero order model.

Consider a magnetic field $\vec{H}$ whose field lines rotate with angular velocity $\vec{\omega}$ rigidally with the star. In an inertial reference frame there is an electric field

$$\vec{E} = -(\vec{\omega} \wedge \vec{r}) \wedge \frac{\vec{H}}{c} \tag{1.1}$$

a particle of charge q and mass m will be subject to a Lorentz force

$$\vec{F} = -q(\frac{\vec{r} \wedge \vec{H}}{c} + \frac{\vec{H}}{c}) \tag{1.2}$$

from Newton's II law one finds

$$\ddot{\vec{r}} = \frac{q}{mc}(\dot{\vec{r}} - \vec{\omega} \wedge \vec{r}) \wedge \vec{H} \tag{1.3}$$

The magnetic field$\vec{H}$ is not uniform but is a function of $\vec{r}$.

Equation (1.3) may be numerically integrated for different values of mass m of charge q for various initial conditions and geometries of the magnetic field. Havnes and Conti did this for a dipolar magnetic field and for $1 \leq \frac{m}{m_H} \leq 25$ and $\frac{m}{m_H} = 150$

The result of such on integration is that the most massive elements fall deeper in the magnetosphere were they are further ionized by the radiation and are definitely captured by the star.

With this mechanism Havnes and Conti predicted that a star with a 2 a.u. accretion radius may change its chemical composition by a factor 10^3 in 10^7 years. They predicted also that the captured elements ought to concentrate in spots arround the polar caps.

The theory was further subject to a quantitative verification by Havnes (1974 and 1975) for Sr Cr, Eu and Si stars and also for stars which are generally classified as non-magnetic. Infact Havnes showed that localized magnetic field

of the order of 1 Tesla may remain undetected if the error on the measurement of H is greater, in modulus, than 0.025 Tesla.

The agreement between theoretical predictions and observations is generally good except for some elements (in particular Ca and Sc); however there is a great number of free parameters (intensity and geometry of the magnetic field, velocity of the field relative to the circumstellar medium, density and chemical composition of the latter in a surronding of the magnetosphere) so that this agreement may not be considered as conclusive evidence in favour of the theory.

Another weak point of the theory is that it neglects the possibility of a collective behaviour of the matter present in the magnetosphere, in particular the screening effects which are tipical of a plasma are totally neglected.

2. Dust accretion

Looking for a more efficient accretion mechanism Havnes (1979) proposed a theory involving accretion from dust grains. The main point of the theory is that dust grains are supposed to be electrically charged. Getting closer to the star they evaporate and the elements which compose them are further ionized by radiation, from here on the mechanism is identical to gas accretion. In order for this accretion to be important it is necessary that at least some elements be present, for a considerable fraction of their total mass, under the form of dust grains of the density of iron (7.86 gcm^{-3})and of radius $r \geq 0.1\mu m$ or even $r \geq 1\mu m$ for hot stars ($8000K \leq T_e \leq 14000K$).

Such requests are compatible with what is known on interplanetary dust. According to Mukai (1977) comets are the main source of interplanetary dust and Mukai himself and Hayakawa *et al.* (1976) claim that cometary dust consists mainly of grains of radius $\geq 1\mu m$. The radii of dust grains at the onset of of stability in a solar nebula are computed by Nakagawa *et al.* (1986) and turn out to be much greater than this: 200000 μm, 59000 μm and 6000 μm for the distances from the star of 1 a.u., 5.2 a.u. and 3 a.u., respectively, corresponding

to the orbits of earth, Jupiter and Neptune in the case of the solar system.

Havnes estimated that if in the space around a star there are comets the accretion efficiency is close to 100%, much greater than the efficiency of gas accretion, which is, at most, 0.1% (Havnes, 1975).

Although promising this theory could not be further developed, lacking detailed knowledge of the fraction of each element which is locked in grains, their shape, size, emission, absorption and evaporation properties. There is also a serious objection to this theory: the elements which are most depleted in the interstellar medium (like e.g. Ca, Al, Mg) should be favoured by this accretion mechanism and therefore be observed to be overabundant, but this is not observed. In fact Mg is usually not affected by anomalies.

3. Solid macroscopic body accretion.

Also Drobyshevsky's theory must be considered as an accretion theory, although completely different from the two so far mentioned.

The idea of Drobyshevsky was that solid macroscopic particles, which he called planetoids, could hit the surface of a star transforming it into an Am star.

Planetoids are not chemically homogeneous, since, due to ignic differentiation, the mantle will be deficient of Mg, Al, Ca and Sc, whereas here will be concentrated elements of large ionic radius: Sr, Y, Zr, Ba and some rare earths, especially Eu.

In support of this theory there is the observational fact that the chemical abundances of lunar rocks measured by Apollo and Luna 20, are similar to those typical of Am stars, except for the iron peak elements. Drobyshevsky claimed that this does not contraddict the theory, since it is likely that the moon is chemically peculiar, being iron deficient.

Drobyshevsky's theory is only capable of explaining Am stars and not Ap or He abnormal. Moreover it seems questionable to build a theory which assumes the existence of planetoids, when we have not any conclusive evidence of the

existence of planets or similar bodies around any star other than the sun. Finally it is not clear why these planetoids should hit A stars and not other spectral types.

3. Diffusion theory

Diffusion theory has the goal of explaining the complex phenomenology of CP stars, as I mentioned before it is the most successfull and most widely accepted.

The theory was originally proposed by Michaud (1970). In the following pages I shall introduce the fundamental equation starting from the basic physics.

We shall assume the atmosphere to be a mixture of classical perfect gases (non- relativistic, non-quantistic). Under this hypothesis for the i^{th} species (be it ion or atom or molecule) we may introduce the distribution function $f(\vec{r},\vec{v},t)$ with the following meaning: $f d\vec{r} d\vec{v}$ is the number of particles of the i^{th} species wich has position between $\vec{r}$ and $\vec{r}+d\vec{r}$ and velocity between $\vec{v}$ and $\vec{v}+d\vec{v}$. Such a function must satisfy the Boltzmann equation

$$\frac{\partial f}{\partial t}+\vec{v}\cdot\frac{\partial f}{\partial \vec{r}}+\frac{\vec{F}}{m}\cdot\frac{\partial f}{\partial \vec{v}}=I_{coll} \tag{1.4}$$

where $\vec{v}$ is the particle velocity, m their mass and $\vec{F}$ the force acting on the particles. I_{coll} is called collision integral and defines the balance between the processes which contribute to populate and those which contribute to depopulate the volume of phase space $d\Gamma = d\vec{p}d\vec{q}$. In a state of thermodynamic equilibrium Liouville's theorem holds

$$\frac{df}{dt}=0 \Rightarrow (I_{coll})_{eq}=0 \tag{1.5}$$

A solution of the Boltzmann equation for thermodynamic equilibrium is the Maxwell-Boltzmann distribution

$$f=n(\frac{m}{2k\mathrm{T}\pi})^{\frac{3}{2}}e^{-\frac{mv^2}{2k\mathrm{T}}} \tag{1.6}$$

Boltzmann's H theorem (law of increase of entropy) proves that it is the only solution to the problem of equilibrium.

Now consider a gas which is in a state which is not too far from equilibrium. It is useful to introduce the concept of a local Maxwellian

$$f_0 = n(\vec{r},t)(\frac{m}{2k\mathrm{T}(\vec{r},\mathrm{t})\pi})^{\frac{3}{2}} e^{-\frac{mv^2}{2k\mathrm{T}(\vec{r},\mathrm{t})}} \tag{1.7}$$

By assuming the system to be described by f_0 we are assuming that each volume element $d\vec{r}$ may be considered for a time dt, to be in thermodynamic equilibrium and, therefore, described by an appropriate Maxwellian.

Under these hypothesis, if the system posesses a particular degree of freedom which reaches equilibrium in times much longer than all the others, so that all other degrees of freedom may be assumed to have their equilibrium values, the collision integral, which, in general, is complex to compute, may be approximated by a rather simple expression

$$I_{coll} \approx -\frac{g}{\tau} = \frac{-f - f_0}{\tau} \tag{1.8}$$

τ has the dimensions of time and it can be shown that it is the time taken by the system to go back to equilibrium after an initial displacement. It is called relaxation time. By substituting this approximate expression in the Boltzmann equation and neglecting terms proportional to $\frac{\partial}{\partial \vec{r}}$ and $\frac{\partial}{\partial \vec{v}}$ which are certainly of superior order to g one finds

$$\frac{\partial f_0}{\partial t} + \vec{v} \cdot \frac{\partial f_0}{\partial \vec{r}} + \frac{\vec{F}}{m} \cdot \frac{\partial f_0}{\partial \vec{v}} = -\frac{f - f_0}{\tau} \tag{1.9}$$

let us now further assume $\frac{\partial f_0}{\partial t} \approx 0$ and calculate the derivatives of f_0 from (1.7) one has

$$\frac{f_0}{k\mathrm{T}} \vec{v} \cdot \frac{\partial \mathrm{T}}{\partial \vec{r}} (\frac{mv^2}{2\mathrm{T}} - \frac{3k}{2}) + \frac{f_0}{n} \vec{v} \cdot \frac{\partial n}{\partial \vec{r}} + \frac{\vec{F}}{m} \cdot \vec{v} \frac{m}{k\mathrm{T}} f_0 = -\frac{f - f_0}{\tau} \tag{1.10}$$

Once the distribution function f is known the macroscopic quantities of interest may be computed. In particular particle current

$$\vec{j} = \int f\vec{v}d\vec{v} \tag{1.11}$$

where the integral is extended to all possible values of velocity. On the other hand in equilibrium there must be no current.

$$\Rightarrow \int f_0\vec{v}d\vec{v} = 0 \tag{1.12}$$

This is easily verified by a direct calculation. Let us now further assume $\frac{\partial T}{\partial \vec{r}}=0$ (this is usually a good approximation since in stellar atmospheres the thermic gradient is usually small. Hence (1.11) given (1.10) becomes

$$\vec{j} = -\tau \int \vec{v}[\vec{v}\cdot(\frac{\vec{F}}{kT} + \frac{1}{n}\frac{\partial n}{\partial \vec{r}})]f_0(\vec{v})d\vec{v} \tag{1.13}$$

all the quantities in this equation must be thought as referring to a particular chemical species. We omitted to note this by using an index to prevent the notation from becoming too clumbersome.

Let us next assume that the atmosphere is formed by plane parallel layers and that both the force and the density gradient are directed along the vertical axis (the direction defined by the gravity acceleration $\vec{g}$) which we shall call z axis

$$\vec{F} = F\vec{e}_z \tag{1.14}$$

$$\frac{\partial n}{\partial \vec{r}} = \frac{dn}{dz}\vec{e}_z \tag{1.15}$$

then the equation for particle current becomes

$$\vec{j} = -\tau \int \vec{v}v_z(\frac{f}{kT} + \frac{1}{n}\frac{dn}{dz})f_0 dv_x dv_y dv_z \tag{1.16}$$

It is easy to verify that the integrals containing the mixed products $v_x v_z$ and $v_y v_z$ vanish identically

$$\Rightarrow \quad j_x = 0 \qquad ; \qquad j_y = 0$$

as was *a priori* obvious by considering the symmetry of the problem. As far as j_z is concerned we have:

$$j_z = -\tau \int v_z^2 (\frac{F}{kT} + \frac{1}{n}\frac{dn}{dz}) f_0 dv_x dv_y dv_z \tag{1.17}$$

The integral appearing in (1.17) may be easily computed by using the formula

$$\int_0^\infty x^n e^{-ax^2} dx = \frac{1}{2}\Gamma(\frac{n+1}{2}) a^{-\frac{n+1}{2}} \tag{1.18}$$

which can be proved by induction. Hence taking into account (1.7) and (1.18), (1.17) becomes

$$j_z = -\tau \frac{kT}{m} n (\frac{F}{kT} + \frac{1}{n}\frac{dn}{dz}) \tag{1.19}$$

Introduce next the quantity W (velocity per particle) defined as $W = \frac{j_z}{n}$ and noting that $\frac{1}{n}\frac{dn}{dz} = \frac{d\ln n}{dz}$ we finally obtain

$$W = \frac{\tau kT}{m} (\frac{-d\ln n}{dz} - \frac{F}{kT}) \tag{1.20}$$

The quantity $\frac{\tau kT}{m}$ is called D the diffusion coefficient.

The forces to which a particle is subject in a stellar atmosphere are (to first order approximation) gravitational force $F = mg$ and radiative force, which we shall write as $F_{rad} = -mg_{rad}$. g_{rad} is called radiative acceleration and must be computed from knowledge of the energy levels and all radiative transitions which may take place between levels for the given species (including ionization). Then the diffusion equation becomes

$$W = D(\frac{-d\ln n}{dz} + \frac{m(g_{rad} - g)}{kT}) \tag{1.21}$$

This is not exactly the equation used by Michaud (1970), however it displays all the basic physics. To use this equation one must compute or estimate radiative accelerations for any given ion. Of particular interest to us are the papers of Michaud *et al.* (1979), in which radiative forces on Helium are computed for B

and O type stars, and that of Michaud *et al.* (1986) who performed calculation of diffusion of heavy elements in sdB stars, in the presence of gallium. The results of the first paper tell us that the observed underabundances of He in B type may be explained by diffusion. In the second paper the authors find that, in order to reproduce the observed abundance patterns for sdB's it is necessary to assume a low mass loss rate.

Diffusion theory is fairly successful, however the diffusion velocities are always of the order of a few centimeters per second, it seems therefore strange that even low microturbulences (whose order of magnitude is of a few kilometers per second) fail to homogenize the atmosphere. In spite of this almost everybody accepts that the He underabundance in HBB and sdB stars is due to diffusion.

Chapter 2

Field blue stars

Blue stars in the halo pose a number of interesting problems related to both stellar and galactic evolution. These stars stars may, a priori, belong to two completely distinct classes of objects, namely they may either be Main Sequence unevolved stars or evolved Horizontal Branch, or post Horizontal Branch, stars. In the former case the main problem to be solved is whether these stars were ejected from the galactic plane, and, if so, which mechanisms caused the ejection, or whether they were formed recently in the halo, and, if so, how could star formation take place in such a dilute environment as we believe to be the halo. In the other two cases we have the opportunity to study the late stages of stellar evolution and compare the field population to the globular cluster population and look for analogies and differences.

Since the two classes of stars have the same effective temperature and gravity a spectroscopic analyses is required to distinguish between the two. Yet on the observational side the matter is complicated by the fact that halo HB stars show a widely varying range of compositions, from deficiencies of some or all heavy elements (see, for example Spite and Spite, 1980) to overabundances of certain heavy elements (Baschek and Sargent, 1976). As pointed out by Conlon *et al.* (1989), a HB star may change its surface composition either due to pre-HB evolution (for example element dredge up following mass loss in the red giant phase (Deupree and Wallace, 1987) or convective mixing (Groth *et al.* 1985)) or during the HB life due to atmospheric phenomena such as diffusion (Michaud, 1970). In spite of these difficulties spectroscopy may be used to discriminate the two classes of objects, in fact Conlon *et al.* (1989) claim that *there is no conclusive evidence for a HB star with a Pop I composition.* The fact that the lower left quadrant of the HR diagram contains a wide variety of objects differing for masses, ages and chemical composition was clearly understood by the early researchers such as Feige (1958) and Luyten (1959), however a systematic

investigation of the physical properties of these stars had to wait until the early seventies.

Newell (1973) determined the effective temperature and gravity of 189 stars. He noticed that stars tend to cluster in well defined areas of the $\log T_{eff}$ $\log g$ plane. Newell counted in all four such areas which he called A, BC, D and HL. In order to explain his observations Newell put forward the hypothesis that the various areas reflected different evolutionary states for stars of different masses.

Greenstein and Sargent (1974) performed a study which is somewhat complementary to that of Newell. On average the stars of Greenstein and Sargent are hotter than Newell's. Several stars are common to both researches, however Greenstein and Sargent could use several medium and high resolution spectrograms, whereas Newell used essentially spectrophotometric data. White dwarfs are more numerous in the Greenstein and Sargent sample, this could be due either to a selection effect in Newell's sample or to an erroneous estimate of g in some cases.

The new fact which emerged from the study of Greenstein and Sargent is the presence of an extended Horizontal Branch (EHB), that is a Horizontal Branch which includes stars hotter than those which are observed on the Horizontal Branches of Globular Clusters. Such stars were classified by Greenstein and Sargent as subdwarfs of type O and B (sdO and sdB).

These pioneering studies were followed by many others (the reader is referred to the reviews of Greenstein (1988) and Sandage (1988) and references therein), our present knowledge is neatly sumarized by Heber (1988), he points out the existence of five classes of objects:

1. Main Sequence B stars

Such stars probably suffered cluster or close binary ejection. Conlon *et al.* (1989) report of the presence of four such stars at 2 kpc or more from the galactic plane . Their Population I nature was established on the basis of a

detailed model atmosphere analysis. Quin *et al.* (1991) studied IUE spectra of 14 high galactic latitude stars, whose distance from the galactic plane ranges from 1.3 to 8.7 kpc, and found all of them to be members of Pop I. Even more intriguing is the presence of B type stars further out in the halo (17 kpc see Brown *et al.* 1989), since if some of these are proved to be Pop I then they cannot possibly have been ejected from the disc, such great distances could not have been covered in their lifetimes; therefore they must have been formed in the halo, in spite of all the theoretical problems that this poses.

2. Horizontal Branch B type stars (HBB)

These stars are present both in the field and in globular clusters. Their atmospheres are, in general, helium deficient (Heber, 1988). Theoretically they are understood as stars with a double source of energy: He burning in the core and H in a shell. It is worth noting that the luminosity of the H shell equals or even exceeds that of the He core. HBB stars may also suffer the ^{3}He anomaly (Hartoog, 1979; Heber 1990), that is that ^{3}He is more abundant than in the sun and in some cases the large isotopic shifts indicate that ^{4}He is almost entirely replaced by ^{3}He (Heber, 1988).

3. Extended Horizontal Branch Stars (EHB)

As said before the existence of such stars was recognized in the field by Greenstein and Sargent (1974). At the time this posed some theoretical problems since evolutionary tracks then available did not reach the region of the EHB; in fact they either turned back redward or had vertical excursions (Rood, 1973;Gross, 1973). However this did not stop Greenstein and Sargent from speculating that *the extreme left end of the EHB is occupied only when the H envelope mass is neglegible.* In fact in such a scenario we would be able to see the deeper, hotter, bluer layers.

As a matter of fact subsequent observations proved the EHB to be present also in globular clusters, the classical example being NGC 6752 (Cannon 1981,

Heber et al. 1986; Glaspey et al., 1989), moreover the Horizontal Branch presents a gap between the EHB and the HB, which is not evident in the diagram for field stars, probably due to errors in distance (and therefore in absolute magnitude) estimates. The stars below the gap (EHB) are those identified as sdB and sdO by Greenstein and Sargent. The evolutionary tracks computed by Caloi (1989), confirm the hypothesis made by Greenstein and Sargent: HB star models with neglegible envelope mass ($M_{env} \leq 0.02 M_{\odot}$) occupy the region in the HR diagram which pertains to the EHB. In fact the main difference between an HBB star and an EHB star is that in the latter the luminosity of the H shell is negligibly small. The structure of an EHB star is similar to that of an He Main Sequence star.

The explanation of the gaps in the HB is still an open question. These were first recognized by Newell (1973) for field stars, and more recently by Crocker et al. (1988) . In disagreement with these findings Caloi (1989) claims that there is a continuity *though through a region of lesser population* (Buonanno *et al.*, 1986).

4. sdO stars

These stars have even higher temperatures ($T_{eff} \geq 35000$) . They differ markedly from HBB and sdB stars because they are He rich, in general. They lie in the zone of the HR diagram which is crossed by the tracks evolving away from the EHB. However their He richness must be explained, if they are to be identified as post-EHB stars. Already Greenstein and Sargent (1974) argued that photospheric convection (driven by HeII ionization) could result in mixing, thus destroying the underabundance built up by diffusion in the progenitor sdB or EHB star. This idea was followed up qualitatively by Groth et al. (1985). The class of sdO's, however seems to be less homogeneous than that of sdB's, in fact several of them lie close to post-AGB tracks and Heber (1988) suggests that they should be identified with AGB descendants. The temperatures and

gravities of these stars are those typical of central stars of planetary nebulae. Spectroscopically the two kinds of objects are indistinguishable except that sdO's lack the nebula.

From what has been said above it seems natural to subdivide the sdO's into two classes: *high gravity* or *classical* sdO's, to be identified as post-EHB stars, and *low gravity* sdO's, to be identified as post-AGB.

5. PG1159 stars

This class was recently discovered and is named after the prototype PG 1159-035 (Mc Graw *et al.* 1989). They are extreemly hot and devoid of hydrogen (like many sdO's). They are characterized by an absorption trough shortwards of 470 nm caused by He 468.6 nm and many CIV lines. The atmospheric abundances closely resemble those of the He-buffer layers of post-AGB star models (Iben,1984), however it is necessary to invoke some mechanism which removes the outer envelope, thus making visible these deep layers, in order to identify these stars with the post-AGB models. One such mechanism could be the born-again post-AGB star scenario of Iben *et al.* (1983), as pointed out by Werner *et al.* (1990). Heber (1988) speculates that, since the born-again post-AGB star scenario can explain the low gravity sdO's as well as the PG 1159 stars *there could be an evolutionary link between these two groups of stars.*

Chapter 3

Feige 86

W.S. Luyten performed a number of studies on the kinematics of field blue stars, thus measuring many proper motions. Among the stars analysed many were taken from the catalogue of J. Feige (1958), in particular star number 86 (which hereafter we shall call Feige 86 or F86) appeared to have a rather high proper motion. Luyten drew the conclusion that it must be subluminous. In fact F86 ought to be rather near, since it is the second brightest star of the catalogue. Its brightness makes it more readily accesible to spectroscopic analysis. The first to obtain a spectrum of F86 was Berger, who in 1963 published a radial velocity measurement on the basis of two spectrograms taken at Mt. Palomar with the Hale reflector, of dispersion 38 Å/mm and 18 Å/mm, respectively. Berger noticed that the visible spectrum is *characterized by weak lines*, and classified it as Pop II. In April 1967 W.L.W Sargent and L. Searle with a six hour exposure obtained a spectrogram of F86 with the dispersion of 9 Å/mm at the coudé focus of the Hale reflector. Their intention was to determine the helium abundance from the analysis of the profiles of neutral He lines. They noticed that at this dispersion the spectrum was characterized by many weak lines, not detectable at lower dispersion and not present in normal Pop I stars. They identified most of these lines as PII. The unusual intensity of PII lines induced Sargent and Searle to compare the spectrum of F86 with that of 3 Cen A, which is a B peculiar Pop I star characterized by many PII lines. From the line widths Sargent and Searle estimated $v \sin i \leq 12\text{km/s}$.

By combining Luyten's proper motion measurements with Berger's radial velocity Sargent and Searle estimated the velocity vector of F86. However to do this it is necessary to know the star's distance. This may be computed if the absolute magnitude is known. As already said for B type stars the most populated zones of the HR diagram are the main sequence and the Horizontal Branch, it is therefore logical to assume that F86 is in one of these two zones.

Balmer line profiles do not allow to decide whether the star is on the MS or on the HB, since they are similar for the two classes of stars around B type (Searle and Rodgers 1966, Sargent 1967).

Given the three usual unit vectors $\vec{u}, \vec{v}, \vec{w}$, $\vec{u}$ towards the galactic center, $\vec{v}$ along the galactic rotation and $\vec{w}$ towards the north galactic pole, Sargent and Searle estimated $(u, v, w) = (+303, -855, +67)$ if F86 is assumed to be on the MS. Sargent and Searle thought this velocity to be implausible for a Pop I star star and unprecedented even for a B runaway star. On the other hand by assuming that F86 is on the HB they find $(u, v, W) = (+95, -250, +8)$, which is a perfectly acceptable velocity for a Pop II star.

Thus the kinematic reasons to believe that F86 is an extreme Pop II star are quite convincing. This, however makes rather surprising the similarity between F86 and 3 Cen A. In fact the two stars ought to have totally different ages, luminosities and masses, but the same peculiar chemical surface composition. From the mass luminosity relation a main sequence B type star, like 3 Cen A, ought to have a mass between 5 and 10 solar masses, whereas a halo HB star of the same spectral type ought to have a mass between 0.4 and 1 solar masses (Greenstein and Sargent, 1974). Newell (1973) included F86 in his BC group and suggested this to be made up by stars of $0.5 M_{\odot}$ on the HB or immediately subsequent phases. Greenstein and Sargent agreed with Newell on the classification of F86 (FB137 in their list) as HBB. They argued that these stars ought to be metal deficient in analogy with what is observed in their globular cluster counterparts. In spite of this argument direct evidence of this hypothesis is, at best, weak. They therefore proposed that some of their stars be observed at high dispersion in order to make a detailed abundance analysis.

Such an analysis was carried out for the visible spectrum by Baschek and Sargent (1976) on the basis of the already mentioned spectrogram of Sargent and Searle, of one taken by Greenstein (1971) and one taken by Greenstein and

Sargent (1974), all at the coudé focus of the Hale reflector. Helium resulted to be ten times underabundant with respect to the sun while for carbon they derived an upper limit $\log(N(C)/N_{tot}) - log(N(C)/N_{tot})_{\odot} < -1.8$.

The analysis of Baschek and Sargent confirmed the similarity of Feige 86 and 3 Cen A, except for carbon which is observed to be more underabundant in F86. Searching for further confirmation of this similarity Hartoog (1979) measured the ^{3}He/^{4}He abundance ratio, in fact this is a lot greater than normal in 3 Cen A. He found ^{3}He/^{4}He = 0.7 , thus enforcing the parallelism between the two stars. In the light of these results one may conclude that there exists some kind of link between Bp stars and the He weak HBB stars. It has already been pointed out that such stars have different masses, radii and luminosities, however they have almost the same temperature and gravity. In fact Bp Pop I stars are more luminous and massive, though they have bigger radii and since one has

$$\mathrm{T}_{eff} \sim (\frac{L}{R^2})^{\frac{1}{4}} \quad ; \quad g \sim \frac{M}{R^2}$$

we can see that an increase in mass and luminosity may be, within ceratin limits, compensated by an increase of radius. It thus appears safe to conclude that the phenomena rsponsible for chemical anomalies depend only upon T_{eff} and g and not on M, L, R.

The abundance analyses carried out by Baschek and Sargent may not be considered to be complete; it is limited by the few lines of measurable equivalent width in the visible spectrum. To overcome this limitation and open up a new field of investigations on F86 M. Hack observed the star in the ultraviolet with IUE. The results of low and high resolution observations are reported in Hack(1979) and Hack (1980). The UV spectrum confirms the carbon underabundance.

A new observational fact is constituted by the possible presence of lines formed by highly ionized species, such as NV and CIV, such lines should not

be formed in the atmosphere of a B type star, since the temperature is too low for such states to be considerably populated. Hack (1980) put forward the hypothesis that these lines pointed at the presence of a hot corona.

Morossi *et al.* (1981) provided an identification list for the UV spectrum, Castelli and Singh (1990) and Bonifacio *et al.* (1990) provided preliminary results for the abundances from the UV spectrum. The fact that, up to now, no complete analysis of the UV spectrum of F86 has been published, in spite of the fact that the spectra were available since 1979, is due to the extreme complexity and surprising aspect of this spectrum. F86 is a slow rotator, this means that many weak lines, which are smeared out in fast rotators, show up. Thus the UV spectrum of F86 is a real forest of lines, most of which were unidentified. There was no hope of obtaining a decent identification list without the aid of spectral synthesis techniques. Only with the new line lists of Kurucz, which became available to us around 1986, a solution of the problem seemed within reach. Yet the uncertainity of many atomic data contained in the lists prevented us from performing an abundance analysis then. We decided that we needed a set of lines with reliable atomic data to determine the abundances. The best way of doing this, we thought, would be to compare a synthetic spectrum with that of a well known standard star of about the same temperature and gravity of F86. The lines with wrong atomic data would show up from such a comparison and consequently be discarded from the number of those useful in determining abundances. The choice of the standard star fell on ι Herculis, because it is well studied in the visible and a UV spectral atlas from Copernicus data is available (Upson and Rogerson, 1981). Thus an extensive work of comparing computed and observed spectra (both Copernicus and IUE) began. This work ended up in the publication of the UV spectral atlas of ι Herculis by Castelli and Bonifacio (1990).

This atlas showed the shortcomings of the synthetic spectrum and allowed

a compilation of a list of lines suitable for abundance analysis. Moreover the comparison we made with F86 showed that the forest of lines detectable in the spectrum of F86 is not a peculiarity, but is typical of a slowly rotating B type star.

Keeping at hand the atlas of ι Herculis the study of the UV spectrum was tackled again by Bonifacio *et al.* (1990). The interesting fact that emerged was that the lines of BII,CI, CII, OI, MgII, SiII, PIII, SI, SII, TiII, FeIII, NiII and Ga III, which originate from the ground level were either shifted or double or asymmetric. Such lines are those indicated by Morton and Smith (1973), Morton (1978) and Morton *et al.* (1988) as characteristic of low density regions such as the interstellar medium, stellar winds and the absorbing material in front of some quasars. This suggests the presence of a quite cool, low density region, different from the photosphere. Singh and Castelli (1990) applied their SiII UV mult 13.04 method to determine the temperature of F86 and found a value much lower than that deduced from Stromgren photometry. Does this support the existence of a cooler outer envelope ? Such an envelope could be expected either due to mass loss during the He-flash or due to mass loss during the red giant phase.

Glaspey *et al.* (1989) studied the abundances of hot horizontal branch stars in globular cluster NGC 6752, using visible spectra. They took also spectra of F86 to be used as a reference. Their results are extreemly interesting. In particular star CL1083 has atmospheric parameters which are very near to those of F86, being somewhat cooler. Moreover, like F86, CL1083 is a slow rotator. One should therefore expect a similar abundance pattern if both are PopII HB objects. Any difference should be ascribed to the different nature of the field and globular cluster populations, if F86 is held to be representative of the field population. The first obvious difference is that P does not show up in the spectrum of CL1083. Interesting is also the data on Mg : the equivalent width

of the line of MgII at 448.12 nm of CL1083 is much smaller than that of F86. The EW of this line measured by Glaspey *et al.* for F86 is similar to that measured by Baschek and Sargent (1976). Baschek and Sargent give [Mg/H]=-0.1, in agreement with the UV result of Bonifacio *et al.* who give [Mg/H]=0.0, it is likely that if Glaspey *et al.* determined the Mg abundance for F86 with their method, using their equivalent width they would find a value similar to those of Baschek and Sargent and ours. On the other hand for CL1083 they give [Mg/H]=-1.22. Consider that the cluster metallicity is -1.5 . This result is puzzling. If we believe the kinematics of F86 it should be a member of extreme PopII, therefore its intinsic metallicity should be of the order of -3.0, well below that of NGC 6752, yet Mg and P behave as though F86 belonged to a more metal rich population than CL1083. If these elements are enhanced by diffusion in F86 then they should be enhanced also in CL1083, since there is no apparent reason for the two stars to behave diferently.

Chapter 4

Data handling

In the future work on F86 we plan to use observational data in the ultraviolet obtained with IUE and in the visible, obtained with the AURELIE spectrograph attached to the 1.5 m telescope of OHP. This data will be compared with synthetic spectra computed with the SYNTHE package (Kurucz and Avrett, 1981), kindly provided to us by R.L. Kurucz.

In this chapter I shall describe how this data is handled and, for observational data, reduced. A brief description of the instruments, IUE and AURELIE, will precede the description of the handling of the relative data. A description of the principles involved in the computation of a synthetic spectrum will be delayed to a later chapter.

THE IUE TELESCOPE AND SPECTROGRAPH

The IUE satellite was launched on January 26^{th} 1978. It follows a geosyncronous orbit and is controlled by two ground based centers situated at Goddard Space Flight Center, Maryland and at Villafranca del Castillo, near Madrid.

The IUE telescope is of conventional type, the diameter is 45 cm, focal ratio f/15. The optical configuration is a Ritchey-Cretiéne. The primary mirror is made in beryllium, in order to guarantee a minimum weight coupled to a high reflectivity in the UV. The secondary, instead is made out of quarz, mainly for the low thermic expansion coefficient.

Since the orbit is geosyncronous, observations must be made also in the sunlight. In order to make this possible IUE has sun-baffles which allow diffraction of sunlight and its subsequent remotion from the optical path before it reaches the focal plane.

On the focal palne there is a metal plate in which are cut four slits, which can send the optical beam into one of two spectrographs. On the plate the stellar field is reflected and this image, viewed from a TV camera is used to

guide the telescope. There are also some tiny lights, on the plate which are used as reference marks to calibrate the coordinates of the star tracker. Moreover there are many microscopic grooves used to asses the quality of the focus. The four slits are divided into two pairs, each of which feeds one of the spectrographs. The pair is made up by one circular slit of 100 μm diameter (corresponding to $3''$ on the sky) and one rectangular slit of 350×700 μm^2 (corresponding to $10'' \times 20''$ on the sky). The spectrographs are two to allow a complete coverage of the wavelength interval from 115 nm to 320 nm with a resolving power not worse than 0.02 nm at any wavelength. One of the two spectrographs covers the range from 115 nm to 200 nm , the other covers the range from 180 nm to 320 nm .

After going through the slit the beam is collimated by a mirror and sent to an echelle grating, from the echelle grating the beam is sent to a concave grating, which focuses the spectrum on a camera. The echelle grating may be masked by a plane mirror, so that the spectrograph may work in low resolution mode (6 Å resolving power). The resolving power in high resolution mode (with the echelle) is 0.2 Å.

The cameras used as detectors are Westinghouse WX 3224 SEC with VIDICON output. Such cameras are only sensitive to visible radiation, but not to UV radiation. It is therefore necessary to use a UV to visible converter. The converters in use are Bendix proximal focus (40 mm) converters. They use a magnesium fluoride window, which is transparent to UV, a CsTe photocatode and an output window of optical fibers, which allows to couple the converter with the SEC tube. Further details are in the papers of Boggess et al. (1978a and 1978b). If the reader is interested to the history of IUE he may refer to Boggess and Wilson (1986).

THE AURELIE SPECTROGRAPH

The AURELIE is a spectrograph designed and manufactured at the Observatoire de Haute Provence to be operated at the coudé focus of the 1.52 m telescope of that observatory. The good quantum efficency (more than 70% between 600 nm and 700 nm) of the solid state detectors employed makes it possible to observe stars which could only be observed with larger telescopes or poor S/N with photographic plates. The AURELIE is a slit spectrograph it has the usual optical scheme: slit-collimator-dispersing medium-camera-detector. The detector is double-barrette Thomson TH7832 each barrette is composed by 2036 photodiodes of dimensions $750\mu m \times 13\mu m$, the photodiodes are coupled with two CCD read-out registers (R1,R2), one is used for odd pixels and the other for even pixels. As mentioned the quantum efficency is quite good in the red but drops below 50% shortwards of, approximately, 500 nm. The factor which limits spectral resolution is not pixel size but the parasitic resistance in the photodiode array, in fact if a single pixel is illuminated the resulting charge leaks to the two neighbouring pixels, therefore the spatial resolution along the direction of the dispersion is at least three pixels. A more accurate analysis of the phenomenon gives a value somewhat larger, the nominal resolutions which I shall quote are all calculated assuming a $\Delta\lambda$ corresponding to 3.23 pixels. The camera has a focal length of 1 m and an aperture of f/10. The dispersing medium is one of six gratings, some of which may be used in two different orders using filters for order separation. The possible combinations of gratings and filters are illustrated in detail in the AURELIE manual. I shall note here just two things:

- the AURELIE may be used in two modes
  a) medium resolution $(4700 < \frac{\lambda}{d\lambda} < 21000)$
  b) high resolution $(30000 < \frac{\lambda}{d\lambda} < 100000)$
- among the "high resolution" gratings there is an echelle grating which uses one of five narrow band filters (but others may be added) as a cross disperser

and obtains a nominal $\frac{\lambda}{d\lambda} = 96000$.

The collimator has a focal length of 1 m and aperture f/10. The slit is circular of $600\mu m$ diameter which corresponds to $3''$ projected on the sky, this does not limit the resolution since $3''$ on the sky correspond to 1.12 pixels on the detector and we saw that the spatial resolution of the detector is somewhat larger than three pixels. The instrument is threfore optimized for the site which has a typical seeing of $3''$ or larger.

To my knowledge visible high resolution spectra of Feige 86 have been obtained only with the coudé spectrograph of the 5 m Hale reflector at mt. Palomar with several hours of exposure (of the order of 6). Attempts have been made with the 1.52 m telescope at OHP and the photographic spectrograph, but the S/N was so low that the spectra could hardly be used for identification. Moreover the Palomar spectra were usable only in the blue range ($\lambda < 480$ nm) because the star is blue and the sensitivity of the photographic plates drops towards the red. However some interesting lines should fall in the red :

H-alpha

C II 657.6 nm , 658.3 nm , 634.6 nm

Si II 637.1 nm

P II 636.7 nm , 646.0 nm , 650.3 nm , 650.8 nm

Ne I 650.6 nm

The AURELIE offers the opportunity of observing these lines which were not accesible even with the mt. Palomar telescope; in fact in this spectral region the sensitivity of the Thomson barrette is at maximum and may, to some extent, compensate the limited diameter of the telescope.

The main problem of the AURELIE is that since the physical dimensions of the detector are small (26.6×0.75 mm^2) in high resolution mode the spectral range is also small.

IUE DATA

The handling of IUE data has been exaustively described elsewhere (Harris and Sonneborn, 1987) and I shall not repeat what has already been said. I shall however mention some of the problems we ran into.

When used on faint stars such, as F86, IUE images yield a poor S/N, the ultimate reason for this is the relatively small aperture of the IUE telescope, no data processing tecnique may overcome this difficulty. The images which are in our possess have been processed with the standard software IUESIPS2 for wavelength and intensity calibration. To further analyze the data one may chose either to normalize the flux to the continuum or to perform absolute flux calibration, according to the calibration of Cassatella et al. (1981, 1982). However this calibration is not included in the standard processing of IUE high resolution spectra. Moreover it is not really necessary in our study. We have thus decided to resort to normalization to the continuum which has the further advantage to make the treatment of the UV data consistent with that of visible data.

For the normalization we used a software which was initially specifically designed for this purpose and successively modified to be used on data other than IUE (NORMA code, Bonifacio, 1989). With this procedure each order was normalized indipendently. The difficulty in choosing the continuum points is that the UV spectrum of a B star and in particular of F86 is crowded with lines. Although the continuum of IUE orders is not straight it is always smooth, this helps to provide a constraint which makes less subjective the choice of the continuum.

AURELIE DATA

The one dimensional nature of the double Thomson barrette used as a detector in the AURELIE spectrograph makes the data handling rather simple

and straightforward.

The raw data consists of a table of the form:

Pixel number	Number of counts
.	.
.	.
.	.
2036	xxx

This table has to be transformed in the calibrated image:

Wavelength	Relative intensity
.	.
.	.
.	.

For our purposes absolute flux calibration, a very complex matter indeed, needs not to be tackled. We are only interested in line strengths relative to the continuum or realtive to each other. This may be readily achieved if the continuum can be safely estimated; this is certainly the case for the visible spectrum of B type stars.

The calibration process consists of three distinct steps:

1. Intensity calibration
2. Wavelength calibration
3. Normalisation to the continuum

1. Intensity calibration

This is aimed at removing two instrumental effects:

a. the wavelength dependence of the instrumental response

b. dark current

a. This is due to several factors: the quantum efficiency of the detector is not constant with wavelength, nor is the efficiency of the optical parts (mirrors, gratings, filters...). As a result of this if a given flux $F(\lambda)$ is input in the spectrograph what is observed is $N(\lambda) = R(\lambda) \times F(\lambda)$, where $R(\lambda)$ is some unknown response function. The $R(\lambda)$ function is typical of a given instrument, but depends also on a number of uncontrollable variables, such as temperature, state of the optics, etc. .. In practice the response function is different from one observation to the other. To remove the instrumental signature one resorts to the so called flat-fielding tecnique. This consists in feeding to the spectrograph a white (i.e. constant over wavelength) spectrum. If the response were, ideally, wavelength independent the output spectrum ought to be flat, hence the name. One then observes $G(\lambda) = R(\lambda) \times K$, where K is the constant input flux. Thus one may compute the function $C(\lambda) = N(\lambda)/G(\lambda) = F(\lambda) \times K$, the multiplicative constant K is unimportant, since we shall normalize the flux to the continuum (see further on).

The white spectrum is provided by a Wr lamp. It is not exactly white, but deviations are unimportant over small spectral ranges, such as those accesible in the high resolution mode of AURELIE. A more serious source of systematic error is that the optical paths of the light from the lamp and from the star are different. So that $G(\lambda) = r(\lambda) \times K$ and$C(\lambda) = F(\lambda) \times K \times [R(\lambda)/r(\lambda)]$. With a careful spectrograph design one should be able to obtain that the ratio in square brackets is almost equal to one. However the validity of this assumption should be checked experimentally for any given spectrograph configuration. One way of doing this would be to take a spectrum of sunlight reflected against the inner surface of the telescope dome, such a spectrum should be reasonably flat.

An even more seriuos source of systematic error is that owing to the physical

properties of the detector and optical system, the response function depends on the absolute flux level. This means that the slope of the flat field may be different if the average number of counts is 1000 or 10000. A careful observer should therefore obtain flat fields with more or less the same number of counts as the image he wants to calibrate. In particular if the image of the star has a low number of counts (because the star is faint) he should obtain a flat field with a low number of counts; however low-level flat fields have a poor S/N, to overcome this difficulty one may take several low- level flat-field exposures and then take the mean, so as to average out the noise. Hence, rather than a single flat-field exposure $G(\lambda)$ one uses an average flat field $g(\lambda) = \frac{\sum_{i=1}^{M} G_i(\lambda) q_i}{M}$, where q_i are some suitable weights and M is the total number of exposures.

b. Due to thermic noise the response of the detector is non-zero even if the spectrograph shutter is kept closed. This results in the fact that what is observed is $P(\lambda) = F(\lambda) \times R(\lambda) + b(\mathrm{T})$, where b is some unknown function of the temperature, in principle it should be independent of λ, although, occasionally a weak wavelength dependence is displayed.

This instrumental effect could be removed by the use of an "offset" exposure, that is a 0 seconds exposure with the spectrogrpah shutter closed. If the temperature is constant during the exposure (and it must be since the barrette is kept in cryostat cooled by liquid nitrogen) one may compute $D(\lambda) = (M(\lambda) - b(\mathrm{T}))/(g(\lambda) - b(\mathrm{T}))$ where $b(\mathrm{T})$ is now the offset exposure. However a serious problem is posed by the charge build-up process in the detector; in practice, owing to the non-zero capacity of the photodiode array b depends also on exposure time: $b(\mathrm{T}, t)$. One should therefore obtain a dark exposure with the same time as the stellar exposure to be calibrated. A good practice would be to take a series of dark exposures with different exposure times, ranging from the minimum to the maximum exposure time we expect to use in the night and

then reduce each image using the dark exposure whose exposure time nearest to that of the image. The above formula may be used if b is the dark exposure.

2. Wavelength Calibration

Wavelength calibration of the AURELIE is in all similar to wavelength calibration with other spectrographs. One takes, with a given spectrograph configuration a spectrum of some reference lamp. Presently available is the Th-Ar lamp, for which the spectral atlas of D'Odorico et al. (1987) is usable for identification.

The calibration image consists of a table:

pixel number	number of counts
.	.
.	.
.	.

i.e. the digital image of the reference spectrum, it is the exact analogue of the stellar spectrum. On this spectrum the lines which are of intensity over some given threshold and of FWHM larger than some other threshold are selected. The threshold values should be chosen in such a way that a convenient number of lines is selected. For AURELIE in high resolution mode this number is something between 15 and 35, depending on the spectral region considered. Too few lines make the dispersion curve unreliable, too many lines make the fitting algorithm unstable. After the lines have been selected 4 or 5 lines must be interactively identified with the help of an atlas. Then an automatic procedure, with the help of a table containing a list of the lines present in the atlas, makes further identifications and tries to fit a first or second degree polynomial for the function $\lambda = \lambda(n)$, where n is pixel number. The procedure should be stopped when most of the lines have been identified and the R.M.S. error is smaller than

or, at least of the order of the nominal resolving power of the spectrograph in that configuration.

Care should be taken in assesing the actual resolution of the spectrum. This may be measured directly by measuring the FWHM of some Th-Ar spectrum lines and taking the average. This is the actual $\Delta\lambda$. The resolving power depends on spectrograph focus. In order to obtain good observations one should always check the spectrograph focus before observing. In the AURELIE spectrograph the factor which ultimately limits the resolution is the parasitical resistance in the photodiode array, which makes charge leak to the neighbouring photodiodes. Illumination of a single pixel results in the charge being distributed over three pixels (the central, illuminated, one and the two neighbouring ones). Remind that the spectrograph's nominal resolution is computed with an assumed $\delta\lambda$ corresponding to 3.23 pixels.

With a careful focusing of the spectrograph one should be able to make the lines of the reference spectrum as narrow as 3.23 pixels or narrower (depending on spectral region). Suppose that we calibrate in wavelength the reference spectrum and measure the average width of the Th-Ar lines, call this width $\Delta\lambda$ and call $\delta\lambda$ the R.M.S. of the calibration curve. Clearly if $\delta\lambda >> \Delta\lambda$ the calibration is no good, it is acceptable if $\delta\lambda \approx \Delta\lambda$ and is very good if $\delta\lambda << \Delta\lambda$. The latter is usually the case. The actual resolving power is $\Delta\lambda$.

The measurement of $\Delta\lambda$ should always be performed to check *a posteriori* both the dispersion curve and the spectrograph focus. It is a very important quantity to asses the quality of the observations. Moreover if the observed spectrum has to be compared with a computed spectrum this should be broadened with an appropriate instrumental profile before the comparison is made. In the case of AURELIE a gaussian of width $\Delta\lambda$ is suitable.

3. Normalisation to the continuum

The final step of the reduction consists in normalising the spectrum. The rationale behind this procedure is the following: the spectrum emitted by the stars is the result of the sum of two terms: $c(\lambda)$ is the flux emitted by all the b-f, f-b and f-f transitions which is called *continuum*, $L(\lambda)$ is the flux emitted by all the b-b transition and is called the *line spectrum*. So $S(\lambda) = c(\lambda) + L(\lambda)$ What we are insterested in is line strengths relative to the continuum rather than absolute line strengths. If absolute line strengths were required absolute flux calibration would become necessary. Absolute flux calibration is very difficult, especially for ground-based observation since the transparency of the atmosphere has to be somehow estimated. However if only relative line strengths are required it is sufficient to estimate the continuum $c(\lambda)$ and then compute $N(\lambda) = S(\lambda)/c(\lambda) = 1 + L(\lambda)/c(\lambda)$. The quantity $L(\lambda)/c(\lambda)$ is called residual intensity. Our problem is then to estimate $c(\lambda)$. Theoretically it is known that the continuum flux distribution is almost everywhere smooth except for some discontinuities or jumps, such as the Balmer jump, the Paschen jump, etc. The smooth bits of the curve may be, to first order approximated by the grey atmosphere flux distribution, or else more refined model atmospheres may be used to approximate the continuum flux. What is important to stress here is that except in the regions of the jumps, over small spectral ranges the continuum flux is smooth and slowly varying with λ . These two facts allow us to state that for small spectral ranges the continuum can be safely estimated by eye. However one should always keep in mind that severe difficulties may arise in spectral regions heavily crowded by lines or dominated by lines with large wings (e.g. autoionization lines); in such cases the continuum is usually placed too low. This is not the case for the visible spectrum of F86, except perhaps near Balmer lines. The procedure for normalising the spectrum thus consists in selecting interactively a certain number of points believed to be

representative of the continuum and then interpolating a smooth curve through these points. It is usually found that spline interpolation yields the best results.

Once the spectrum has been intensity and wavelength calibrated and normalized to the continuum it is ready for the extraction of scientific information. Such information is essentially: line positions, line widths, equivalent widths. With this data one may proceed to line identification, readily obtained with the aid of a synthetic spectrum, and even to the determination of the element abundance. How this is done is explained in the next chapter.

SUCCESSIVE ANALYSIS

At the end of calibration procedure both IUE and AURELIE spectra are written in a machine-readable form compatible with the SYNTHE package of Kurucz.

For UV spectra we shall not perform any equivalent width measurement since all the algorithms for line fitting known to us are very unstable in a line crowded region such as the UV spectrum of F86. On the other hand such measurements will be performed on the visual spectrum where, on the contrary, the scarcences of lines makes algorithms such as that of Fraser and Suzuki (1970) both very stable and reliable.

Both UV and visible spectra will be compared with synthetic spectra in the case of UV spectra this is the best way of determining the abundances since no reliable EW is available. In the case of the visible spectra the comparison provides a useful cross- check of internal consistency of synthetic spectra calculations and EW measurements.

COMPARISON WITH SYNTHETIC SPECTRA

This chapter deals with data handling, thus also with the handling of synthetic spectra. Once a synthetic spectrum has been computed (how this may

be done is the topic of the next chapter) it is just another set of data. Kurucz provided us, along with has synthetic spectra programs with a series of programs which allow handling and presentation of both synthetic and observed spectra. The spectrum itself consists of a table of wavelength values (in nm) and residual intensity values, written in a machine readable form. This is true for both computed and observed spectra. However computed spectra have attached to them a lot more information, namely a list of all the lines, with their atomic data, used in the computation. This line data may be read separately with specifically designed programs. In order to compare a computed spectrum with an observed one the form must be broadened to take into account the effects of stellar rotation, Doppler broadening due to micro and macro turbolence, and instrumental profile. This may be readily done with programs specifically written by Kurucz for this purpose. (Programs Broaden and Rotate). Ultimately the comparison is done by superimposing observed and synthetic spectra on the same plot. The plotting package made available to us by Kurucz is both powerful and flexible. The most interesting feature is that it may use the line data read in from the synthetic spectrun to produce labels which display the data on the plot at the wavelength at which the line occurs. Usually not all the line labels are displayed but only these of lines whose stenght is above some fixed threshold. One of the advantages of this presentation method is that one is provided immediately with line identification and may see easily which lines are blended. Clearily before superimposing the computed and the observed spectrum the latter must be shifted in wavelength to take into account the Doppler shift due to the stellar radial velocity. For IUE spectra it is usually found that the shifts which is necessary to adopt to obtain an overall agreement between observed and computed spectra, is slightly different for each order, this is interpreted as small errors in the wavelength calibration procedure. I wrote a number of simple programs

which act as a user interface to make easier the use of the plotting package, in future these may evolve, if the need is felt, into a proper user-friendily interface.

Chapter 5

The art of computing synthetic spectra

Statement of the problem

The emergent spectrum from a star is the rather complex result of many physical phenomena. It is generated in a thin region of the star which we shall call the atmosphere. At the basis of the atmosphere is input a photon flux which comes indirectly from the thermonuclear reactions in the star's core. This photon flux interacts with the matter present in the atmosphere which modifies its energy spectrum. The total energy must be conserved or, to put it differently, there must be no creation or destruction of energy within the atmosphere itself. An example of a situation when this requirement is not met is if in the atmosphere takes place the decay of some radioactive species, the energy liberated in this process is in excess of that input at the basis of the atmosphere.

Before proceeding further in this discussion let us introduce some quantities apt to describe the radiation field

$$I_\nu = \frac{dE}{dS\cos\theta d\omega d\nu dt} = \text{specific intensity} \tag{5.1}$$

it is the energy which crosses the surface element dS, carried by photons of frequency between ν and $\nu + d\nu$ moving in solid angle $d\omega$ in time dt . θ is the angle between the direction of propagation of photons and the normal to the surface dS.

Specific intensity is simply linked to the distribution function for photons, which is the number of photons with energy between $h\nu$ and $h\nu + hd\nu$ moving in directions comprised in the solid angle $d\omega$

$$I_\nu = ch\nu f_\nu \tag{5.2}$$

Other quantities of interest are: the energy flux, simply called flux, which is a vector quantity

$$\vec{F} = \oint I_\nu \vec{n} d\omega \tag{5.3}$$

where $\vec{n}$ is the direction of propagation of the photons.

The radiation pressure tensor is a second order tensor defined as

$$\mathbf{P} = \frac{1}{c} \oint I_\nu \vec{n}\vec{n} d\omega \tag{5.4}$$

or in component form

$$P_{ij} = \frac{1}{c} \oint I_\nu n_i n_j d\omega \tag{5.5}$$

Notice that, since $I_\nu = ch\nu f_\nu$

$$P_{ij} = \frac{1}{c} \oint ch\nu f_\nu n_i n_j d\omega = \oint (cn_i f_\nu)(\frac{h\nu}{c} n_j) d\omega \tag{5.6}$$

It is then obvious to interpret P_{ij} as the momentum carried by photons ($= h\nu n_j/c$) in the direction n_j going through a surface normal to n_i at time dt. The physical meaning of the flux is very straightforward. Not so the radiation pressure tensor. Let us investigate its properties in order to gain some physical insight on its significance. There is an obvious relation between $\mathbf{P}$ and the volume forces exerted by the radiation field. The force $\vec{\mathcal{F}}$ acting on a closed surface $\mathcal{S}$, due to radiation is

$$\vec{\mathcal{F}} = -\oint_{\mathcal{S}} \mathbf{P} \cdot d\vec{\mathcal{S}} = -\int_{\mathcal{V}} \mathrm{div}\mathbf{P} d\mathcal{V} \tag{5.7}$$

the second equality is guaranteed by the divergence theorem. The minus sign is due to the fact that we defined $\mathbf{P}$ in such a way that $\vec{n}$ is the outward normal to the surface, so that $\oint_{\mathcal{S}} \mathbf{P} \cdot d\vec{\mathcal{S}}$ gives the decrease of momentum enclosed by surface $\mathcal{S}$. If we denote by $\vec{G}$ the momentum we have

$$\oint_{\mathcal{S}} \mathbf{P} \cdot d\vec{\mathcal{S}} = -\frac{d\vec{G}}{dt} \tag{5.8}$$

For an electromagnetic field the conservation of momentum may be written as

$$\frac{d\vec{G}}{dt} = \frac{d\vec{G}_{mec}}{dt} + \frac{d\vec{G}_{e.m.}}{dt} = \int_{\mathcal{V}} \mathrm{div}\mathbf{T} d\mathcal{V} \tag{5.9}$$

where $G_{mec}$is the mechanical momentum and

$G_{e.m.}$ = electromagnetic momentum

$$G_{e.m.} = \int_{\mathcal{V}} \vec{g} d\mathcal{V} \tag{5.10}$$

where $\vec{g} = \frac{\epsilon\mu}{c^2}\vec{S}$ and $\vec{S}$ is the Poynting vector and

$$\mathbf{T} = \frac{1}{4\pi}(\epsilon(\vec{E}\vec{E} - \frac{1}{2}(\vec{E}\cdot\vec{E})\delta) + \mu(\vec{H}\vec{H} - \frac{1}{2}(\vec{H}\cdot\vec{H})\delta) \tag{5.11}$$

$\mathbf{T}$ is the Maxwell stress tensor and δ is the unit tensor (Kronecker's δ). For an electromagnetic field in the absence of matter $G_{mec} = 0$

$$\Rightarrow \vec{\mathcal{F}} = \frac{d\vec{G}_{e.m.}}{dt} = \int_{\mathcal{V}} \mathrm{div}\mathbf{T} d\mathcal{V} \tag{5.12}$$

from which follows $\mathbf{T} = -\mathbf{P}$. Hence the radiation pressure tensor is just the Maxwell stress tensor, apart from the sign. Other quantities which we are interested in are:

$$J_\nu = \frac{1}{4\pi}\oint I_\nu d\omega = \text{mean intensity} \tag{5.13}$$

extinction coefficient or opacity, which is the energy fraction removed from the elementary photon beam of frequency between ν and $\nu + d\nu$ which propagates in solid angle $d\omega$

$$\mathrm{k}_\nu = \frac{dE^-}{I_\nu dS dx d\omega d\nu dt} \tag{5.14}$$

it is measured in cm^{-1}.

Emissivity, defined as the fraction of energy added to the elementary photon beam of frequency between ν and $\nu + d\nu$, which propagates in solid angle $d\omega$

$$j_\nu = \frac{dE^+}{dS dx d\omega d\nu dt} \tag{5.15}$$

The source function, defined as

$$S_\nu = \frac{j_\nu}{\mathrm{k}_\nu} \tag{5.16}$$

For a black body at temperature T

$$S_\nu = B_\nu = \frac{2\pi h}{c^2}\nu^3(e^{(\frac{h\nu}{kT})} - 1)^{-1} \tag{5.17}$$

B_ν is the Planck function. In the following discussion we shall make no distinction between true absorption and emission and scattering.

The energy transfer is described by a Boltzmann equation, which is usually called the transfer equation. It is usually written in terms of specific intensity, rather than photon distribution function. However for clarity let us derive it unconventionally in terms of $f(\vec{r},\vec{k},t)$ = the number of wave packets in volume $\vec{r}$ to $\vec{r}+d\vec{r}$ with wavenumber between $\vec{k}$ and $\vec{k}+d\vec{k}$ at time t . The Boltzmann equation is

$$\frac{df}{dt} = I_{coll} = \text{the collision integral} \tag{5.18}$$

I_{coll} is, as usual (see chapter 1) the sum of two terms : In + Out

In increases the number of wavepackets in volume$d\vec{r}d\vec{k}$

Out decreases the number of wavepackets in volume $d\vec{r}d\vec{k}$

If we introduce two new quantities

$$\eta(\vec{r},\vec{k},t) = \text{number of wavepackets created in volume } d\vec{r}d\vec{k} \text{ at time } t$$

$$\chi(\vec{r},\vec{k},t) = \text{number of wavepackets destroyed in volume } d\vec{r}d\vec{k} \text{ at time } t$$

With the aid of these new quantities the collision integral may be expressed as:

$$I_{coll} = \eta - f\chi \tag{5.19}$$

Let us expand the total derivative

$$\frac{df}{dt} = \frac{\partial f}{\partial \vec{r}}\frac{d\vec{r}}{dt} + \frac{\partial f}{\partial \vec{k}}\frac{d\vec{k}}{dt} + \frac{\partial f}{\partial t} \tag{5.20}$$

Now, for photons $\frac{d\vec{r}}{dt} = v_g$, the group velocity, in vacuum this coincides with the phase velocity $c\vec{n}$. Moreover $\vec{k} = \frac{\omega}{c}\vec{n} = \frac{2\pi\nu}{c}\vec{n} = \frac{1}{\hbar}\vec{p}$ where $\vec{p}$ is the photon momentum.

$$\Rightarrow \frac{d\vec{k}}{dt} = \frac{1}{\hbar}\frac{d\vec{p}}{dt} = \frac{1}{\hbar}\vec{F} \tag{5.21}$$

where $\vec{F}$ represents the forces acting on the photons. In the absence of general relativistic effects, which is always the case in the atmospheres of normal stars, we can safely put $\vec{F} = 0$, hence the Boltzmann equation becomes simply:

$$\frac{df}{dt} = \frac{\partial f}{\partial \vec{r}} \cdot \vec{n}c + \frac{\partial f}{\partial t} = I_{coll} = \eta - \chi f \tag{5.22}$$

Let us rewrite it using specific intensity (remember that $I_\nu = ch\nu f_\nu$) and multiply by $ch\nu$ the whole equation

$$c\vec{\nabla} I_\nu \cdot \vec{n} + \frac{\partial I_\nu}{\partial t} = \eta ch\nu - \chi I_\nu \tag{5.23}$$

it is easy to see that the previously defined j_ν and k_ν are related to η and χ through the following relations:

$$j_\nu = \eta h\nu$$

$$\mathrm{k}_\nu = \frac{\chi}{c}$$

hence the transfer equation takes up the more familiar form

$$\vec{\nabla} I_\nu \cdot \vec{n} + \frac{1}{c}\frac{\partial I_\nu}{\partial t} = j_\nu - \mathrm{k}_\nu I_\nu \tag{5.24}$$

A result which we shall use further on is obtained by taking the second moment of this equation: apply operator $\frac{1}{c}\oint \vec{n} d\omega$, recalling that

$$\frac{1}{c}\oint I_\nu \vec{n}\vec{n} d\omega = \mathbf{P}_\nu \tag{5.25}$$

and

$$\oint I_\nu \vec{n} d\omega = \vec{F} \tag{5.26}$$

one has

$$\frac{1}{c}\oint \vec{\nabla} I_\nu \cdot \vec{n}\vec{n} d\omega + \frac{1}{c^2}\oint \frac{\partial I_\nu}{\partial t}\vec{n} d\omega = \frac{1}{c}\oint (j_\nu - \mathrm{k}_\nu I_\nu)\vec{n} d\omega \tag{5.27}$$

if we invert the order of the operators $\vec{\nabla}$ and $\oint$ and $\frac{\partial}{\partial t}$ and $\oint$ we obtain

$$\vec{\nabla}\mathbf{P}_\nu + \frac{1}{c^2}\frac{\partial \vec{F}_\nu}{\partial t} = \frac{1}{c}\oint (j_\nu - \mathrm{k}_\nu I_\nu)\vec{n} d\omega \tag{5.28}$$

let us further apply operator $\int_0^\infty d\nu$ to this equation

$$\vec{\nabla}\mathbf{P} + \frac{1}{c^2}\frac{\partial \vec{F}}{\partial t} = \frac{1}{c}\int_0^\infty \oint (j_\nu - \mathrm{k}_\nu I_\nu)\vec{n} d\omega \tag{5.29}$$

if the medium is isotropic

$$\oint j_\nu \vec{n} d\omega = j_\nu \oint \vec{n} d\omega = 0 \tag{5.30}$$

$$\oint \mathrm{k}_\nu I_\nu \vec{n} d\omega = \mathrm{k}_\nu \oint I_\nu \vec{n} d\omega = \mathrm{k}_\nu \vec{F}_\nu \tag{5.31}$$

hence our equation becomes

$$\vec{\nabla}\mathbf{P} + \frac{1}{c^2}\frac{\partial \vec{F}}{\partial t} = -\frac{1}{c}\int_0^\infty \mathrm{k}_\nu \vec{F}_\nu d\nu \tag{5.32}$$

let us examine the case of a plane parallel layer atmosphere, then tensor $\mathbf{P}$ is diagonal and takes up the simple form

$$\mathbf{P} = \begin{pmatrix} -p_r & 0 & 0 \\ 0 & 1 & 0 \\ 0 & 0 & 1 \end{pmatrix} \tag{5.33}$$

in a coordinate system such that x is orthogonal to the layers and positive outwards. p_r is a scalar called radiation pressure. $\vec{F}$ has a single non-vanishing component, the x component which is $F_\nu = \oint I_\nu \cos\theta d\omega$, replace operator $\vec{\nabla}$ by $\frac{d}{dx}$ and the equation becomes

$$\frac{dp_r}{dx} = \frac{1}{c}\int_0^\infty \mathrm{k}_\nu F_\nu d\nu \tag{5.34}$$

we shall need this equation later.

What is observed trough the spectrograph is $\phi_\nu = \frac{R^2 F_\nu}{d^2} \alpha_\nu$ where R is the star radius, d is the distance to the star and α_ν is the transparency of the earth's atmosphere. If we are using high resolution spectroscopy, over small spectral ranges so that $\alpha_\nu \approx$ constant (except for strong telluric in absorption or geocoronal lines in emission, which must be taken into account explicitly), we may remove this effect through normalisation (see chapter 4); so, in practice, what we observe is something which is proportional to F_ν (we are assuming that we are capable of removing the instrumental signature by an appropriate calibration procedure).

Now the problem of spectral synthesis may be stated as follows: produce a model whose output is a theoretical spectrum ${}^tF_\nu$ which may be compared with the observed ${}^oF_\nu$. As will become clear in the following discussion it is necessary to split the calculation into two steps:

1) Build a model atmosphere

2) Compute a synthetic spectrum for a given model atmosphere.

Building a model atmosphere

In what follows we shall always assume that the atmosphere is composed by plane parellel layers. A further assumption which shall considerably simplify our task is to assume that each layer is a quasi-isolated subsystem of an isolated system. Under this hypothesis each layer may be treated separately and it may be ascribed thermodynamic quantities such as $\mathrm{T}, \mathrm{P}, \mathrm{N_e}$ ..... etc. If we further assume that each layer is in thermodynamic equilibrium occupation numbers will be given Boltzmann's law and ionization stages by Saha's law. This hypothesis is called Local Thermodynamic Equilibrium (LTE). Much emphasis is often put in favor of the so-called NON-LTE calculations, where the Boltzmann law is not used, but statistical equilibrium equations are solved directly. I should like to

make a few comments about such models:

- Although not in thermodynamic equilibrium they are ususally assumed to be not too far from equilibrium, in fact occupation numbers are expressed as $n_j = n_j^* b_j$ where n_j^* is the Boltzmann occupation number and b_j is a deviation factor, close to 1

- They remain strictly local, that is that the occupation number at a given depth depends on the radiation field at that depth, whereas the problem is intrinsically non-local

- Experience has shown that LTE is a good approximation for continuum and for most lines. Other lines may be "treated in NON-LTE", as is often said in the literature. What this really means is that for the line under study the equations of statistical equilibrium are solved throughout the atmosphere, thus yielding the appropriate b factors at each depth.

From these comments follows that such models ought to be called QUASI-LTE, rather than NON-LTE. The most severe limitation is the assumed local-ness. In what follows we shall assume an LTE framework, although much of what will be said applies to NON-LTE calculations as well.

The problem of building a model atmosphere may be stated as follows: construct a table which contains thermodynamic quantities of interest for each layer. The layer must be identified by some convenient independent variable. Candidates for the independent variable to use are: geometrical depth x, optical depth $\tau_\nu = \int -\mathrm{k}_\nu dx$, column mass density $m = \int \rho dx$. The geometrical depth is the least convenient, since it has little relation to the radiation field and certain quantities such as opacity or emissivity may have abrupt changes, thus generating numerical instability. Optical depth has great physical significance, but also the complication that it is frequency dependent, optical depth at some fixed frequency (e.g. τ_{5000}) or some kind of mean optical depth (e.g. $\tau_{Rosseland}$) are sometimes used, however they may suffer the same limitations of geometrical

depth, being simply proportional ($d\tau_{Ross} = -\mathrm{k}_{Ross}dx$). The Kurucz models (as usual by this I mean any model computed by some version of ATLAS) use the column mass density m as an indipendent variable, this has the advantage that we may use the mass absorption and emission coefficients, rather than opacity and emissivity, thus removing the rapid variation caused by the change in number densities as we pass through the atmosphere (Kurucz,1970). In the case of plane parallel layers the transfer equation reads:

$$\cos\theta\frac{dI_\nu}{dx} = j_\nu - \mathrm{k}_\nu I_\nu = \mathrm{k}_\nu(S_\nu - I_\nu) \tag{5.35}$$

if we introduce the mass absorption and emission coefficients through

$$h_\nu = \frac{j_\nu}{\rho} \quad ; \quad k_\nu = \frac{\mathrm{k}_\nu}{\rho} \tag{5.36}$$

the transfer equation becomes:

$$\cos\theta\frac{dI_\nu}{dm} = k_\nu(S_\nu - I_\nu) \tag{5.37}$$

we shall assume that the atmosphere is static, i.e. there are no mass motions on macroscopic scale. Staticity implies that the equation of hydrostatic equilibrium must be satisfied

$$\vec{\nabla}p = \rho\vec{g} \tag{5.38}$$

Other effects such as that of temperature gradient or chemical potential gradient could, in principle, be included, but these effects are always small in a stellar atmosphere. We shall now use equation (5.34) that we derived previously. For plane parallel layers the above equation becomes

$$\frac{dp}{dx} = \rho g \tag{5.39}$$

since $p = p_g + p_r$ where p_g is the gas pressure and p_r is the radiation pressure we may write

$$\frac{dp_g}{dx} + \frac{dp_r}{dx} = \rho g \tag{5.40}$$

and, in light of (5.34)

$$\frac{dp_g}{dx} + \frac{1}{c}\int_0^\infty \mathrm{k}_\nu F_\nu d\nu = \rho g \tag{5.41}$$

or, passing to column mass density and rearranging the terms we find

$$\frac{dp_g}{dm} = g - \frac{1}{c}\int_0^\infty k_\nu F_\nu d\nu \tag{5.42}$$

which is identical to formula (7-8) of Mihalas (1974), which has been derived in a different way.

We shall further assume that the atmosphere is in radiative equilibrium, which means that the energy absorbed is exactly balanced by that emitted in the atmosphere. This not only assumes that there is no production or dissipation of energy within the atmosphere, but also that there is no energy exchange between radiative and non-radiative modes (such as acoustic waves, shocks, convective zones...). This condition is met by stars of effective temperature greater than, about 8500 K. Mathematically speaking the condition that there is no creation or destruction of radiative energy may be expressed by the requirement

$$\oint\int_0^\infty (j_\nu - \mathrm{k}_\nu I_\nu) d\nu d\omega = 0 \tag{5.43}$$

To gain further physical insight in the significance of this equation let us take the first moment of the transfer equation. Apply to the equation the operator $\oint d\omega$

$$\oint \vec{\nabla} I_\nu \cdot \vec{n} d\omega + \frac{1}{c}\oint \frac{\partial I_\nu}{\partial t} d\omega = \oint (j_\nu - \mathrm{k}_\nu I_\nu) d\omega \tag{5.44}$$

let us invert, as usual the order of operators $\oint$ and $\vec{\nabla}$ and $\oint$ and $\frac{\partial}{\partial t}$ and recall that $\oint I_\nu \vec{n} d\omega = \vec{F}_\nu$ and $\oint I_\nu d\omega = 4\pi J_\nu$, the equation becomes

$$\vec{\nabla} \cdot \vec{F} + \frac{4\pi}{c}\frac{\partial J_\nu}{\partial t} = \oint (j_\nu - \mathrm{k}_\nu I_\nu) d\omega \tag{5.45}$$

We want to better understand the second term on the left-hand side

$$J_\nu = \frac{1}{4\pi}\oint ch\nu f_\nu d\omega = \frac{c}{4\pi}\oint h\nu d\omega = \frac{c}{4\pi} E_r(\nu) \tag{5.46}$$

E_r is simply the energy transported by the photons. Hence the equation may be written in the illuminating form

$$\vec{\nabla} \cdot \vec{F}_\nu + \frac{\partial E_r(\nu)}{\partial t} = \oint (j_\nu - \mathrm{k}_\nu I_\nu) d\omega \tag{5.47}$$

let us apply the operator $\int_0^\infty d\nu$ to this equation, and, as usual, invert the order of operators $\vec{\nabla}$ and $\frac{\partial}{\partial t}$, we obtain

$$\mathrm{div}\vec{F} + \frac{\partial E_r}{\partial t} = \int_0^\infty \oint (j_\nu - \mathrm{k}_\nu I_\nu) d\omega d\nu \tag{5.48}$$

in radiative equilibrium the right hand side vanishes and one is left with

$$\mathrm{div}\vec{F} + \frac{\partial E_r}{\partial t} = 0 \tag{5.49}$$

which is the usual continuity equation for an incompressible fluid, moreover, since the atmosphere is static the term with $\frac{\partial}{\partial t}$ vanishes identically, hence the condition of radiative equilibrium is equivalent to

$$\mathrm{div}\vec{F} = 0 \tag{5.50}$$

i.e. the radiation field is solenoidal, like any other field without sinks or sources (e.g. magnetic induction $\vec{B}$).

We can now proceed to illustrate the strategy to build an LTE model atmosphere in radiative equilibrium. Since $\vec{F}$ is solenoidal, in a plane parallel atmosphere this implies that its only non-vanishing component is a constant F, this is related to effective temperature through

$$F = \sigma \mathrm{T}_e^4 \tag{5.51}$$

where σ is the Stefan-Boltzmann constant. Then the equation of hydrostatic equilibrium becomes

$$\frac{dp_g}{dm} = g - \frac{\sigma}{c}\overline{k}\mathrm{T}_e^4 \tag{5.52}$$

where $\overline{k}$ is some suitable mean opacity. This equation may be integrated to give the pressure structure of the stmosphere. The next step is to compute occupation numbers for each m. However to do this one needs to know, the density structure, the temperature structure and the electron pressure, to be used in Boltzmann's and Saha's laws. One starts off with an initial guess of the temperature structure T(m) and derives density from

$$N(m) = \frac{p_g(m)}{k\mathrm{T}(m)} \tag{5.53}$$

electron pressure may be derived by considering that $p_g = (N_N + N_e)k\mathrm{T}$, where N_N is the number of nuclei. Moreover $N_N = N_0 + N_1 + N_2 + ...$ where N_0 is the number of neutral atoms, N_1 is the number of singly ionized atoms, etc. For any chemical species Saha's law may be put in the form

$$\frac{N_1}{N_0} = \frac{\phi(\mathrm{T})}{p_e} \tag{5.54}$$

since

$$\frac{p_e}{p_g} = \frac{N_e}{(N_N + N_e)} = \frac{N_e}{N_0 + N_1 + N_2 + ...} \tag{5.55}$$

through repeated application of Saha's law each term in the denominator may be put in terms of N_0, p_e and ϕ(T) and since $N_e = \frac{p_e}{k\mathrm{T}}$ this equation, with the constraint $N_e - (N_1 + 2N_2 + 3N_3 + ...) = 0$ (charge conservation) gives an equation to be solved for p_e. Knowledge of $p_e(m)$ and $N(m)$ coupled with Saha's and Boltzmann's laws and atomic constants, allows the computation of $h_\nu(m)$ and $k_\nu(m)$. These must be computed for a mesh of values of ν. Continuum opacities have an almost everywhere smooth behaviour, moreover their slope with ν is gentle. This allows us to consider relatively few frequency points, without loosing information. However the matter is different if one takes into account also the line spectrum. The most straightforward way to deal with it would be to include enough frequency points in the calculation to describe all the profiles of the lines under consideration (the so-called "direct approach"). We

would be then tackling directly the problem of spectrum synthesis. However this is prohibitively expensive in terms of computer time, so that one has to solve the problem in some other way. The most widely used technique is that of the so-called "Opacity Distribution Functions" (hereafter ODF). These are constructed in the following fashion: consider a spectral band, narrow enough so that the exact position of the line does not matter. Find the fraction of the band which is covered by lines of opacity greater than or equal to some fixed value X_i, call this number f. If we plot X_i as a function of f the result will be a smooth function. Then, if we call W the bandwidth and ν_0 the lower frequency of the band we have, for any frequency ν in the band, $\nu = \nu_0 + Wf$. We may then replace the true mass absorption coefficient k_ν by a smooth function $Y(\nu) = X(\frac{\nu-\nu_0}{W})$. These ODF's must be pretabulated for a mesh of temperatures and densities, so that, when computing a model atmosphere, the needed opacities may be obtained by interpolating in the tables. Such a procedure is both quick and stable. This method is exploited by the ATLAS code (Kurucz, 1970 ; see also Castelli, 1988), which reads ODF's tabulated for different bandwidths and different metallicities.

Once the opacity (due both to lines and continua) is known, the transfer equation may be solved, in fact once the source function is known the radiation field may be determined at the expense of a quadrature. The next step is to check whether the constraint of radiative equilibrium is satisfied, if it isn't one must somehow correct the temperature distribution and iterate the whole procedure until radiative equilibrium is satisfied to some fixed accuracy. It must be emphasized that there is no guarantee that the model will converge, nor that it will converge to the correct solution. It must be stressed, in fact, what pointed out by Mihalas (1978), that *temperature correction methods tend to stabylize rather than converge*. In this respect the computation of a model atmosphere must be considered as a numerical experiment (Kurucz, 1970). Its success or failure must be checked *a posteriori* when comparing observed quantities with

those derived from the model.

The way of obtaining temperature corrections is, by no means unique or obvious. The reader is referred to the book of Mihalas (1978) for a discussion of these methods.

Computing the synthetic spectrum

Suppose that, somehow, we have a model atmosphere, which may be either the result of a converged computation, or else be an empirical model, such as the Vernazza *et al.* (1981). The model gives us T, P, N and other quantities of interest (such as b factors, if the model was computed in NON-LTE). We are then in the position to tackle spectrum synthesis, which is the heart of this chapter.

Clearly the synthetic spectrum may be computed for relatively small wavelength intervals, much smaller than the interval included in the model calculation. However, some computations may be carried out only once, even if we want to compute the spectrum for several wavelength intervals. This is the case of continuum opacity, which, owing to its smoothness may be computed for relatively few values of λ, however, care must be taken to evaluate the continuum opacity on both sides of any photoionization edge (Kurucz and Avrett, 1981). The bulk of the computation is the calculation of line opacities and source functions. This is straightforward ,in principle, $S_\nu = \frac{j_\nu}{k_\nu}$ and depends only on the atomic constants, occupation numbers and temperature. For example the SYNTHE code (Kurucz and Avrett, 1981), which will be used by us, computes the line absorption coefficient as

$$l_\nu = [\frac{\pi e^2}{mc}\frac{\mathrm{N}}{U}\frac{1}{\sqrt{\pi}\Delta\nu_D}][e^{-\frac{E}{k\mathrm{T}}}][H(a,v)][1-e^{-\frac{h\nu}{k\mathrm{T}}}] \qquad (5.56)$$

where N is the number density, U is the partition function, ρ is the mass density, g is the statistical weight of the lower energy level, f is the oscillator strength,

$\Delta\nu_D$ is the doppler width, E is the energy of the lower level and

$$H(a,v) = \frac{a}{\pi}\int_{-\infty}^{+\infty} \frac{e^{-y^2}}{(v-y)^2+a^3}dy \tag{5.57}$$

is the Voigt profile, with $v = \frac{\Delta\nu}{\Delta\nu_D}$ and $a = \frac{\Gamma_R+\Gamma_s+\Gamma_W}{4\pi\Delta\nu_D}$, where Γ_R is the radiative damping constant Γ_S is the stark damping constant and Γ_W is the Van der Waals damping constant.

This line opacity must be computed for each depth in the atmosphere. It may be used to compute the source function, together with the continuum opacity, in a later stage of the computation.

Once the source function is known one may obtain the surface flux or the surface intensity, for a mesh of angles, by direct quadrature

$$I_\nu(0,\mu) = \frac{1}{\mu}\int_0^\infty S_\nu(t)e^{-\frac{t}{\mu}}dt \tag{5.58}$$

$$F_\nu(0) = \frac{2}{\pi}\int_0^\infty S_\nu(t)E_2(t)dt \tag{5.59}$$

where we have put $\mu = \cos\theta$ and E_2 is the well known integro-exponential function of index 2.

$$E_n(x) = \int_1^\infty y^{-n}e^{-xy}dy \tag{5.60}$$

Thus, contrary to the construction of a model atmosphere, the computation of a synthetic spectrum is a straightforward and unambiguous process. However it necessitates an enormous amount of atomic data, which carry along their uncertainity. Furthermore its reliability rests, ultimately on the reliability of the input model atmosphere. In spite of its conceptual simplicity it is quite costly as regards to computer time and storage requirements. This is the reason why only in the late eighties spectrum synthesis began to be widely used.

Chapter 6

Temperature and gravity determinations for B type stars

In order to perform a model atmosphere analysis or to compute a synthetic spectrum it is necessary to fix somehow a model which best represents the stars being analyzed. The optimum criterium to be used is crucial. We must bear in mind that a star is a very complex object and the presently available models are such that often a single model is not capable of describing all the properities of the star. A model suitable to reproduce the visible spectrum may be inadequate to reproduce the UV spectrum or else a model which fits the continuum energy distribution may not be used to reproduce the line spectrum. The nature of the problem is twofold: on the one hand one may argue that this behaviour is due to shortcomings of the model, such as lack of atomic data, NLTE, etc. ... ,which is not refined enough to explain all the details of the observations. On the other hand one may claim that a model-atmosphere is not a two parameter problem: g and T_{eff} don't fix a unique model but other parameters such as abundances, stellar rotation, micro and macro turbulence, play an important role.

Having clarified this point we may state precisely the problem we are trying to solve: find the temperature and gravity of the Kurucz model which best reproduces the observed spectrum. By Kurucz model we mean any model from the grids of Kurucz (1979 and unpublished) or computed with ATLAS. We would like the same Kurucz model to reproduce both the UV and the visible spectrum, but this is an extra condition which may not always be satisfied. Two comments are in order here:

1) The choice of a Kurucz model is, to some extent, arbitrary, however NLTE effects should be unimportant for the temperature range we are interested in (Kundritzki, 1979). The Kurucz models are those with the most complete and accurate set of opacities known to us. By use of these models we cannot deal the effects of rotation, spots, inhomogenities, ... (see Castelli, 1988).

2) On the basis of numerical simulations made with ATLAS we assume that abundances affect the structure of the model only as a second order effect. This assumption allows us to look for a method of fixing T_{eff} and g whatever the abundances. The methods used in the literature to fix g and T_{eff} are almost as many as the paper published on model atmosphere analysis. (This is perhaps a little exaggerated, but not all the much). In the following paragraphs I shall attempt to give a quick survey of all the methods which I have come across with no claim of completness.

1) Methods using absolute flux

The basic assumption underlying these methods is that the model which best reproduces the continuum flux is also that which will best reproduce the observed spectrum.

The method has been applied to visible spectrum scans (e.g. Baschek and Sargent 1976), however since for B stars most of the flux is carried in the UV, some feel that a UV absolute flux, such as that provided by absolutely calibrated IUE low resolution spectra, is best suited for this purpous (see, e.g. Heber *et al.* 1986, Heber 1986, Heber *et al.* 1984). On the grounds that the some model ought to fit both the UV and the visible spectrum a fit of the continuum energy distribution (coming from IUE and ground base observations) has been used (e.g. Hack 1979, 1980).

The results of this method are usually satisfactory, the great drawback is the need of absolute flux measurements which often are not available, especially for faint stars.

2) Methods using broad band photometry

Any broad band photometric system (UVB, Geneva, Vilnius, VILGEN) allows the extraction of reddening free parameters which may be empirically related to temperature. The first and most widely used of such methods is

Johnson's Q method.

One defines the reddening free parameter

$$Q = (U - B) + S(B - V)$$

where S is a constant to be determinated empirically for each spectral type. Values of S are given by Heintze (1973). Q may be empirically linked by a linear relation to the reciprocal temperature $\theta_{eff} = \frac{5040}{T_{eff}}$ (Schild *et al.* , 1971)

$$\theta_{eff} = aQ + b$$

where $a = 0.377$, $b = 0.500$ for $Q \leq -0.1$ and $a = 0.625$, $b = 0.525$ for $Q > -0.1$

Johnson photometry is more easily available than absolute fluxes and this is an advantage of the method. The drawback is that an indipendent way must be sought to estimate the gravity g . One possible solution is to use Balmer line profiles (see further on).

3) Methods using narrow band photometry

There is no conceptual difference between narrow band and broad band photometry. Narrow band photometry is best suited to discriminate between spectral features which vary markedly across neighbouring spectral types. One such feature is the Balmer discontinuity for stars from A0 to B0.

The most widely used narrow band photometric system is Stromgren's uvby to which is almost universally associated Crawford's β index (Crawford, 1958). The most useful color indices which may be formed in the Stromgren system are

$(b - y)$ (analogous to Johnson's $(B - V)$)

$m_1 = (v - b) - (b - y)$ (gives a measure of metal line blanketing)

$c_1 = (U - V) - (V - b)$ (it is a measure of Balmer's discontinuity.)

A number of methods have been proposed based on the comparison between observed and computed colour indices. A computed colour index or, more appropriately, a synthetic colour index, is obtained by computing the emergent flux from a model atmosphere and convolving it with the filter profile. A grid of synthetic colours must be calibrated by requiring that observed and synthetic colours coincide for some standard star. Such a grid was computed by Relyea and Kurucz (1978) and calibrated on Vega. The same grid was recalibrated together with newly computed β indices, by Lester, Gray and Kurucz (1986) using 5 standard stars .

Synthetic beta indices where computed by Schmidt (1979). Moon and Dworetsky (1985) also applied corrections to the Relyea and Kurucz and Schmidt grids. The correction concerned the c_0 (dereddened c_1) and β index and were obtained by comparing the computed values with the observed values for stars of known temperature and gravity. The corrections were relative to stars in the temperature range 8500 $K \leq \mathrm{T}_{eff} \leq 20000$ K.

The grids may be used in several ways to estimate T_{eff} and g . Huenemoerder *et al.* (1986) used the Relyea and Kurucz grid to plot in the $(b-y)$, m_1 plane the curves of constant temperature and constant $\log g$. From the position of a star in this plane its T_{eff} and $\log g$ may be estimated (e.g. by graphic interpolation).

Conlon *et al.* (1989) used the reddening free parameters $[c_1]$ and $[u-b]$ to determine the temperature and Balmer line profiles to determine the gravity.

Castelli (1991) has thoroughly investigated the use of the c_0 and beta indices and the grids of Moon and Dworetsky (1985) and Lester *et al.* (1986) to determine T_{eff} and g . One possibility is to determine T_{eff} , directly from c_0. For any fixed gravity there is a tight relationship between c_0 and T_{eff} (cfr. fig.1 of Castelli, 1991). Having fixed the temperature g may be determined directly from β (see fig.4 of Castelli, 1991). The comparison made by Castelli leads to

the conclusion that the Moon and Dworetsky (1985) grid is more reliable than the Lester *et al.* (1986) grid, for B-type stars, she suggests that this is due to the fact that the zero point, B-type standard star η U Ma, used by Lester *et al.* (1986) has a high rotational velocity ($v \sin i = 205$ Km/s) and this may alter the emergent flux distribution causing anomalous colours for its temperature.

Another possibility is that exploited by the TEFFLOGG code of Moon (1985), namely to find $\log T_{eff}$ and $\log g$ as polynomials of c_0 and β, the polynomial coefficients are computed from a least square fit to the Moon and Dworetsky grid. Castelli (1991) recomputed the fitting polinomial for the MD grid and computed it also for the LGK grid.

The rationale behind the method is the following: let

$$\log g = f_1(c_0, \beta, \log T_{eff})$$

$$\log T_{eff} = f_2(c_0, \beta, \log g)$$

This is equivalent to saying that the locus of points $(\log g, \log T_{eff}, c_0, \beta)$ defined by the models is a two-dimensional affine topological variety embedded in $\Re^4$. Suppose next that this variety is differentiable then in the surronding of any point of the variety

$$\log g =$$

$$q_1 + \sum_{j=1}^{J} \lambda_j (\log T_{eff})^j + \sum_{k=1}^{K} \mu_k c_0^k + \sum_{l=1}^{L} \nu_l \beta^l + o((\log T_{eff})^{J+1}, c_0^{K+1}, \beta^{L+1}) \quad (6.1)$$

$$\log T_{eff} =$$

$$p_1 + \sum_{m=1}^{M} \rho_m (\log g)^m + \sum_{n=1}^{N} \sigma_n c_0^n + \sum_{r=1}^{R} \tau_r \beta^r + o((\log T_{eff})^{M+1}, c_0^{N+1}, \beta^{R+1}) \quad (6.2)$$

numbers J, K, L, M, N, R are, in principle, all different since the variety is in general steeper in certain directions than in others. Moon (1985) adopts $J = 1$; $K = L = 4$; $M = N = R = 2$. The values of λ, μ, ν, ρ, σ, τ are obtained by least square fits of these approximate formulas to sets points known

to be on the variety (i.e. points taken from the grid). Since these formulas are valid only locally it is natural that different parameters are found for different ranges in $\log T_{eff}$ and $\log g$.

Once the parameters are fixed these formulas may be used to find $\log g$ and T_{eff} for any pair of values (c_0, β) given, through a simple iteration scheme: guess a value of T_{eff} and use (6.1) to compute $\log g$, use the $\log g$ thus computed to compute an updated estimate of T_{eff} from (6.2). Iterate the procedure until $|\log T_{eff}^{n+1} - \log T_{eff}^{n}| < \epsilon$. I have seen no proof of the convergence of this method. For high temperatures ($20000 < T_{eff} < 30000$) the dependences of $\log g$ on $\log T_{eff}$ and of $\log T_{eff}$ on $\log g$ is so weak thet it may be neglected. Non iterative relations, similar to that linking θ_{eff} and Q may be used

$$\theta_{eff} = w_1 + w_2 a_0 + w_3 r + w_4 a_0^2 + w_5 r^2 \tag{6.3}$$

$$\log g = v_1 + v_2 a_0 + v_3 r + v_4 r^2 + v_5 r^3 \tag{6.4}$$

where a_0 and r are linear combinations of the indices $(b-y)$, m_0, c_0, and β (Stromgren 1966). This method, devised by Moon (1985) and extensively investigated by Castelli (1991) is very quick and powerful.

4) Methods using the line spectrum

It has already been mentioned that Balmer lines profiles are powerful gravity indicators (used by e.g. Conlon *et al.* 1989). If one has somehow fixed the temperature one may compute line profiles for different gravities until a match between the observed and computed spectrum is found. The main uncertainity is linked to the different theories used to compute the Balmer line broadening.

Another method which uses the line spectrum is that of ionization equilibria. If one is able to observe lines of an ion in two successive stages of ionization (e.g. SiII/SiIII) one may determine the temperature by forcing the two sets of lines to yield the same abundance. Instead if one observes lines of the neutral atom and

of an ion (e.g. TiI/TiII) (FeI/FeII), since the line strenghts of the neutral atom are insensitive to gravity, one may determine the gravity by forcing the two sets of lines to yield the same abundance. These ionization equilibria methods rest on the assumption that the line formation region is the same for both species.

Recently Singh and Castelli (1991) in an extreemly exciting paper have proposed a method for determining temperature of B stars from SiII lines of UV multiplet 13.04. These lines are caused by transitions between the $3s3p^2\,^2D$ and $3s3p(^3P^0)3d\,^2F^0$ levels. The lower ^2D term is composed of levels with J=3/2 and J=5/2; the $^2F^0$ upper term is composed of levels with J=5/2 and J=7/2. The J=7/2 level lies 80.7 cm^{-1} above the ionization limit of SiII (131838.4 cm^{-1} corresponding to 16.35 eV) whereas the J=5/2 level lies 161.0 cm^{-1} below this limit. Hence the upper level of the line at 130.5592 nm (J-J')=(5/2-7/2) should autoionize while the upper levels of the lines 130.9453 nm (J-J'=3/2-5/2) and 130.9725 (J-J'=5/2-5/2) should not. However the ionization energy depends on electron density in the plasma. Underhill (1981) showed that in the atmospheres of B-type stars the ionization limit is depressed so that both the levels with J=5/2 and J=7/2 of the upper term autoionize (Singh and Castelli, 1991).

This phenomenon provides the explanation of the broad features observed in the spectra of B-type stars at 130.5592 nm and 130.9 nm . Underhill (1981) pointed out that the intensity of these autoionization lines depends on temperature. Through a careful analysis Singh and Castelli (1991) demonstrated that the temperature may be determined (having fixed g e.g. though the β index) by adopting that of the model for which the computed profiles of SiII 13.04 multiplet best match the observed profiles. The crucial point is that the silicon abundance must be somehow fixed. Singh and Castelli have shown that the Si abundance may be conveniently determined using lines of SiIII, UV mult.4.

The Singh and Castelli method is very interesting because the temperature thus determined should be the most appropriate to describe the region where

the UV spectrum forms. The drawback is that it is necessary to posses good quality far UV spectra, which implies space- based observations.

BIBLIOGRAPHY

ABT H.A. and SNOWDEN M.A. - 1973 - Ap. J. Suppl. **25**, 137

BABU G.S.D. and SHYLAJA B.S. - 1981 - Astr.& Space Sci. **79**, 243

BASCHEK B. and SARGENT A.I. - 1976 - A.&A. **53**, 47

BERGER J. - 1963 - P.A.S.P. **75**, 393

BONIFACIO P. - 1989 - NORMA : *A program for the normalisation of spectra*, University of Trieste, Astronomy department, Internal Report 20 - IV - 1989

BONIFACIO P., CASTELLI F. and HACK M. - 1990 - Poster paper presented at I.A.U. Symp. 145 , p. 123

BOGGESS A. *et al.* - 1978a - NATURE **275**, 372

BOGGESS A. *et al.* - 1978b - NATURE **275**, 377

BOGGESS A. and WILSON R. - 1987 - in "Exploring the universe with the IUE Satellite "Y. KONDO ed. Kluver Academic Publishers, Dodrecht The Netherlands, p. 3

BROWN P.J.F., DUFTON P.L., KEENAN F.P., BOKSENBERG A., KING O.L. and PETTINI M. - 1989 - Ap. J.

BURBIDGE G.R. and BURBIDGE E.M. - 1955 - Ap. J. Suppl. **1**, 431

BURBIDGE G.R., BURBIDGE E.M. and FOWLER W.A. - 1958 - I.A.U. Symp. 6, p. 222

BUONANNO R., CALOI V.,CASTELLANI V.,CORSI C., FUSI PECCI F. and GRATTON R. - 1988 - A.& A. **102**, 25

CALOI V. - 1989 - A.& A. **221**, 27

CANNON R.D. - 1981 - I.A.U. Symp. 105, p. 123

CASSATELLA A., PONZ D. and SELVELLI P.L. - 1981 - NASA IUE Newsletter 14, 170

CASSATELLA A. , PONZ D. and SELVELLI P.L. - 1982 - ESA IUE Newsletter 15, 43

CASTELLI F. -1988 - " Kurucz's models, Kurucz's fluxes and the ATLAS code. Models and fluxes availables at O.A.T." Pub. O.A.T. 1164

CASTELLI F. - 1991 - to be published in A.& A.

CASTELLI F. and BONIFACIO P. - 1990 - A.& A. Suppl. Ser. **84**, 259

CASTELLI F. and SINGH J. - 1990 - Proc. Int. Symp. "Evolution in Astrophysics" - ESA SP-310, 261

CASTELLI F. and SINGH J. - 1991 - to be published in A.& A.

CONLON E.S., BROWN P.J.F., DUFTON P.L. and KEENAN F.P. - 1989 - A.& A. **224**, 65

COWLEY C. - 1979 - I.A.U. Coll. **47**, 375

COWLEY C.R., SEARS R.L., AIKMAN G.C.L. and SADAKANE K. - 1982- Ap.J:,**254**, 191

CRAWFORD D.L. - 1958 - Ap. J. **128**, 158

CROCKER D.A., ROOD R.T. and O'CONNELL R.W - 1988 - Ap. J. **322**, 236

DEUPREE R.G. and WALLACE R.K. - 1987 - Ap. J. **317**, 724

D'ODORICO S., GHIGO M. and PONZ D. - 1987 - ESO Sci. Rep. 6

DROBYSHEVSKY E.M. - 1985 - I.A.U. Coll. 90, p. 473

FARAGGIANA R. - 1987 - Astr. & Space Sci. **134**, 381

FEIGE J. -1958 - Ap. J. **128**, 267

FRASER R.D.P. and SUZUKI E. -1970 - in " Spectral anlysis methods and techniques" J.A. BLACKBURN ed., Marcel Dekker INC. New York

GLASPEY J.W., MICHAUD G., MOFFAT A.F.J. and DEMERS S. - 1989 - Ap. J. **339**, 926

GREENSTEIN J.L. - 1971 - I.A.U. Symp. 42, p. 46

GREENSTEIN J.L. - 1988 - I.A.U. Coll. 95

GREENSTEIN J.L. and SARGENT A.I. - 1974 - Ap. J. Suppl **28**, 157

GROOTE D., HUNGER K. and SCHULTZ G.V. - 1980 - A.&A. **83**, L5

GROOTE D. e KAUFMANN J.P. - 1981 - A.&A. **94**, L23

GROSS P.G. - 1973 - M.N.R.A.S. **164**, 65

GROTH H.G., KUDRITZKI R.P. and HEBER U. - 1985 - A.& A. **152**, 107

HACK M. - 1974 - Ap. J. **194**, L143

HACK M. - 1979 - A.&A. **74**, L4

HARDROP J. and SHORE S.S. - 1971 - P.A.S.P. **83**, 605

HARRIS A.W. and SONNEBORN G. - 1987 - in "Exploring the universe with the IUE satellite " Y. KONDO ed. Kluver Academic Publishers, Dodrecht The Netherlands

HAVNES O. - 1974 - A.&A. **32**, 161

HAVNES O. - 1975 - I.A.U. Coll. 32, p. 135

HAVNES O. - 1979 - A.&A. **75**, 197

HAVNES O. and CONTI P.S. - 1971 - A.&A. **14**, 1

HAYAKAWA S., MATSUMOTO T. and ONO T. - 1976 - I.A.U. Coll. 31, p. 323

HEBER U. - 1986 - A.& A. **155**, 33

HEBER U. - 1990 - I.A.U. Symp. 145,

HEBER U., HUNGER K., JONAS G., KUDRITZKI R.P. - 1984 - A. & A. **130**, 119

HEBER U., KUDRITZKI R.P., CALOI V., CASTELLANI V., DANZIGER J., GILMOZZI R. - 1986 - A.& A. **162**, 171

HENSENBERGE H. and VAN RENSENBERGEN - 1985 - I.A.U. Coll. 90, p. 151

HUENEMOERDER D.P., de BOER K.S. and CODE A.D. - 1984 - Astron. J. **89**, 851

IBEN I. Jr. - 1984 - Ap. J. **277**, 333

IBEN I. Jr., KALER J.B., TRURAN J.W. and RENZINI A. - 1983 - Ap. J. **264**, 605

JASCHEK C. e GOMEZ A.E. - 1970 - P.A.S.P. **82**, 809

JASCHEK M. and EGRET D. - 1982 - Catalogue of Stellar Groups Part 1 - Publ speciale du C.D.S. 4

JACKSON J.D. - 1975 - Classical Electrodynamics, John Wiley & Sons Inc. New York

KLOCHKOVA V.G. e KOPYLOV I.M. - 1985 - I.A.U. Coll. 90, p. 159

KUDRITZKI R.P. - 1979 - 22 Liége International Astrophys. Symp. p. 117

KURUCZ R.L. - 1970 - S.A.O. Spec. Rep. 309

KURUCZ R.L. - 1979 - Ap. J. Suppl. **40**, 1

KURUCZ R.L. and AVRETT E.H. - 1981 - S.A.O. Spec. Report 391

LUYTEN W.J. - 1959 - Pub. Un. Minn. Obs. ,A Search for faint blue stars XVII

LESTER J.B.,GRAY R.O, and KURUCZ R.L. - 1986 - Ap. J. Suppl. **61**, 509

Mc GRAW J.T., STARRFIELD S., GILBERT J. and GREEN R.F. - 1989 - I.A.U. Coll. 53, p. 377

MICHAUD G. - 1970 - Ap.J. **160**, 641

MIHALAS D. - 1978 - Stellar Atmospheres, Freeman & Co.

MOON T.T. - 1985 - "Stellar parameters from Stromgren photometry" Comm. from University of London Observatory 78

MOON T.T. and DWORETSKY M.M. - 1985 - M.N.R.A.S. **217**, 305

MOROSSI C., RAMELLA M., HACK M. and CASTELLI F. - 1981 - in 23 Liége International Astrophys. Symp.

MORTON D.C. - 1978 - Ap. J. **222**, 863

MORTON D.C., YORK D.G., JENKINS E.B. - 1988 - Ap. J. Suppl. **68**, 449

MORTON D.C. and SMITH Wm. H. - 1973 - Ap. J. Suppl. **26**, 333

MUKAI T. - 1977 - A.&A. **61**, 69

NEWELL - 1973 - Ap. J. Suppl. **26**, 37

NORTH P. - 1985 - I.A.U. Coll. 90, p. 321

OETKEN L. - 1985 - I.A.U. Coll. 90, p. 355

POPPER D. - 1980 - A.&A. Ann. Rev. **18**, 115

QUIN D.A., BROWN P.J.F., CONLON E.S., DUFTON P.L. and KEENAN F.P. - 1991 - Ap. J. **375**, 342

RELYEA L.J. and KURUCZ R.L. - 1978 - Ap. J. Suppl. **37**, 45

RIDDIFORD L. and BUTLER S.T. - 1952 - Phil. Mag. **43**, 447

ROOD R.T. - 1973 - Ap. J. **184**, 815

SANDAGE A. - 1988 - I.A.U. Coll. 95

SARGENT W.L.W. - 1967 - Ap. J. **148**, L147

SARGENT W.L.W. and SEARLE L. - 1967 - Ap. J. **150**, L33

SCHMIDT E.G. - 1979 - Astron. J. **84**, 1193

SHALLIS M.J., BARUCH J.E.F., BOOTH A.J. and SELBY M.J. - 1985 - M.N.R.A.S. **213**, 307

SLETTEBAK A. - 1954 - Ap. J. **119**, 146

SLETTEBAK A. - 1955 - Ap. J. **121**, 653

SPITE M. and SPITE F. - 1980 - A.& A. **89**, 118

STROMGREN B. - 1966 - A.& A. Ann. Rev. **4**, 433

SWANN W.F.G. - 1933 - Phys. Rev. 43,447

VAUCLAIR G. - 1976 - A.&A., **50**, 435

UESUGI A. and FUKUDA I. - 1970 - Contr. Inst. Ap. Kwasan Obs. Univ. Kyoto No 189

UNDERHILL A.B. - 1981 - A. &A. **97**, L11

UPSON W.L. and ROGERSON J.B. - 1980 - Ap. J. Suppl **42**, 175

VERNAZZA T.E., AVRETT E.H. and LOESER H. - 1981 - Ap. J. Suppl. **45**, 619

WERNER K., HEBER U. and HUNGER K. - 1990 - 7 European White Dwarf Workshop

Appendix A

In this appendix I present the observations made by me at OHP in January 1990, plus one image kindly taken at my request by D. Mangiacapra in May 1990. The images were reduced by me at the Astronomical Observatory of Trieste using MIDAS to implement the procedures outlined in chapter 4. Unfortunately these images may only be used for a qualitative study and line identifications. In fact the dark exposures taken before and after the observations may not be used to reliably calibrate the spectra, since there is a thermic drift of one or two °C starting from each replenishing of the nitrogen bottle.

I made some tests to asses how much did this uncertainity affects the measurement of the equivalent widths. The result is that for a faint star such as F86 a difference of 50 counts in the level of the dark results in a difference of 1.0 – 1.5 pm in the measured equivalent widths.

The observed spectra are compared with computed spectra. The spectra have been computed using the model atmosphere reported in Table 1. The phosporous abundance is that published by Baschek and Sargent (1976), for other elements I assumed the abundances determined by us from the UV spectra. Computed spectra have been convolved with a gaussian instrumental profile corresponding to a resolution of 50000 for the red spectra and 12000 for the blue spectra, this takes into account both instrumental profile and microturbulence. Since F86 is a slow rotator and the actual resolution of the spectra never exceeds 20000 I decided not to further convolve the computed spectra with a rotational profile which would be not influent. To match observed wavelengths to laboratory wavelengths of identified lines it was necessary to give a shift of +52.44 km/s for the images taken in January 1990 and +9 km/s for the image taken by D. Mangiacapra in May 1990. On the leftmost side of each plot there is a label which identifies the image which is being plotted. Labels are also appended on top of each computed line of predicted residual intensity greater or equal to 0.1 ;

the exact wavelength is stated and the ion which gives rise to the line (e.g. 15.01 is PII). Looking at the spectra one may note that all the PII lines are correctly identified, however computed lines are systematically deeper than observed lines. Possible causes of this discrepancy may be:

(1.) A wrong $\log gf$ assumed in the computations

(2.) A systematic error in the intensity calibration of the spectra

In the near future I hope we shall be able to decide which is the main cause of the discrepancy.

Although these spectra should not be used for quantitative analysis I measured the equivalent widths of all the measurable lines. Then I plotted my measurements (CB) against those of Sargent and Searle (1967; SS) and of Baschek and Sargent (1976; BS) for the lines we had in common, as well as the BS against the SS. As can be seen from the plots reported in this appendix the differences are not dramatic, in particular there is good agreement with the Sargent and Searle data, whereas my EW's are systematically smaller than those of Baschek and Sargent; however this is true also for the Sargent and Searle EW's. From these plots one could argue that the uncertainity in the calibration affects the EW's by no more than 10%.

Observation's log

IMAGE IDENTIFIER	GRATING	ORDER	FILTER	λ_c (nm)	R (nominal)	t_{exp} (seconds)	DATE
J84	5	I	OG590	663.0	31000	5400	2/1/1990
J104	5	I	OG590	643.3	31000	4500	2/1/1990
J196	5	I	OG590	650.5	31000	11000	3/1/1990
J275	2	Blaze 5000	NONE	430.0	20000	3000	4/1/1990
M232*	2	Blaze 5000	NONE	451.0	20000	4868	9/5/1990

*This image has been kindly observed at our request by D. Mangiacapra.

Image quality parameters

IMAGE	estimated S/N	$\Delta\lambda$ (nm) measured from the width of lines in Th-Ar spectra
J84	30	0.035
J104	10	0.034
J196	40	0.029
J275	20	0.036
M232	10	0.032

Gratings of AURELIE

Grating number	Type	lines per mm		R reciprocal dispersion (Å/mm)
1	Holographic	3000	40000	2.5
2	Blaze 5000 Å	1200	20000	8
3	Blaze 5000 Å	600	8000	16.5
4	Blaze 6000 Å	300	4700	33
5	Red	1200	31000*	7
6	Echelle	79	96000	1.5

* If used in the first order. In the second order the resolution is 60000 and the reciprocal dispersion 2.6 Å/mm.Order separation is achieved through the use of filters.

TABLE 1

the model atmosphere used for the computation of the synthetic spectra in appendix A

```
SURFACE INTENSI 17 1.,.9,.8,.7,.6,.5,.4,.3,.25,.2,.15,.125,.1,.075,.05,.025,.01
ITERATIONS 1 PRINT 2 PUNCH 2
CORRECTION OFF
PRESSURE OFF
 CONVECTION OFF  1.00 TURBULENCE OFF  0.00  0.00  0.00  0.00
ABUNDANCE SCALE   1.000 ABUNDANCE CHANGE 1 0.900 2 0.100
ABUNDANCE CHANGE 15 -4.7
ABUNDANCE CHANGE 5 -10.24 6 -5.37 7 -4.65 14 -5.54 16 -5.44
TITLE FEIGE 86 VISIBLE
TEFF  17000. GRAVITY 4.000 LTE
READ DECK6 40 RHOX,T,P,XNE,ABROSS,ACCRAD,VTURB
  9.14804550E-05   10227.1 9.051E-01 3.037E+11 3.625E-01 1.108E+02 0.000E+00
  1.33128895E-04   10530.9 1.317E+00 4.296E+11 3.625E-01 1.032E+02 0.000E+00
  1.90725419E-04   10542.3 1.887E+00 6.142E+11 3.875E-01 1.189E+02 0.000E+00
  2.69595999E-04   10606.1 2.667E+00 8.627E+11 4.169E-01 1.340E+02 0.000E+00
  3.76822660E-04   10692.9 3.725E+00 1.195E+12 4.514E-01 1.477E+02 0.000E+00
  5.21358510E-04   10803.4 5.149E+00 1.635E+12 4.916E-01 1.596E+02 0.000E+00
  7.15195551E-04   10927.5 7.055E+00 2.215E+12 5.386E-01 1.702E+02 0.000E+00
  9.74087801E-04   11060.3 9.600E+00 2.977E+12 5.939E-01 1.805E+02 0.000E+00
  1.31810550E-03   11198.8 1.298E+01 3.974E+12 6.592E-01 1.913E+02 0.000E+00
  1.77118671E-03   11341.0 1.742E+01 5.268E+12 7.369E-01 2.041E+02 0.000E+00
  2.36360193E-03   11483.3 2.322E+01 6.934E+12 8.283E-01 2.179E+02 0.000E+00
  3.13386344E-03   11622.4 3.074E+01 9.072E+12 9.361E-01 2.341E+02 0.000E+00
  4.12900280E-03   11764.0 4.045E+01 1.179E+13 1.062E+00 2.524E+02 0.000E+00
  5.40788844E-03   11904.0 5.290E+01 1.524E+13 1.211E+00 2.747E+02 0.000E+00
  7.04764389E-03   12042.4 6.883E+01 1.960E+13 1.385E+00 3.020E+02 0.000E+00
  9.14798956E-03   12184.1 8.916E+01 2.509E+13 1.589E+00 3.344E+02 0.000E+00
  1.18397856E-02   12335.3 1.151E+02 3.199E+13 1.821E+00 3.717E+02 0.000E+00
  1.52911982E-02   12501.0 1.483E+02 4.066E+13 2.082E+00 4.134E+02 0.000E+00
  1.97333675E-02   12687.6 1.908E+02 5.155E+13 2.371E+00 4.614E+02 0.000E+00
  2.54519731E-02   12905.3 2.452E+02 6.515E+13 2.679E+00 5.142E+02 0.000E+00
  3.28952447E-02   13170.6 3.156E+02 8.224E+13 2.985E+00 5.670E+02 0.000E+00
  4.27567624E-02   13503.7 4.083E+02 1.039E+14 3.266E+00 6.157E+02 0.000E+00
  5.62564209E-02   13934.9 5.347E+02 1.323E+14 3.515E+00 6.580E+02 0.000E+00
  7.49000162E-02   14475.9 7.085E+02 1.695E+14 3.735E+00 6.967E+02 0.000E+00
  1.00991577E-01   15149.8 9.508E+02 2.192E+14 3.909E+00 7.264E+02 0.000E+00
  1.37945145E-01   15972.0 1.293E+03 2.858E+14 4.029E+00 7.418E+02 0.000E+00
  1.91027015E-01   16952.1 1.784E+03 3.754E+14 4.138E+00 7.537E+02 0.000E+00
  2.67611980E-01   18111.8 2.493E+03 4.944E+14 4.165E+00 7.455E+02 0.000E+00
  3.78601760E-01   19424.7 3.520E+03 6.534E+14 4.214E+00 7.392E+02 0.000E+00
  5.39399028E-01   20931.1 5.010E+03 8.644E+14 4.262E+00 7.292E+02 0.000E+00
  7.70052731E-01   22608.3 7.148E+03 1.143E+15 4.399E+00 7.322E+02 0.000E+00
  1.09921896E+00   24486.1 1.020E+04 1.506E+15 4.527E+00 7.293E+02 0.000E+00
  1.56679010E+00   26586.7 1.453E+04 1.976E+15 4.725E+00 7.404E+02 0.000E+00
  2.22145891E+00   28943.4 2.059E+04 2.572E+15 5.004E+00 7.662E+02 0.000E+00
  3.12384081E+00   31606.1 2.890E+04 3.308E+15 5.377E+00 8.026E+02 0.000E+00
  4.31794977E+00   34528.9 3.985E+04 4.183E+15 5.930E+00 8.575E+02 0.000E+00
  5.83550072E+00   37735.6 5.366E+04 5.183E+15 6.745E+00 9.418E+02 0.000E+00
  7.95605755E+00   41679.2 7.275E+04 6.456E+15 8.094E+00 1.054E+03 0.000E+00
  1.10907698E+01   46751.1 1.007E+05 8.095E+15 9.329E+00 1.093E+03 0.000E+00
  1.64336777E+01   53319.8 1.486E+05 1.054E+16 1.006E+01 9.716E+02 0.000E+00
PRADK 1.1389E+02
```

J275NOR.BIN
.0
.1
.2
.3
.4
.5
.6
.7
.8
.9
1.0
422.0
422.5
423.0
423.5
424.0
198 15.02 117835 694
522 15.01 107360 640
172 26.01 20830 554

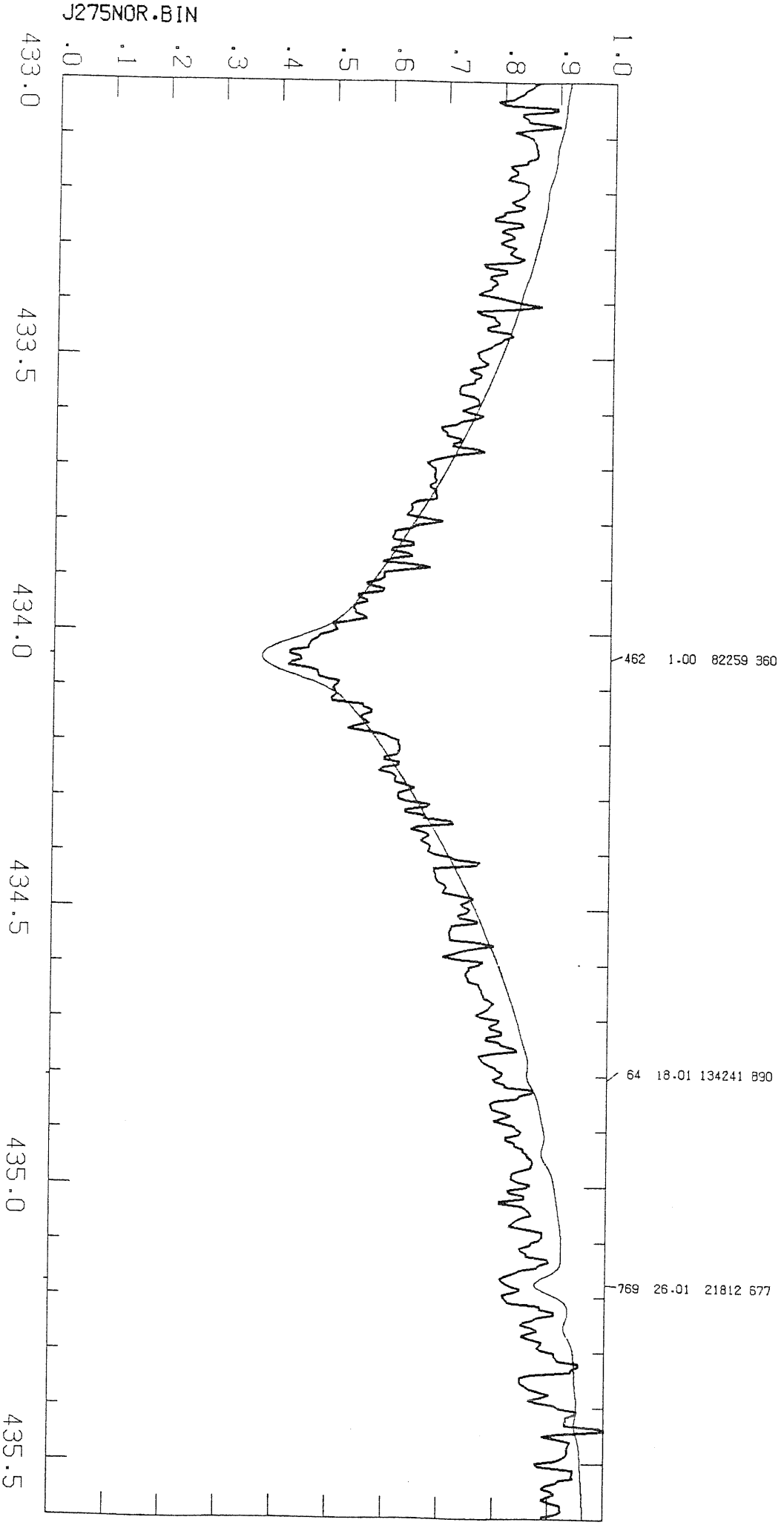
J275NOR.BIN
.0
.1
.2
.3
.4
.5
.6
.7
.8
.9
1.0
433.0
433.5
434.0
434.5
435.0
435.5
462 1.00 82259 360
64 18.01 134241 890
769 26.01 21812 677

.0
.1
.2
.3
.4
.5
.6
.7
.8
.9
1.0
438.0
438.5
439.0
439.5
440.0
440.5
637 12.01 80619 833
393 15.01 101635 747
387 26.01 22409 831
929 2.00 171135 614
572 12.01 80650 761
755 26.02 66591 862
104 15.01 105224 840

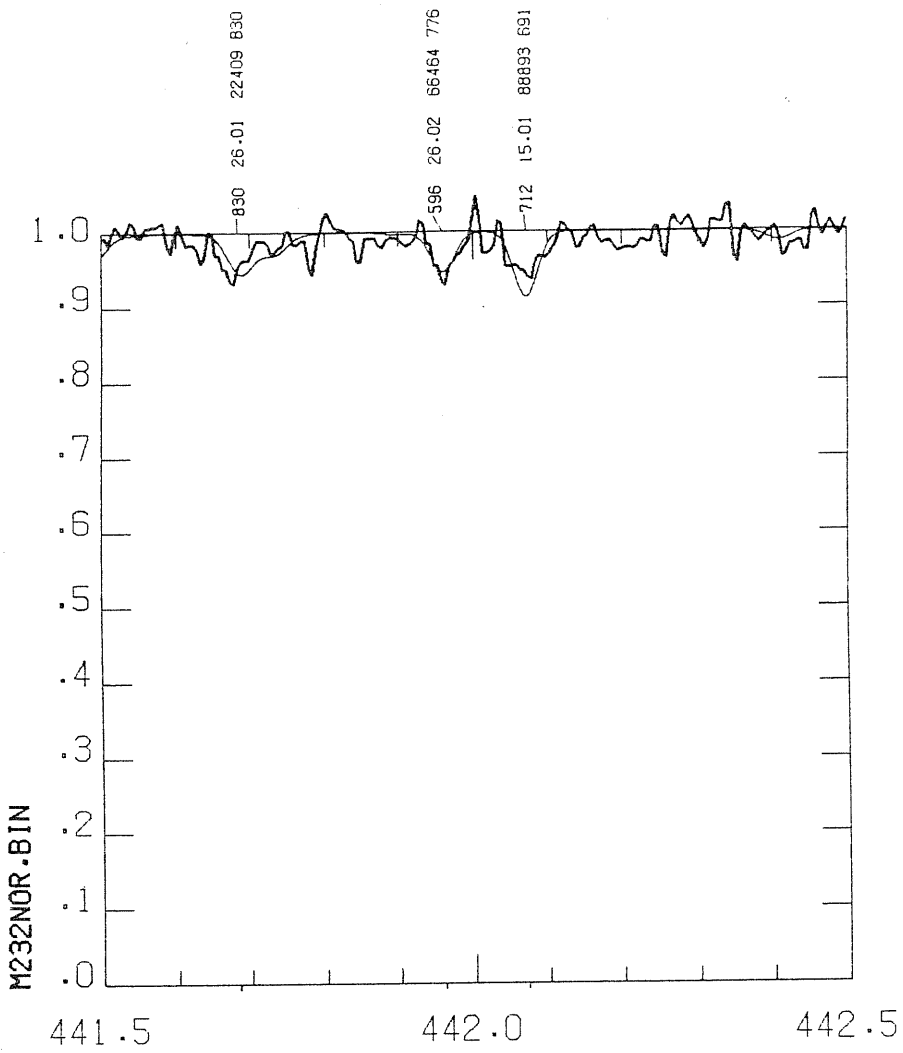
22409 830
26.01
830
66464 776
26.02
596
88893 691
15.01
712
1.0
.9
.8
.7
.6
.5
.4
.3
.2
.1
.0
M232NOR.BIN
441.5
442.0
442.5

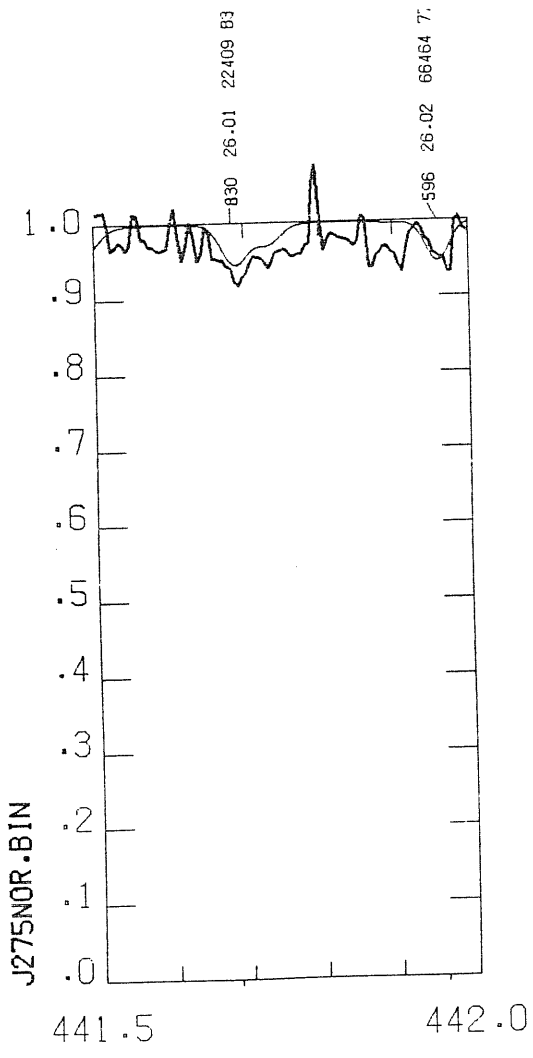
22409 83
26.01
830
66464 7
26.02
596
1.0
.9
.8
.7
.6
.5
.4
.3
.2
.1
.0
J275NOR.BIN
441.5
442.0

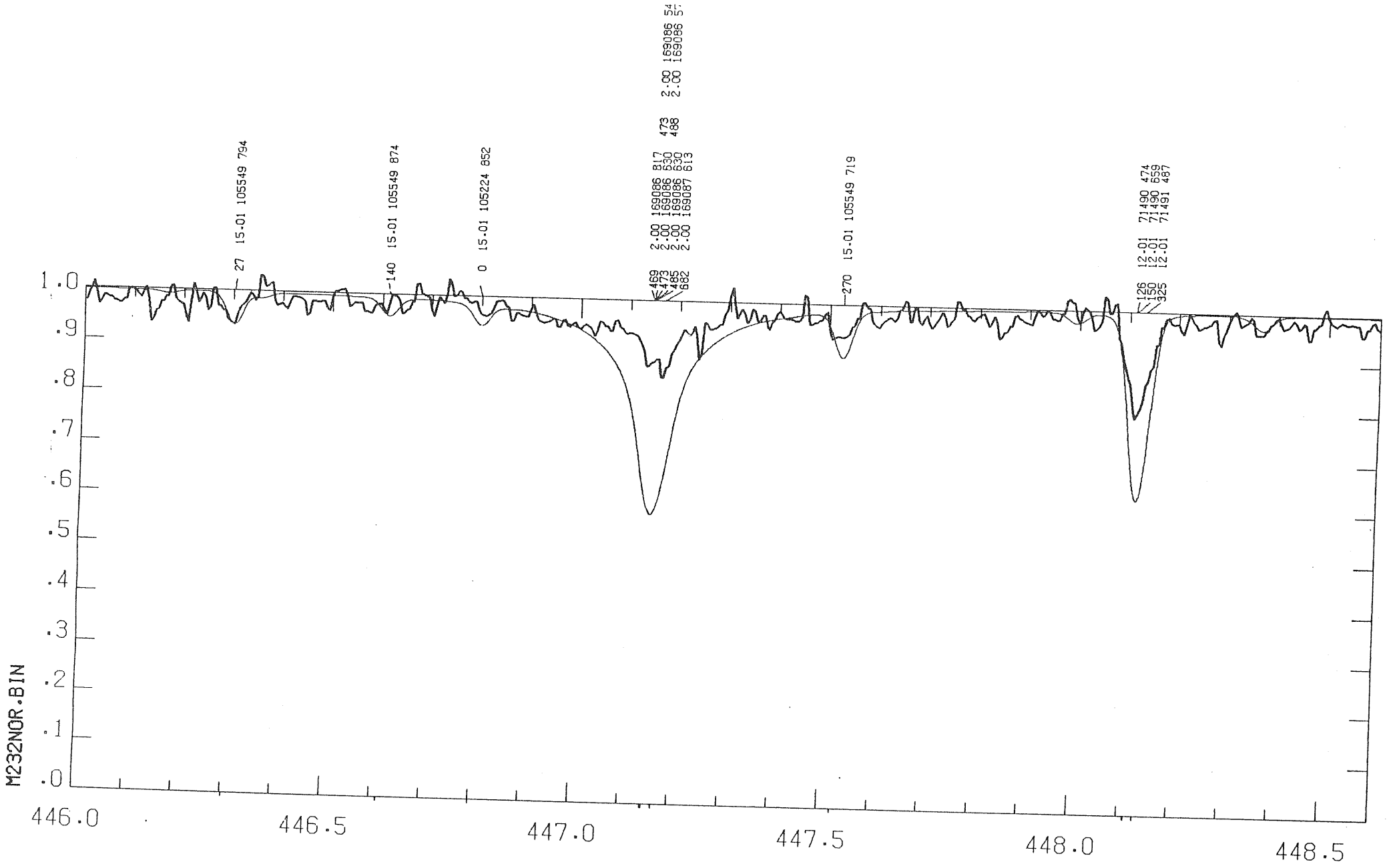
M232NOR.BIN
1.0
.9
.8
.7
.6
.5
.4
.3
.2
.1
.0
446.0
446.5
447.0
447.5
448.0
448.5
27 15-01 105549 794
140 15-01 105549 874
0 15-01 105224 852
2.00 169086 817
2.00 169086 530
2.00 169086 630
2.00 169087 613
469
473
485
682
2.00 169086 473
2.00 169086 488
270 15-01 105549 719
12-01 71490 474
12-01 71490 659
12-01 71491 487
126
150
325

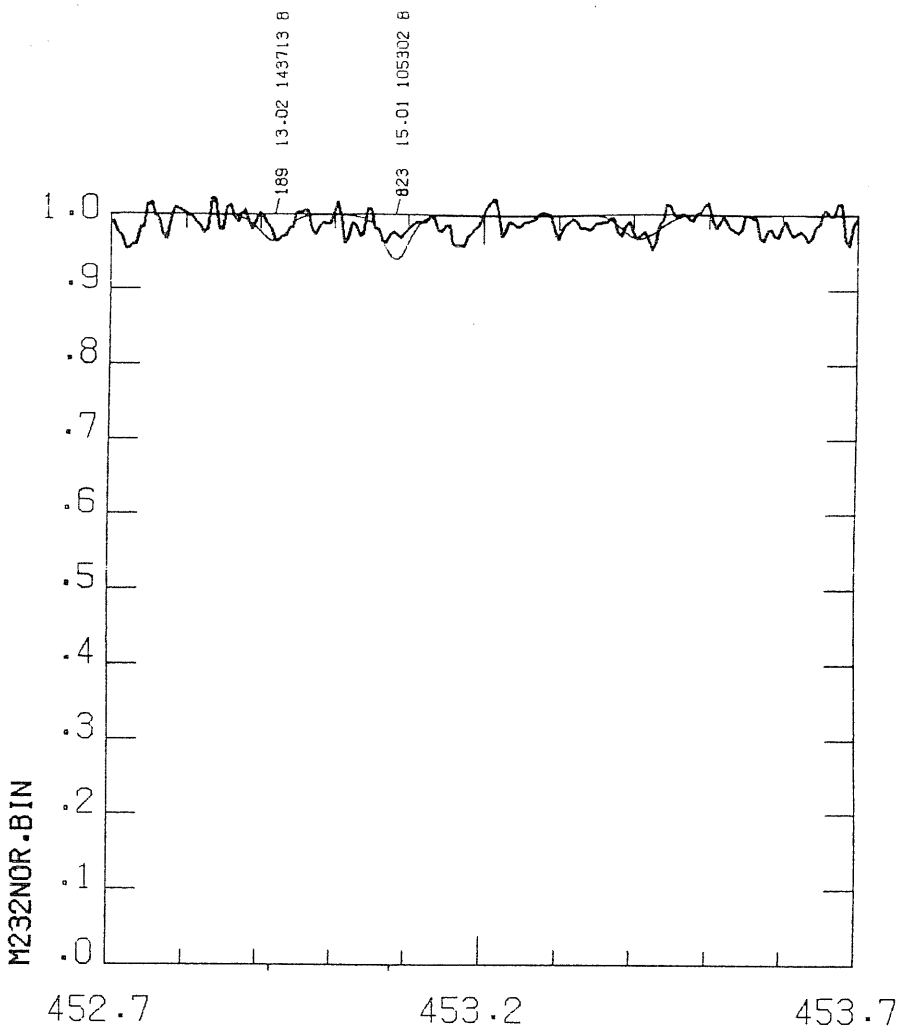
13.02 143713 8
189
15-01 105302 8
823
1.0
.9
.8
.7
.6
.5
.4
.3
.2
.1
.0
M232NOR.BIN
452.7
453.2
453.7

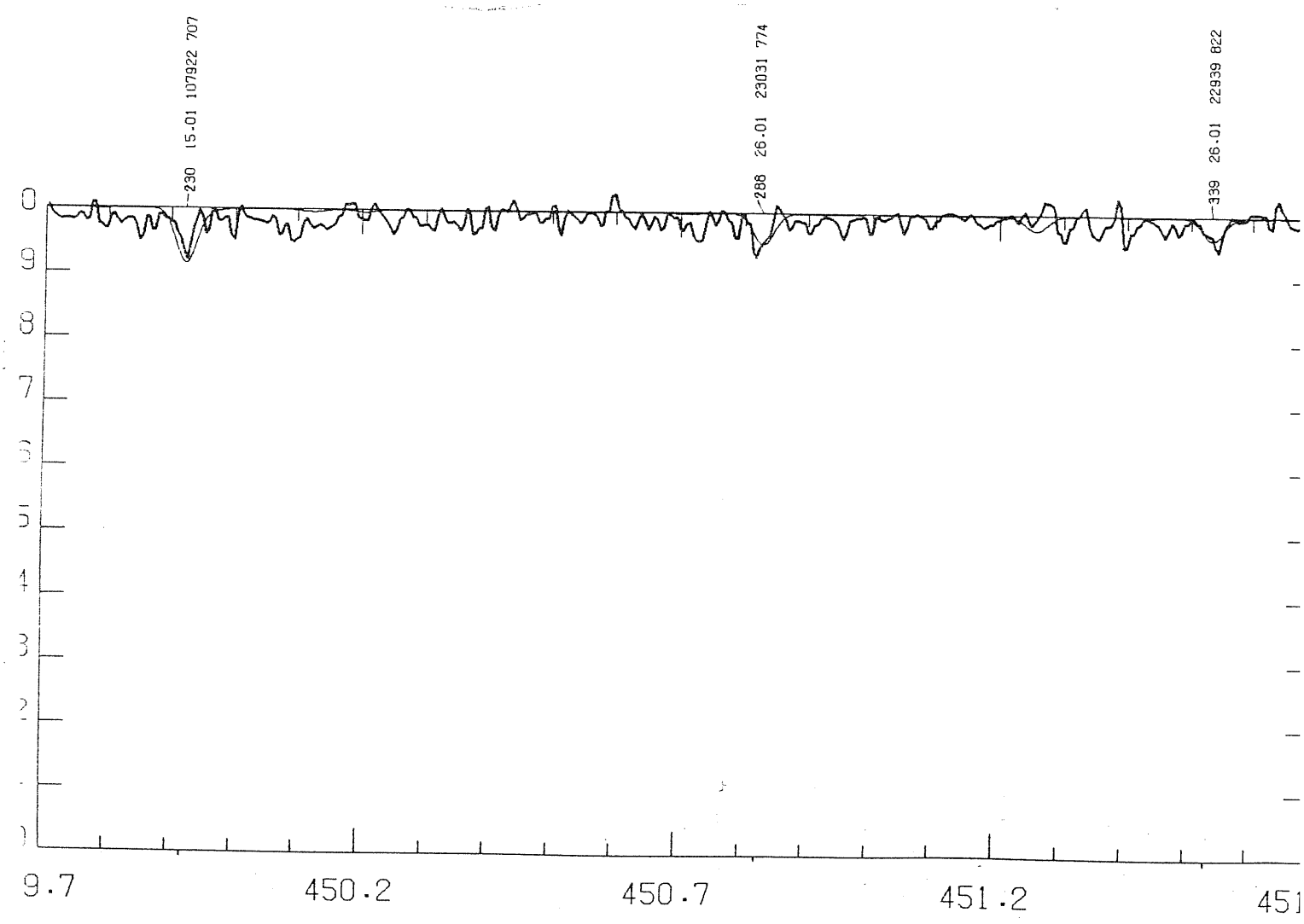
15-01 107922 707
230
26.01 23031 774
288
26.01 22939 822
339
9
8
7
5
4
3
2
450.2
450.7
451.2

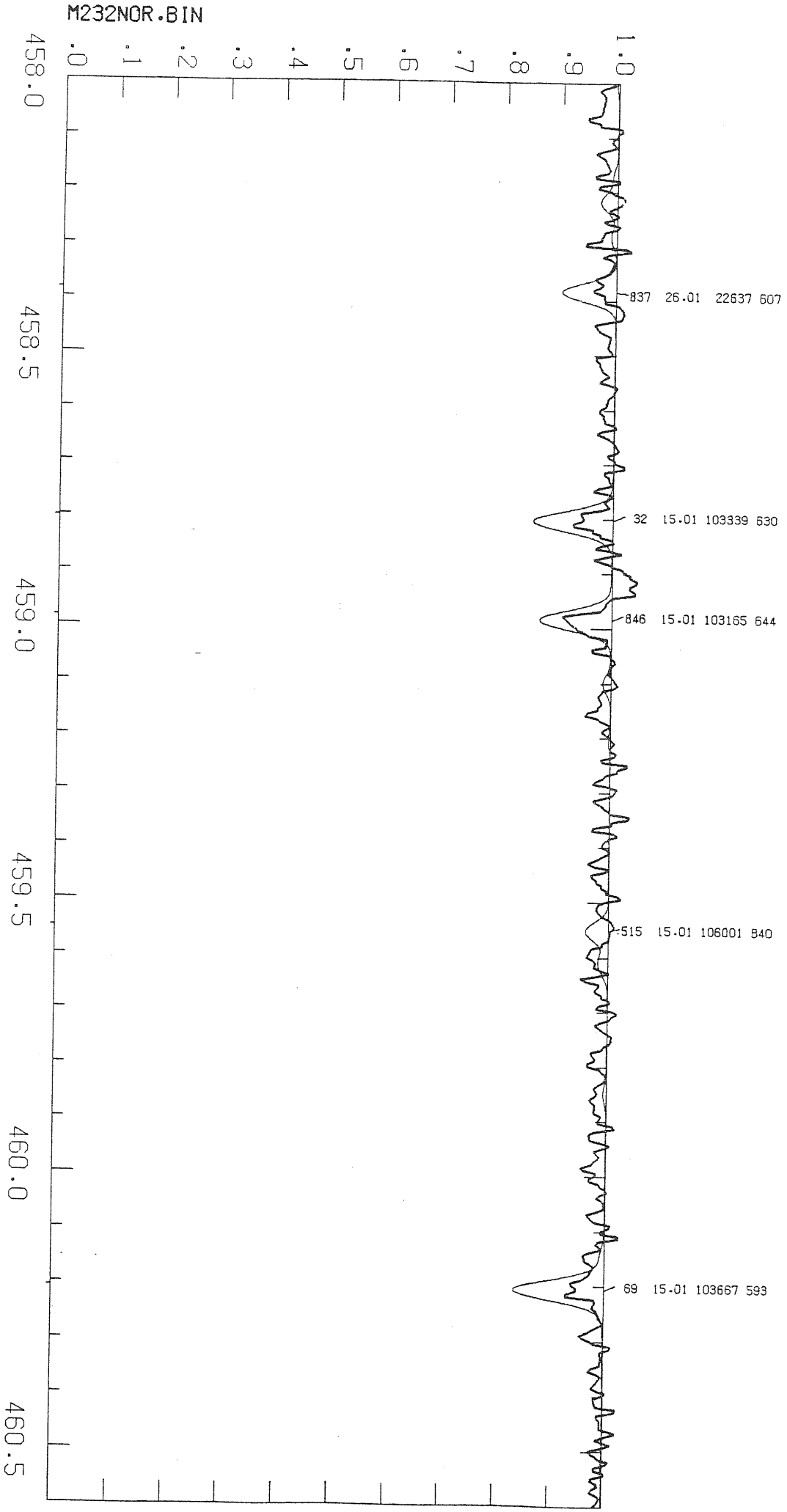
M232NOR.BIN
458.0
458.5
459.0
459.5
460.0
460.5
.0
.1
.2
.3
.4
.5
.6
.7
.8
.9
1.0
837 26.01 22637 607
32 15.01 103339 630
846 15.01 103165 644
515 15.01 106001 840
69 15.01 103667 593

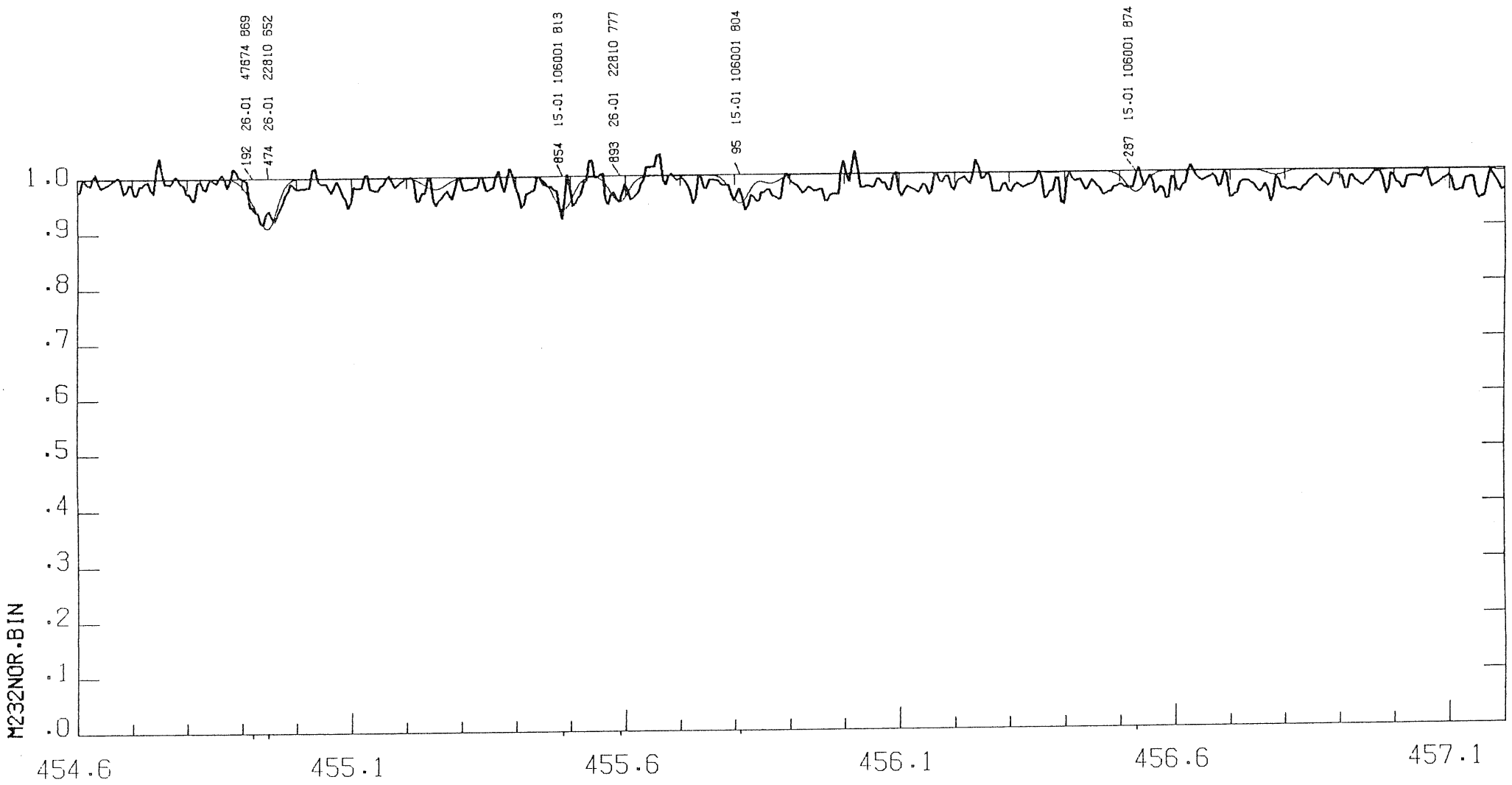
26.01 47674 869
192
26.01 22810 552
474
15.01 106001 813
854
26.01 22810 777
893
15.01 106001 804
95
15.01 106001 874
287
1.0
.9
.8
.7
.6
.5
.4
.3
.2
.1
.0
M232NOR.BIN
454.6
455.1
455.6
456.1
456.6
457.1

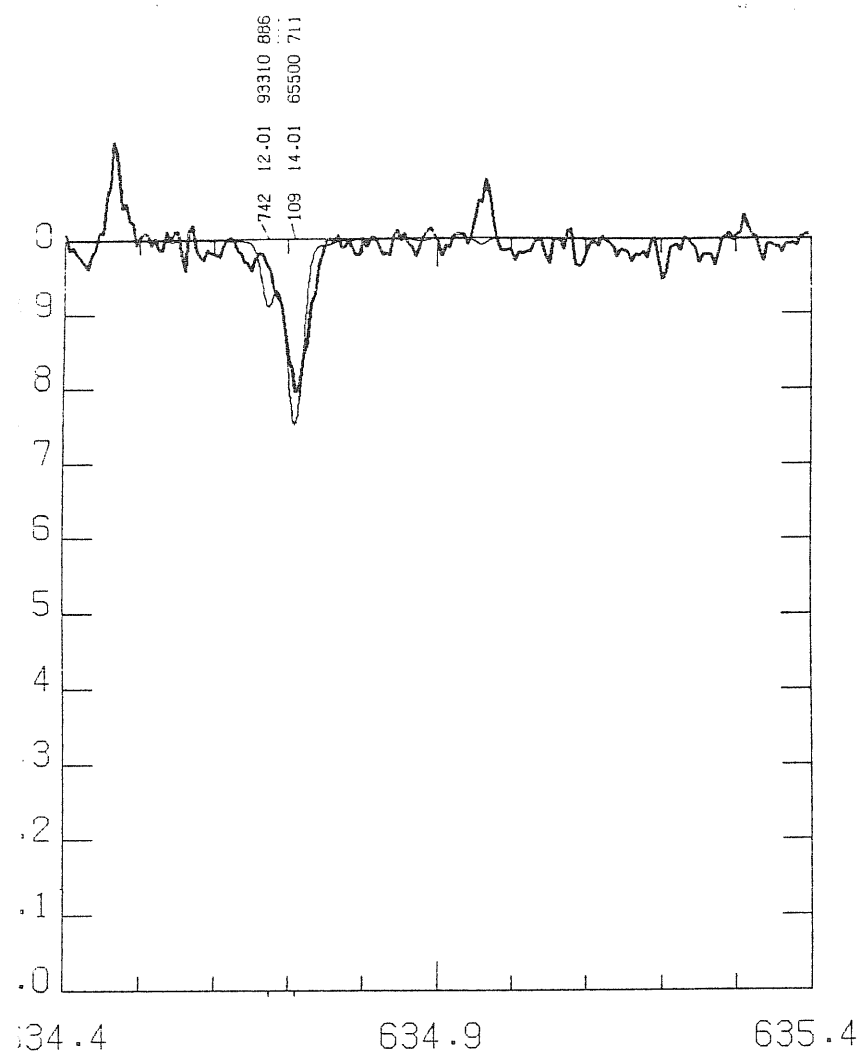
742 12.01 93310 886
109 14.01 65500 711
.0
.1
.2
.3
.4
.5
.6
.7
.8
.9
634.4
634.9
635.4

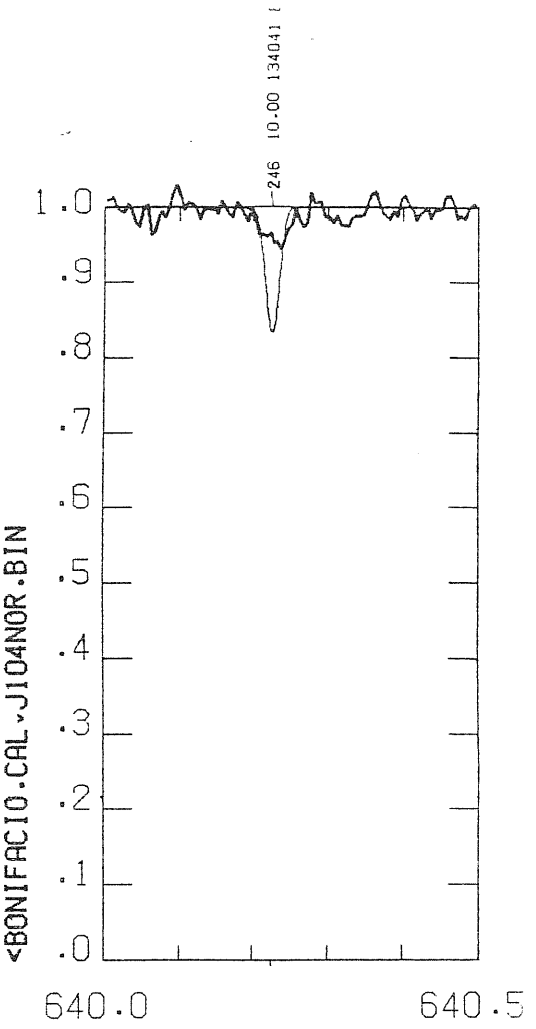
246 10.00 134041
1.0
.9
.8
.7
.6
.5
.4
.3
.2
.1
.0
<BONIFACIO.CAL›J104NOR.BIN
640.0
640.5

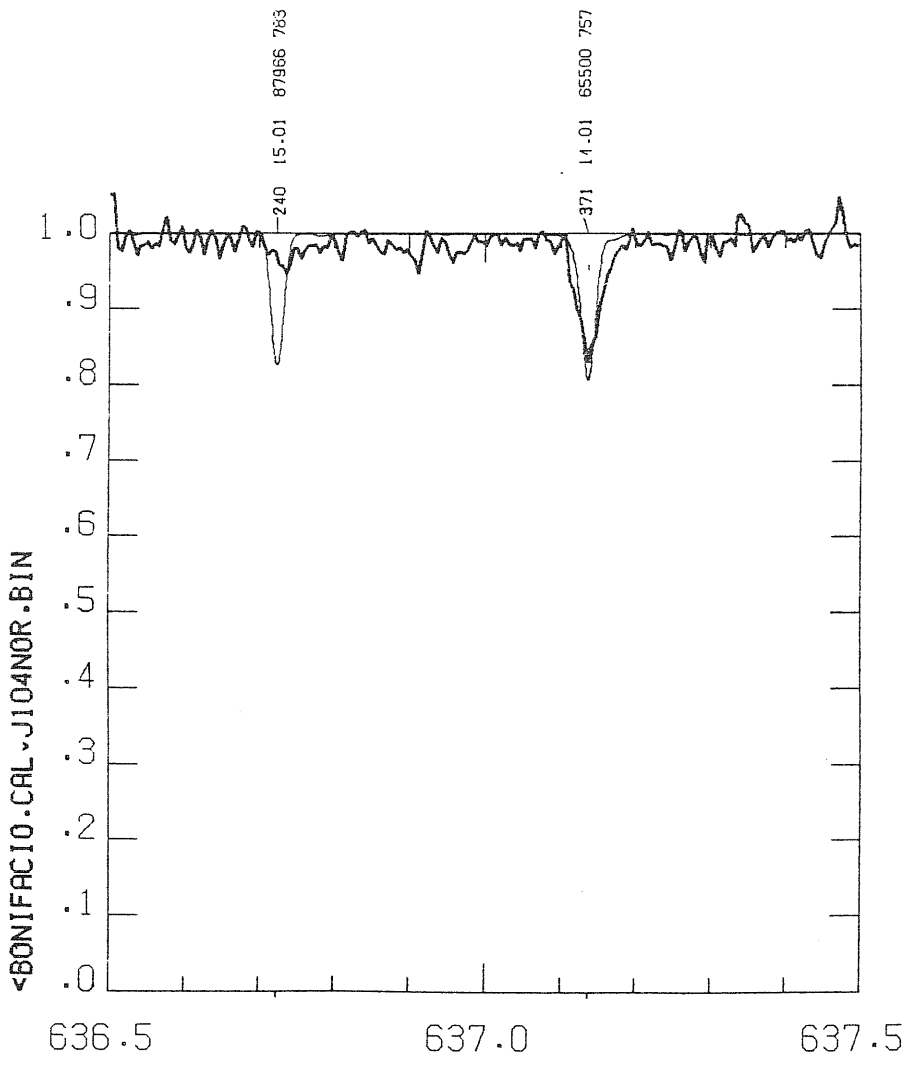
240 15.01 87966 783
371 14.01 65500 757
1.0
.9
.8
.7
.6
.5
.4
.3
.2
.1
.0
<BONIFACIO.CAL›J104NOR.BIN
636.5
637.0
637.5

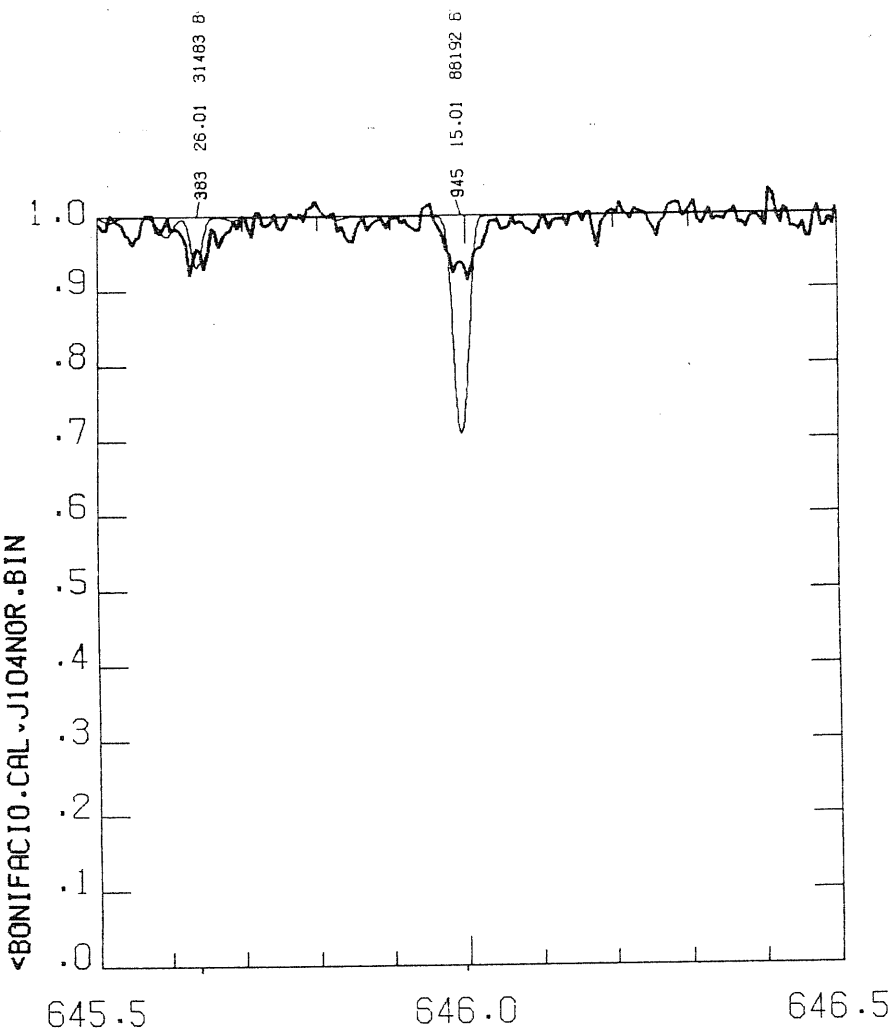
383 26.01 31483 8
945 15.01 88192 6
1.0
.9
.8
.7
.6
.5
.4
.3
.2
.1
.0
<BONIFACIO.CAL>J104NOR.BIN
645.5
646.0
646.5

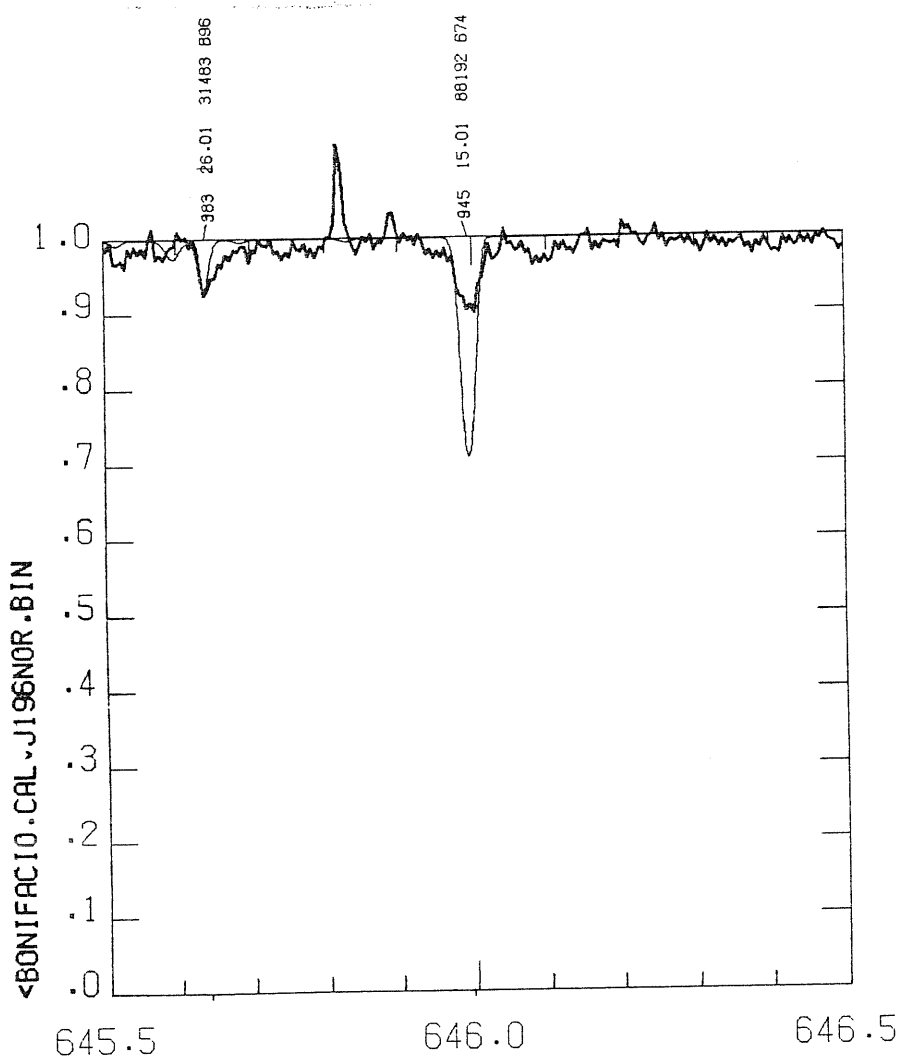
383 26.01 31483 896
945 15.01 88192 674
1.0
.9
.8
.7
.6
.5
.4
.3
.2
.1
.0
<BONIFACIO.CAL>J196NOR.BIN
645.5
646.0
646.5

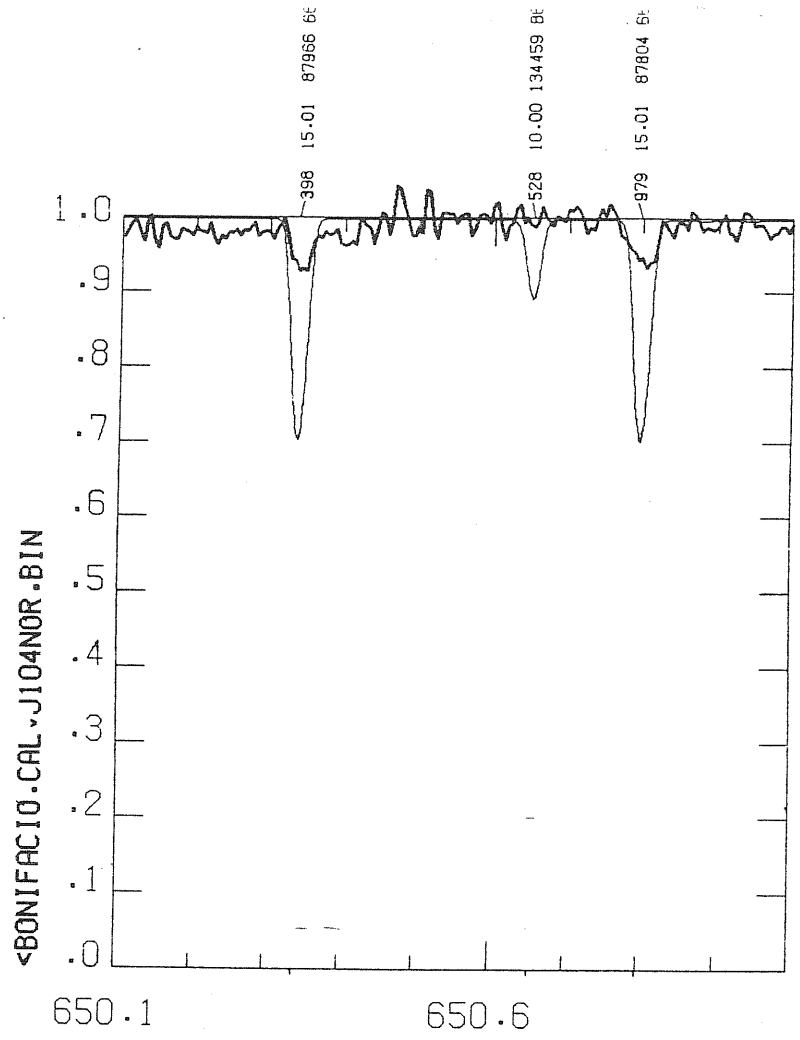
398 15.01 87966 6
528 10.00 134459 8
979 15.01 87804 6
1.0
.9
.8
.7
.6
.5
.4
.3
.2
.1
.0
<BONIFACIO.CAL>J104NOR.BIN
650.1
650.6

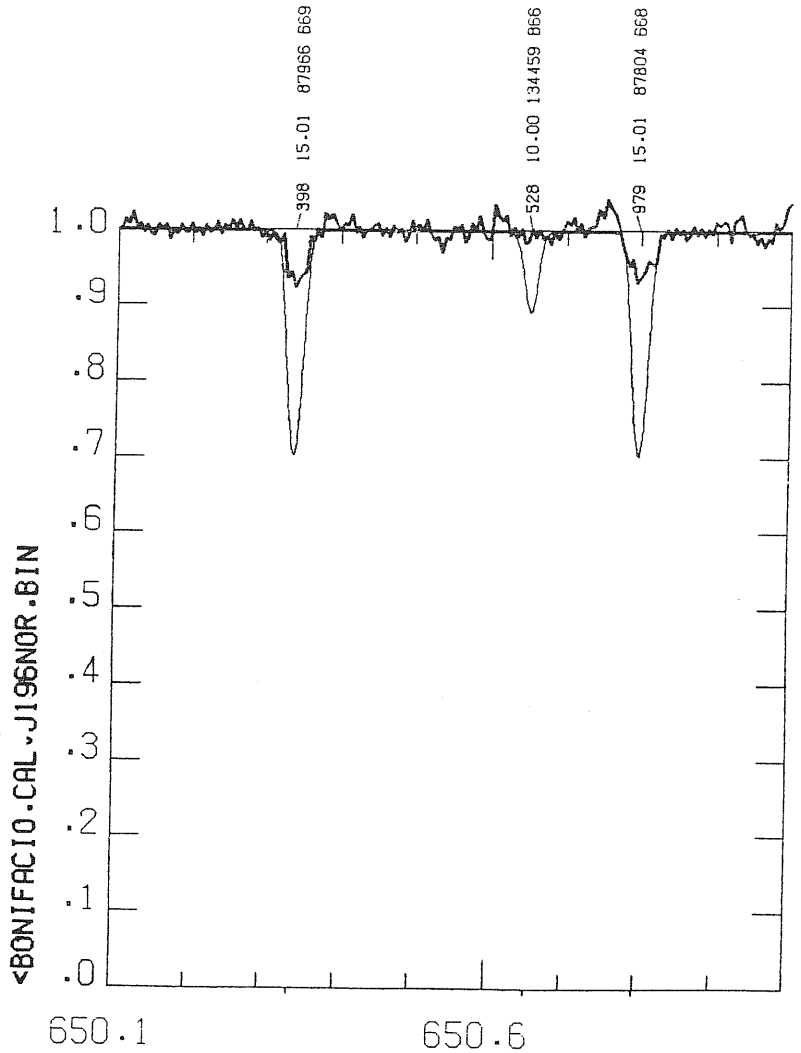
398 15.01 87966 669
528 10.00 134459 866
979 15.01 87804 668
1.0
.9
.8
.7
.6
.5
.4
.3
.2
.1
.0
<BONIFACIO.CAL>J196NOR.BIN
650.1
650.6

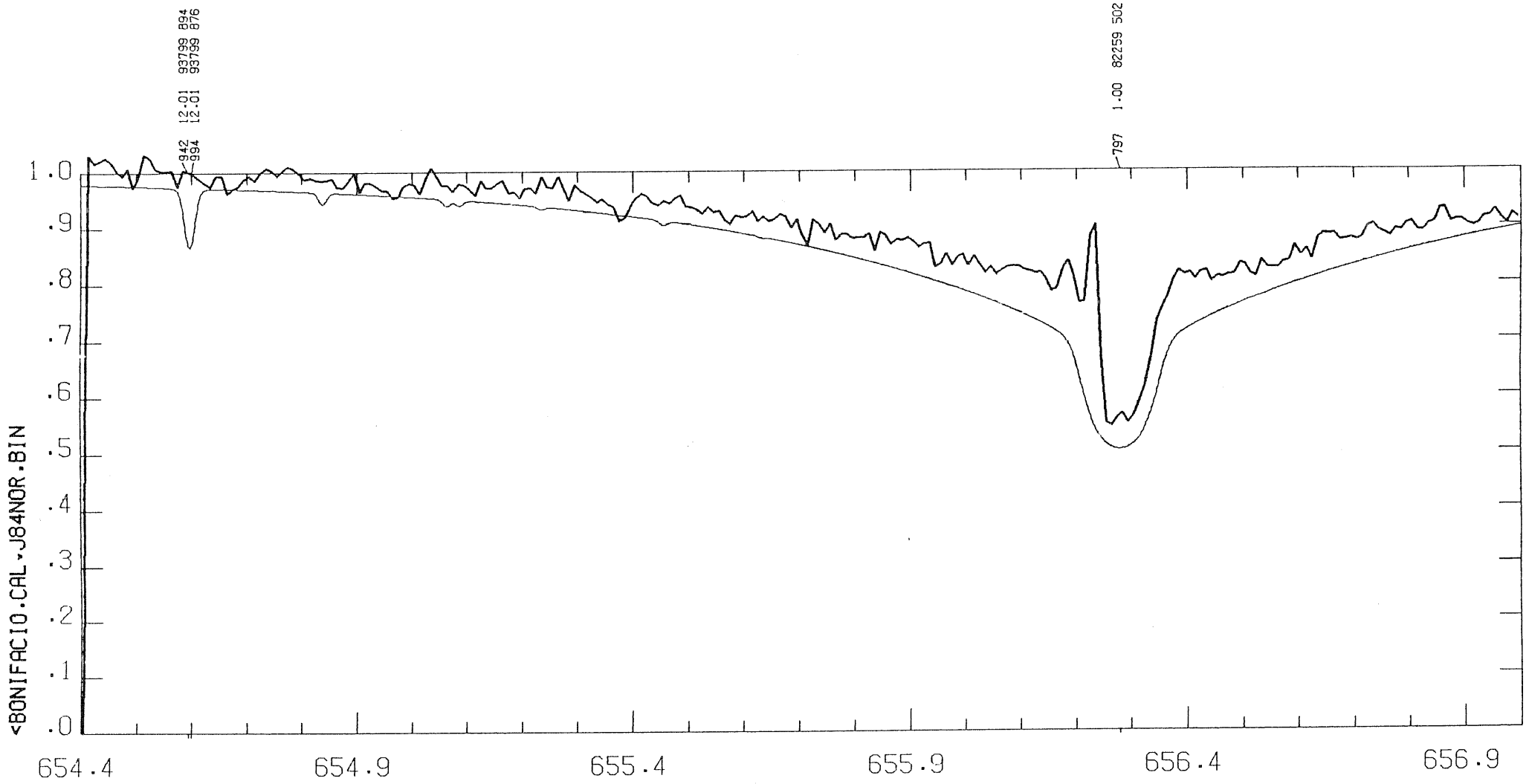
12-01 93799 894
12-01 93799 876
942
894
1.00 82259 502
797
1.0
.9
.8
.7
.6
.5
.4
.3
.2
.1
.0
<BONIFAC10.CAL+J84NOR.BIN
654.4
654.9
655.4
655.9
656.4
656.9

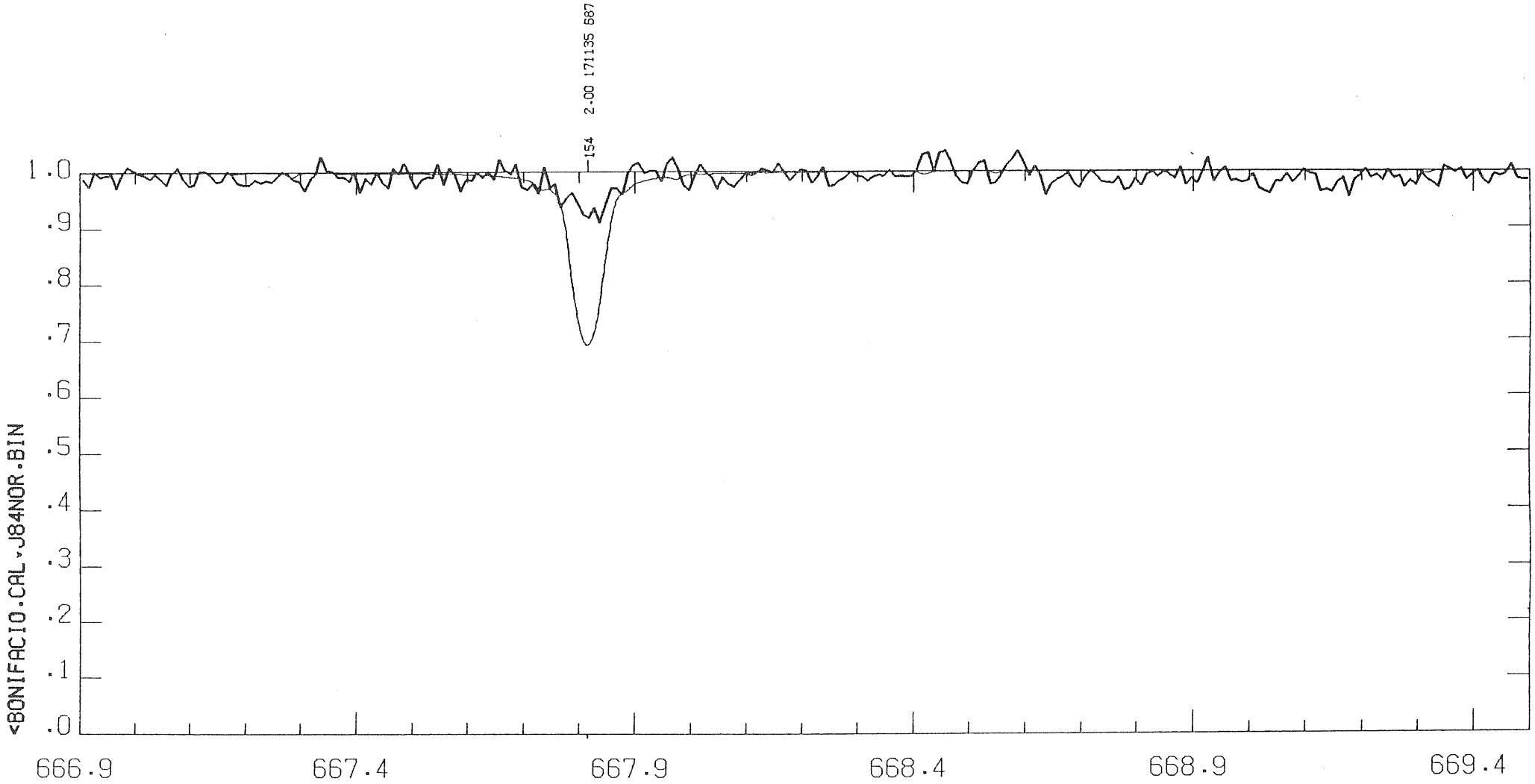
154 2.00 171135 687
1.0
.9
.8
.7
.6
.5
.4
.3
.2
.1
.0
<BONIFACIO.CAL-J84NOR.BIN
666.9
667.4
667.9
668.4
668.9
669.4

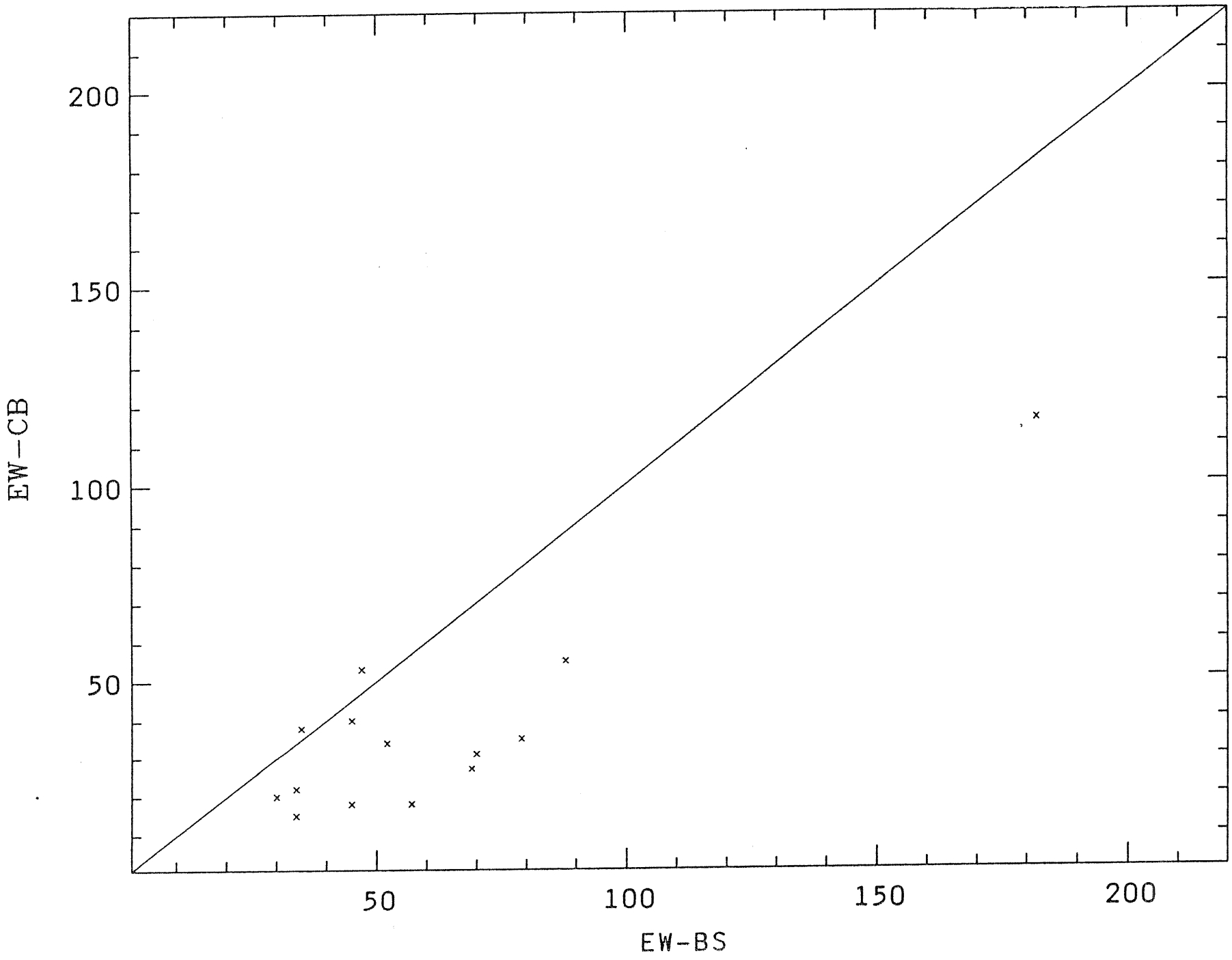
200
150
100
50
EW-CB
50
100
150
200
EW-BS

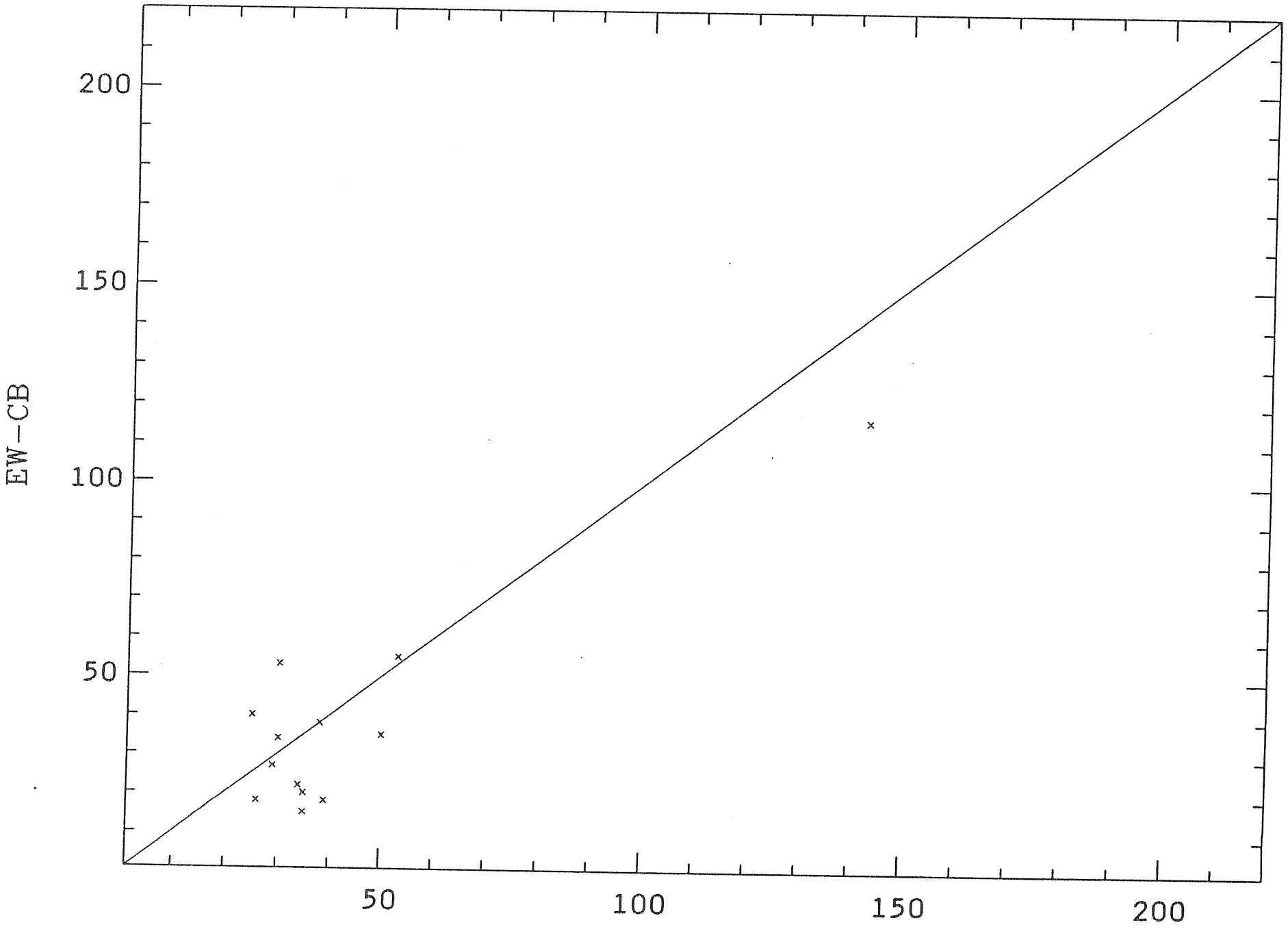
EW−CB
200
150
100
50
50
100
150
200

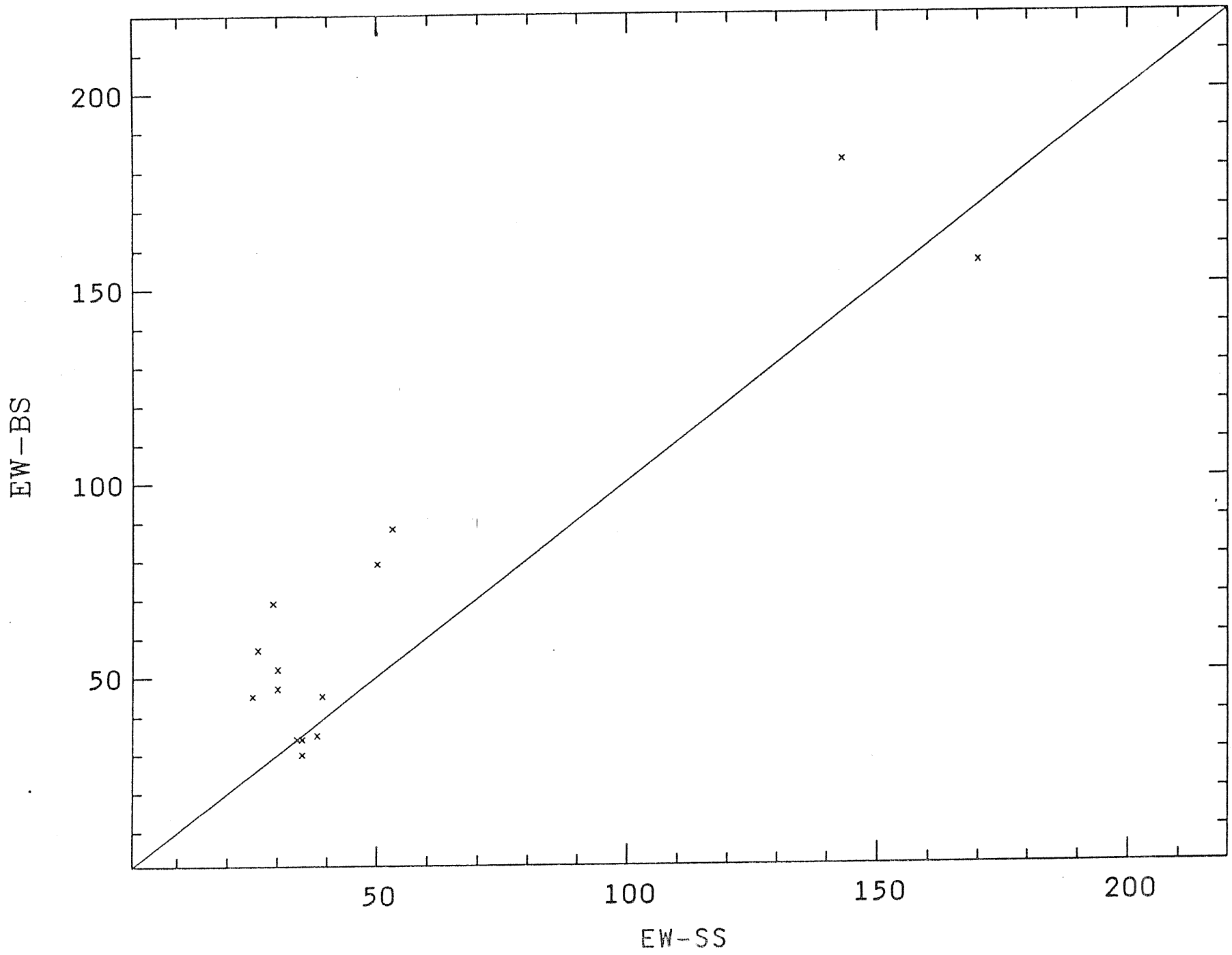
200
150
100
50
EW-BS
50
100
150
200
EW-SS

Appendix B

In this appendix I show some examples of plots of IUE spectra and synthetic spectra for Feige 86. The IUE image used is SWP15592, which was observed by P.L. Selvelli on November 29^{th}, 1981 with an exposure time of 293 minutes.

The image has been reprocessed at Vilspa in autumn 1986 with the IUE-SIPS2 reduction package. In order to match observed wavelengths to laboratory wavelengths of identified lines it was necessary to give a shift of +53.16 km/s to the observed spectra. For presentation the image was smoothed with a gaussian filter of FWHM 0.05 Å.

The synthetic spectra were computed using the model atmosphere reported in table 2. This has an effective temperature of 16800 K and $\log g = 4.08$, the microturbulence is 2 km/s. The abundances are those indicated in the control card ABUNDANCE CHANGE (if an element is not present in this list its abundace is solar). They were determined by requiring that computed profiles of some selected lines matched the observed ones (see Bonifacio *et al.* 1991). The spectra were rotationally broadened for $v \sin i = 15$ km/s and further convolved with a gaussian instrumental profile of FWHM 17 km/s, which corresponds to about 0.1 Å, the nominal resolving power of IUE in the short wavelength range.

The most remarkable anomalies are displayed by CI, notice the complex structure of multiplets 2 and 3 in the region 165.6 nm — 165.9 nm ; the line at 127.72 nm of multiplet 7 is clearly red-shifted, while lines of multiplet 5, in the region 156.0 nm — 156.2 nm are both enhanced and red-shifted.

The resonance line of BII at 136.2461 nm shows clearly that boron is under-abundant (the computed spectrum shown here matches rather well the observed line and it assumes a $\log(N_B/N_{tot}) = -11.6$ while $\log(N_B/N_{tot})_\odot = -9.44$), the FeII line at 136.2267 is probably computed with a wrong $\log gf$.

The PII lines at 130.4492 nm and 131.0703 nm support a phosphorous overabundace of a factor 300, so does also the PIII line at 133.4813, although

other PIII lines are much weaker, implying an abundance of only, about, 4 times the solar one. This discrepancy between the abundance inferred from PII and PIII lines was already note for the visible spectrum by Baschek and Sargent (1976). Note that the $\log gf$ values adopted in the computation are those of the Kurucz and Peytremann list (KP ; 1975), which are derived under the hypothesis of LS coupling which is certainly not valid for several P lines. In the future I plan to do a compilation of $\log gf$ values for phosphorous and recompute the spectra using better values than the KP, whenever possible.

The resonance line of HgII at 165.0 nm is either absent or, at best, very weak. This line has been extensively studied by Leckrone (1984) and shows up if Hg is overabundant.

The few plots shown in this appendix illustrate that a lot of effort is still necessary to satisfactorily analyse these spectra. One of the aims is to gather conclusive evidence in favour or against the existence of a cool circumstellar region where some of the CI lines could form.

Bibliography

Baschek, B. and Sargent, A.I.:1976, A.&A. **53**, 47

Bonifacio P., Castelli F. and Hack M.:1990, Poster paper presented at I.A.U. Symp. 145 , p. 123

Kurucz, R.L. and Peytremann, E.:1975 S.A.O. Spec. Rep. 362

Leckrone, D.S.:1984, Ap.J. **286**,, 275

TABLE 2

the model atmosphere used for the computation of the synthetic spectra in appendix B

```
SURFACE INTENSI 17 1.,.9,.8,.7,.6,.5,.4,.3,.25,.2,.15,.125,.1,.075,.05,.025,.0
ITERATIONS 1 PRINT 2 PUNCH 2
CORRECTION OFF
PRESSURE OFF
TEFF  16800. GRAVITY 4.080 LTE
ABUNDANCE CHANGE 5 -11. 6 -5.25 7 -5.0 13 -6.75 14 -5.0 15 -4.5
TITLE TEST MODEL WITH SDSC OPACITY  VTURB 2 KM/S
OPACITY IFOP 1 1 1 1 1 1 1 1 1 1 1 1 1 1 0 1 0 0 0 0 0 0
CONVECTION OFF  1.00 TURBULENCE OFF  0.00  0.00  0.00  0.00
ABUNDANCE SCALE   1.00000 ABUNDANCE CHANGE 1 0.91100 2 0.08900
READ DECK6 64 RHOX,T,P,XNE,ABROSS,ACCRAD,VTURB
4.33420209E-06   8864.6 5.133E-02 1.999E+10 3.089E-01 1.805E+02 2.000E+05
5.77235452E-06   9256.6 6.836E-02 2.551E+10 3.089E-01 1.695E+02 2.000E+05
7.67342357E-06   9339.1 9.090E-02 3.362E+10 3.120E-01 1.716E+02 2.000E+05
1.01877264E-05   9440.8 1.207E-01 4.416E+10 3.157E-01 1.718E+02 2.000E+05
1.35030745E-05   9550.4 1.600E-01 5.787E+10 3.198E-01 1.703E+02 2.000E+05
1.78647599E-05   9667.0 2.117E-01 7.566E+10 3.244E-01 1.671E+02 2.000E+05
2.35951096E-05   9788.4 2.796E-01 9.871E+10 3.296E-01 1.622E+02 2.000E+05
3.11107388E-05   9913.3 3.688E-01 1.286E+11 3.356E-01 1.562E+02 2.000E+05
4.09449610E-05  10039.3 4.855E-01 1.671E+11 3.428E-01 1.500E+02 2.000E+05
5.37572214E-05  10160.4 6.377E-01 2.169E+11 3.516E-01 1.450E+02 2.000E+05
7.03887065E-05  10268.1 8.352E-01 2.812E+11 3.620E-01 1.415E+02 2.000E+05
9.19377664E-05  10359.8 1.091E+00 3.641E+11 3.747E-01 1.411E+02 2.000E+05
1.19677914E-04  10436.6 1.421E+00 4.705E+11 3.901E-01 1.451E+02 2.000E+05
1.55094047E-04  10501.6 1.841E+00 6.058E+11 4.086E-01 1.533E+02 2.000E+05
2.00088192E-04  10564.3 2.375E+00 7.766E+11 4.305E-01 1.644E+02 2.000E+05
2.56969323E-04  10634.0 3.049E+00 9.904E+11 4.555E-01 1.761E+02 2.000E+05
3.28677920E-04  10717.6 3.898E+00 1.256E+12 4.837E-01 1.862E+02 2.000E+05
4.18613707E-04  10811.5 4.962E+00 1.585E+12 5.154E-01 1.943E+02 2.000E+05
5.31245357E-04  10913.0 6.294E+00 1.991E+12 5.510E-01 2.008E+02 2.000E+05
6.71864145E-04  11019.2 7.956E+00 2.493E+12 5.914E-01 2.064E+02 2.000E+05
8.47083355E-04  11127.6 1.003E+01 3.111E+12 6.372E-01 2.120E+02 2.000E+05
1.06440046E-03  11239.2 1.259E+01 3.868E+12 6.898E-01 2.185E+02 2.000E+05
1.33160341E-03  11349.5 1.574E+01 4.789E+12 7.510E-01 2.279E+02 2.000E+05
1.65875036E-03  11458.1 1.960E+01 5.906E+12 8.204E-01 2.381E+02 2.000E+05
2.05771555E-03  11565.1 2.430E+01 7.254E+12 8.990E-01 2.493E+02 2.000E+05
2.54255920E-03  11670.3 3.001E+01 8.875E+12 9.877E-01 2.616E+02 2.000E+05
3.12982087E-03  11775.0 3.691E+01 1.082E+13 1.088E+00 2.756E+02 2.000E+05
3.83916848E-03  11878.2 4.524E+01 1.314E+13 1.202E+00 2.914E+02 2.000E+05
4.69530675E-03  11979.7 5.527E+01 1.592E+13 1.331E+00 3.095E+02 2.000E+05
5.72651811E-03  12080.0 6.734E+01 1.924E+13 1.477E+00 3.304E+02 2.000E+05
6.96869869E-03  12180.3 8.185E+01 2.318E+13 1.641E+00 3.543E+02 2.000E+05
8.46228371E-03  12281.1 9.926E+01 2.788E+13 1.826E+00 3.820E+02 2.000E+05
1.02570891E-02  12389.2 1.201E+02 3.344E+13 2.031E+00 4.131E+02 2.000E+05
1.24112024E-02  12501.7 1.451E+02 4.003E+13 2.259E+00 4.486E+02 2.000E+05
1.50005081E-02  12624.0 1.750E+02 4.781E+13 2.508E+00 4.888E+02 2.000E+05
1.81125254E-02  12762.1 2.108E+02 5.698E+13 2.775E+00 5.328E+02 2.000E+05
2.18690897E-02  12920.2 2.539E+02 6.780E+13 3.050E+00 5.773E+02 2.000E+05
2.64368923E-02  13102.8 3.061E+02 8.063E+13 3.328E+00 6.215E+02 2.000E+05
3.20420515E-02  13320.4 3.699E+02 9.590E+13 3.597E+00 6.633E+02 2.000E+05
3.90045907E-02  13576.3 4.488E+02 1.143E+14 3.853E+00 7.021E+02 2.000E+05
4.77797569E-02  13879.6 5.480E+02 1.367E+14 4.084E+00 7.365E+02 2.000E+05
```

5.89815817E-02	14242.3	6.742E+02	1.644E+14	4.289E+00	7.673E+02	2.000E+05
7.33932523E-02	14678.4	8.362E+02	1.985E+14	4.472E+00	7.952E+02	2.000E+05
9.19305529E-02	15187.9	1.044E+03	2.409E+14	4.603E+00	8.127E+02	2.000E+05
1.16260058E-01	15785.3	1.317E+03	2.943E+14	4.694E+00	8.218E+02	2.000E+05
1.48281930E-01	16483.1	1.675E+03	3.612E+14	4.800E+00	8.325E+02	2.000E+05
1.90822655E-01	17276.5	2.151E+03	4.454E+14	4.851E+00	8.320E+02	2.000E+05
2.47079461E-01	18173.5	2.781E+03	5.499E+14	4.863E+00	8.230E+02	2.000E+05
3.21842209E-01	19165.0	3.619E+03	6.804E+14	4.924E+00	8.199E+02	2.000E+05
4.20958383E-01	20267.5	4.729E+03	8.422E+14	4.977E+00	8.145E+02	2.000E+05
5.51767978E-01	21470.4	6.196E+03	1.042E+15	5.058E+00	8.112E+02	2.000E+05
7.23309921E-01	22783.7	8.119E+03	1.288E+15	5.153E+00	8.128E+02	2.000E+05
9.49254602E-01	24218.2	1.065E+04	1.590E+15	5.240E+00	8.086E+02	2.000E+05
1.24335327E+00	25773.9	1.395E+04	1.957E+15	5.426E+00	8.214E+02	2.000E+05
1.62088292E+00	27465.8	1.817E+04	2.392E+15	5.650E+00	8.388E+02	2.000E+05
2.10202378E+00	29311.7	2.355E+04	2.905E+15	6.000E+00	8.746E+02	2.000E+05
2.70112337E+00	31316.2	3.021E+04	3.490E+15	6.412E+00	9.181E+02	2.000E+05
3.43311525E+00	33489.1	3.831E+04	4.142E+15	7.065E+00	9.876E+02	2.000E+05
4.31602008E+00	35852.5	4.802E+04	4.860E+15	7.827E+00	1.064E+03	2.000E+05
5.37338217E+00	38416.9	5.957E+04	5.655E+15	8.739E+00	1E+03	2.000E+05
6.65248025E+00	41229.8	7.343E+04	6.557E+15	9.789E+00	1.223E+03	2.000E+05
8.28654709E+00	44442.5	9.103E+04	7.624E+15	1.073E+01	1.265E+03	2.000E+05
1.05462645E+01	48232.5	1.154E+05	8.970E+15	1.137E+01	1.237E+03	2.000E+05
1.40186020E+01	52928.5	1.530E+05	1.088E+16	1.185E+01	1.122E+03	2.000E+05

RADK 1.4251E+02

EGIN ITERATION 15 COMPLETED

ND

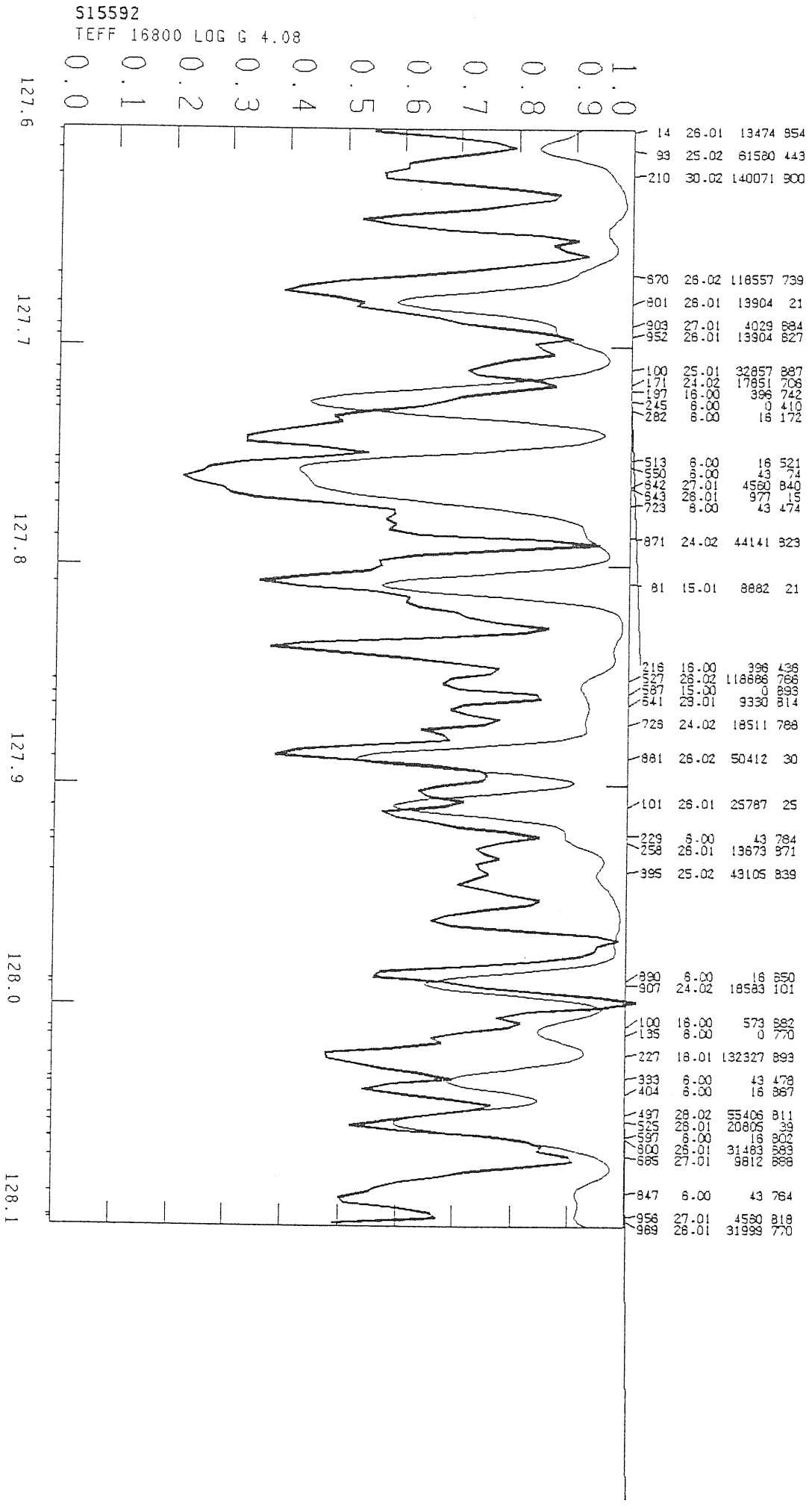
S15592
TEFF 16800 LOG G 4.08
0.0 0.1 0.2 0.3 0.4 0.5 0.6 0.7 0.8 0.9 1.0
127.6
127.7
127.8
127.9
128.0
128.1
14 26.01 13474 854
93 25.02 61580 443
210 30.02 140071 900
870 26.02 118557 739
801 26.01 13904 21
903 27.01 4029 684
952 26.01 13904 827
100 25.01 32857 887
171 24.02 17851 706
197 16.00 396 742
245 6.00 0 410
282 6.00 16 172
513 6.00 16 521
550 6.00 43 74
642 27.01 4580 840
643 28.01 977 15
723 6.00 43 474
871 24.02 44141 823
81 15.01 8882 21
216 16.00 396 436
527 26.02 118688 766
587 15.00 0 893
641 28.01 9330 814
728 24.02 18511 788
881 26.02 50412 30
101 26.01 25787 25
229 6.00 43 784
258 26.01 13673 971
395 25.02 43105 839
890 6.00 16 650
907 24.02 18583 101
100 16.00 573 882
135 6.00 0 770
227 18.01 132327 893
333 6.00 43 478
404 6.00 16 867
497 28.02 55406 811
525 28.01 20805 39
597 6.00 16 902
800 25.01 31483 583
685 27.01 9812 688
847 6.00 43 764
956 27.01 4580 818
989 28.01 31999 770

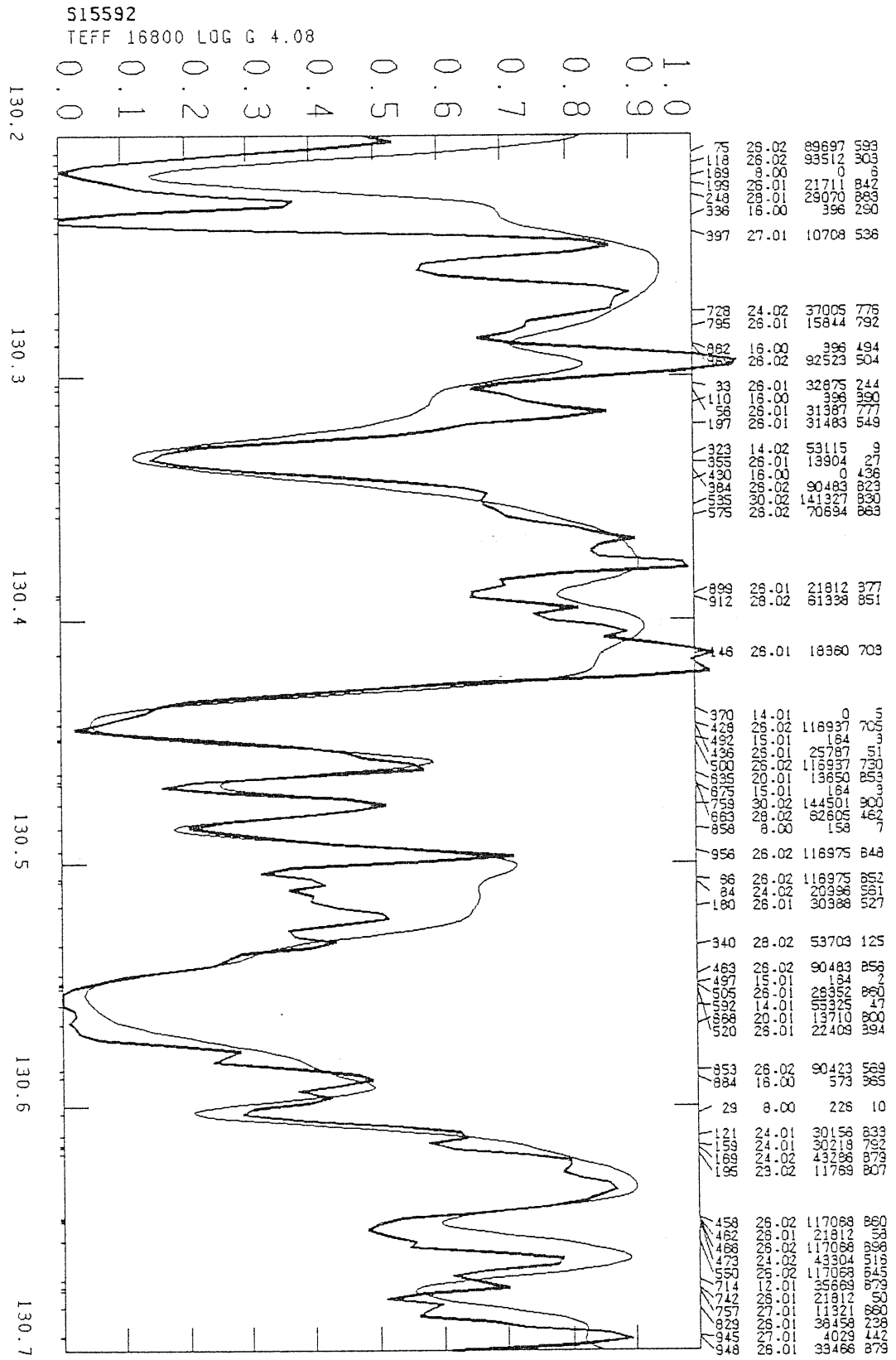
S15592
TEFF 16800 LOG G 4.08
0.0
0.1
0.2
0.3
0.4
0.5
0.6
0.7
0.8
1.0
130.2
130.3
130.4
130.5
130.6
130.7
75 26.02 89697 593
118 26.02 93512 303
168 8.00 0 8
199 26.01 21711 842
248 26.01 29070 883
336 16.00 396 290
397 27.01 10708 536
728 24.02 37005 776
795 26.01 15844 792
862 16.00 396 494
26.02 92523 504
33 26.01 32875 244
110 16.00 396 390
56 26.01 31387 777
197 26.01 31483 549
323 14.02 53115 9
355 26.01 13904 27
430 16.00 0 436
384 26.02 90483 823
535 30.02 141327 830
575 26.02 70694 883
898 26.01 21812 377
912 26.02 61338 851
146 26.01 18360 703
370 14.01 0 5
428 26.02 116937 705
482 15.01 184 3
436 26.01 25787 51
508 26.02 116937 730
535 20.01 13650 853
675 15.01 184 3
759 30.02 144501 900
663 26.02 82605 462
858 8.00 158 7
956 26.02 116975 848
86 26.02 116975 852
84 24.02 20986 551
180 26.01 30388 527
940 28.02 53703 125
463 26.02 90483 856
497 15.01 184 2
505 26.01 28352 860
592 14.01 55325 47
668 20.01 13710 800
520 26.01 22409 394
853 26.02 90423 569
884 16.00 573 365
29 8.00 226 10
121 24.01 30156 833
159 24.01 30218 792
169 24.02 43286 879
195 23.02 11769 807
458 26.02 117068 860
462 26.01 21812 58
466 26.02 117068 898
473 24.02 43304 515
550 26.02 117068 645
714 12.01 35669 879
742 26.01 21812 50
757 27.01 11321 860
829 26.01 38458 238
945 27.01 4029 442
948 26.01 33466 879

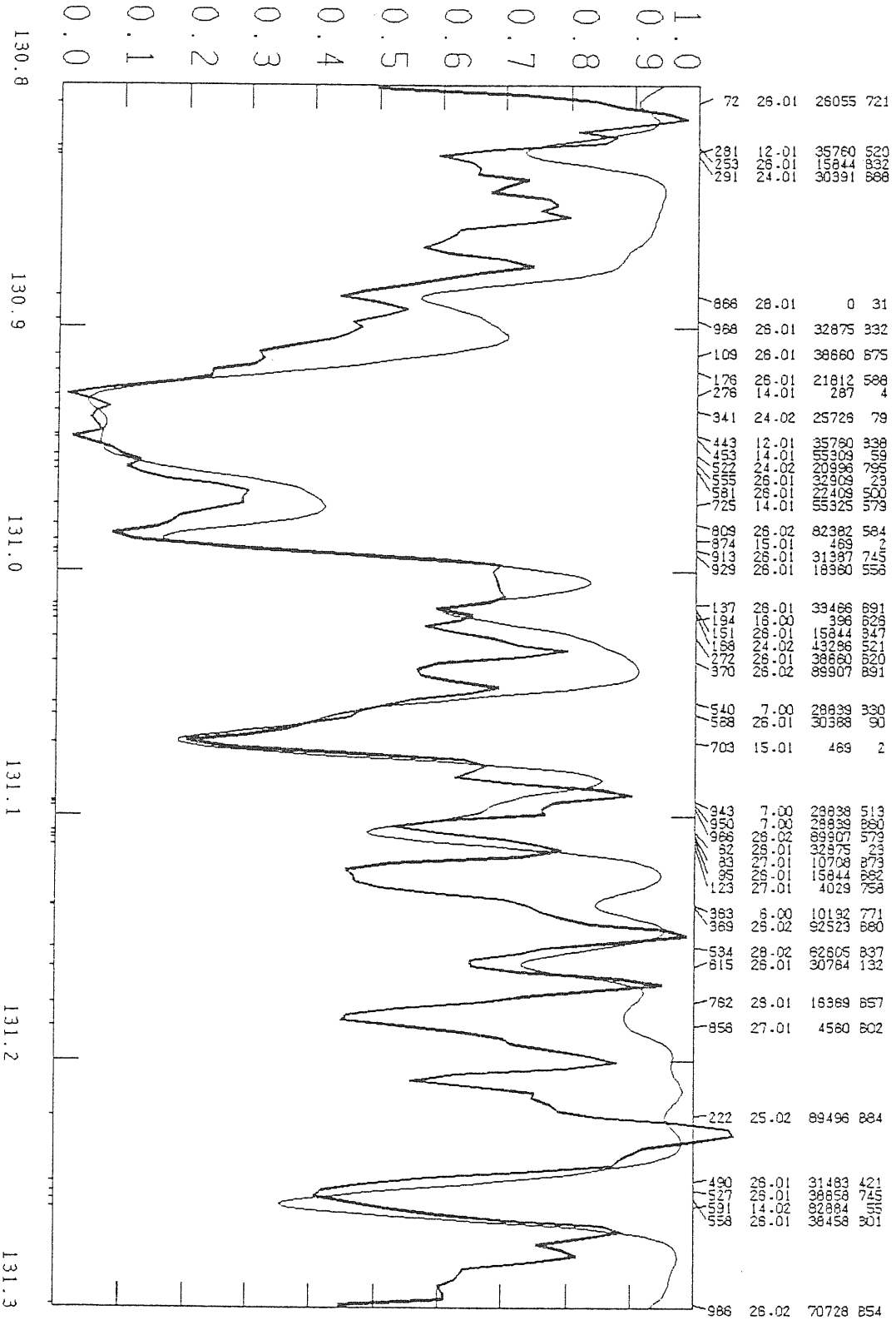
S15592
TEFF 16800 LOG G 4.08
0.0
0.1
0.2
0.3
0.4
0.5
0.6
0.7
0.8
0.9
1.0
130.8
130.9
131.0
131.1
131.2
131.3
72 26.01 28055 721
281 12.01 35760 520
253 26.01 15844 832
291 24.01 30391 688
866 28.01 0 31
968 26.01 32875 332
109 26.01 38660 575
176 26.01 21812 588
278 14.01 287 4
341 24.02 25726 79
443 12.01 35760 338
453 14.01 55309 59
522 24.02 20996 795
555 26.01 32909 23
581 26.01 22409 500
725 14.01 55325 579
809 26.02 82382 584
874 15.01 469 2
913 26.01 31387 745
929 26.01 18960 556
137 26.01 33486 691
194 16.00 396 626
151 26.01 15844 847
158 24.02 43286 521
272 26.01 38660 620
370 26.02 89907 891
540 7.00 28838 330
568 26.01 30388 90
703 15.01 469 2
943 7.00 28838 513
950 7.00 28838 860
986 26.02 89907 579
52 26.01 32875 23
83 27.01 10708 873
95 26.01 15844 882
123 27.01 4029 758
383 6.00 10192 771
389 26.02 92523 680
534 26.02 62605 837
815 26.01 30784 132
782 26.01 18389 857
856 27.01 4580 802
222 25.02 89496 884
490 26.01 31483 421
527 26.01 38858 745
591 14.02 82884 55
558 26.01 38458 301
986 26.02 70728 854

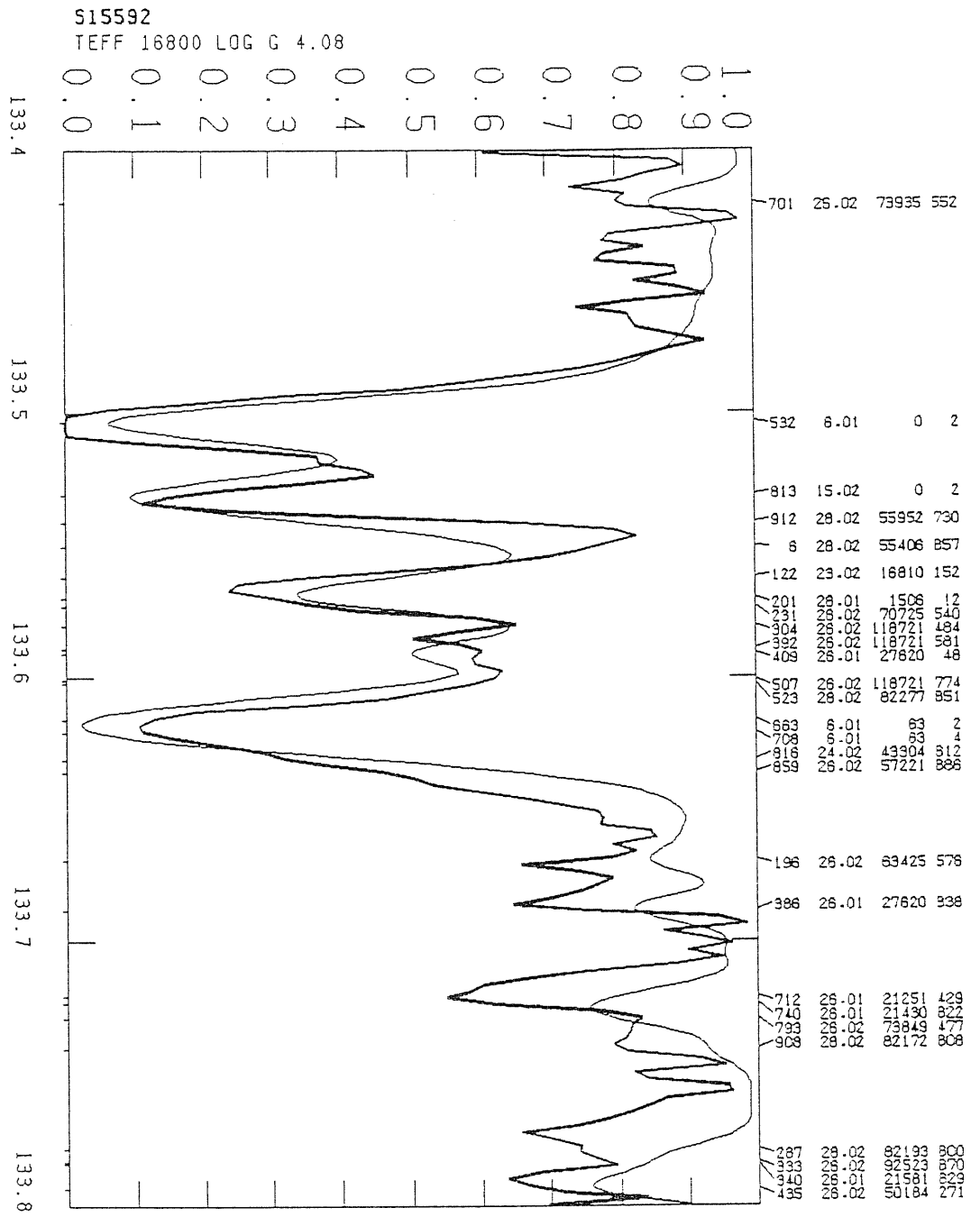
S15592
TEFF 16800 LOG G 4.08
0.0
0.1
0.2
0.3
0.4
0.5
0.6
0.7
0.8
0.9
1.0
133.4
133.5
133.6
133.7
133.8
701 26.02 73935 552
532 8.01 0 2
813 15.02 0 2
912 28.02 55952 730
6 28.02 55406 857
122 23.02 16810 152
201 28.01 1506 12
231 28.02 70725 540
304 28.02 118721 484
392 28.02 118721 581
409 28.01 27820 48
507 28.02 118721 774
523 28.02 82277 851
663 6.01 63 2
708 6.01 63 4
816 24.02 43304 812
859 26.02 57221 886
196 26.02 83425 576
386 26.01 27820 938
712 26.01 21251 429
740 26.01 21430 822
793 28.02 79849 477
908 28.02 82172 808
287 28.02 82193 800
333 28.02 92523 870
340 26.01 21581 829
435 28.02 50184 271

S15592

TEFF 16800 LOG G 4.08

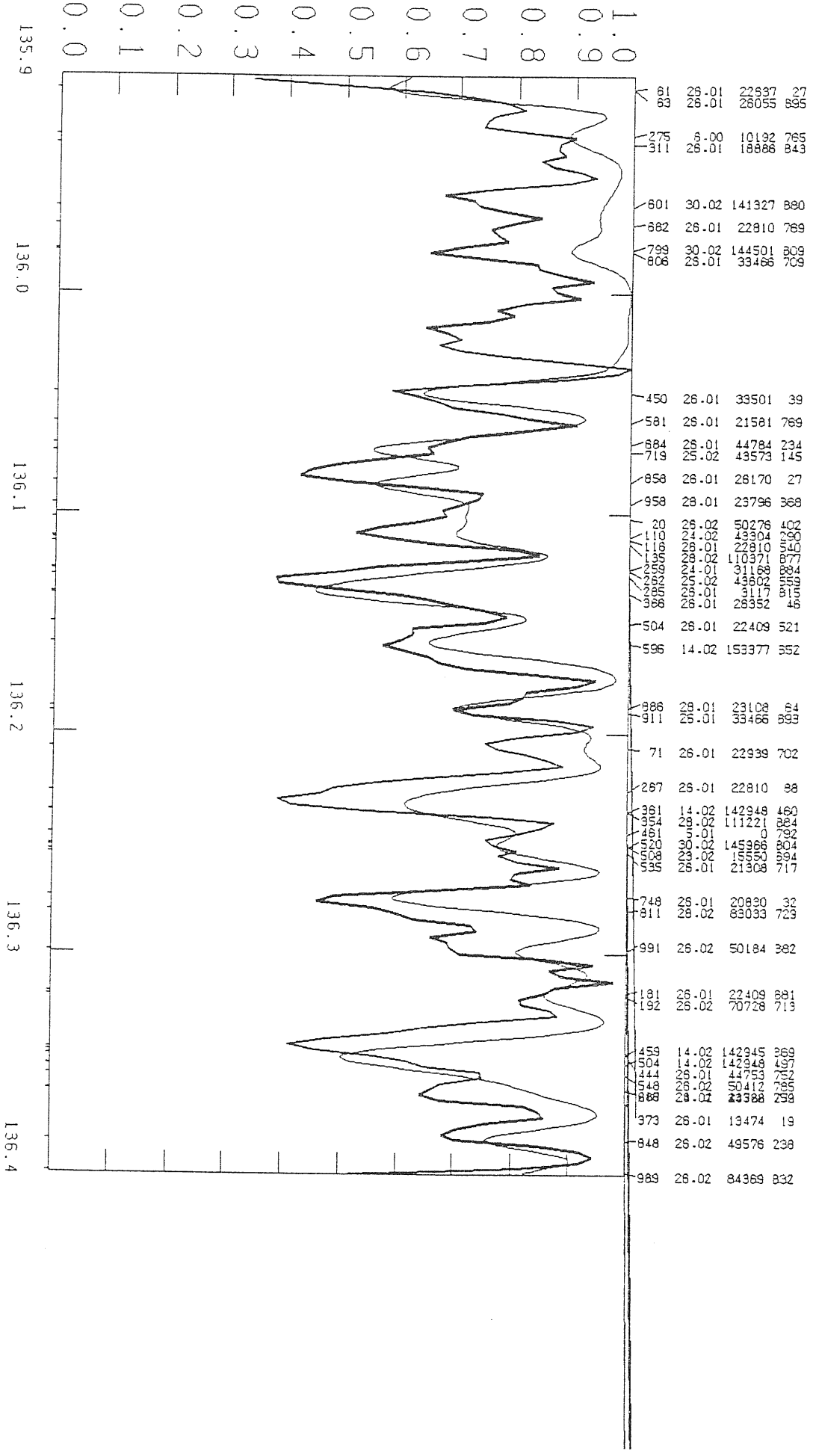

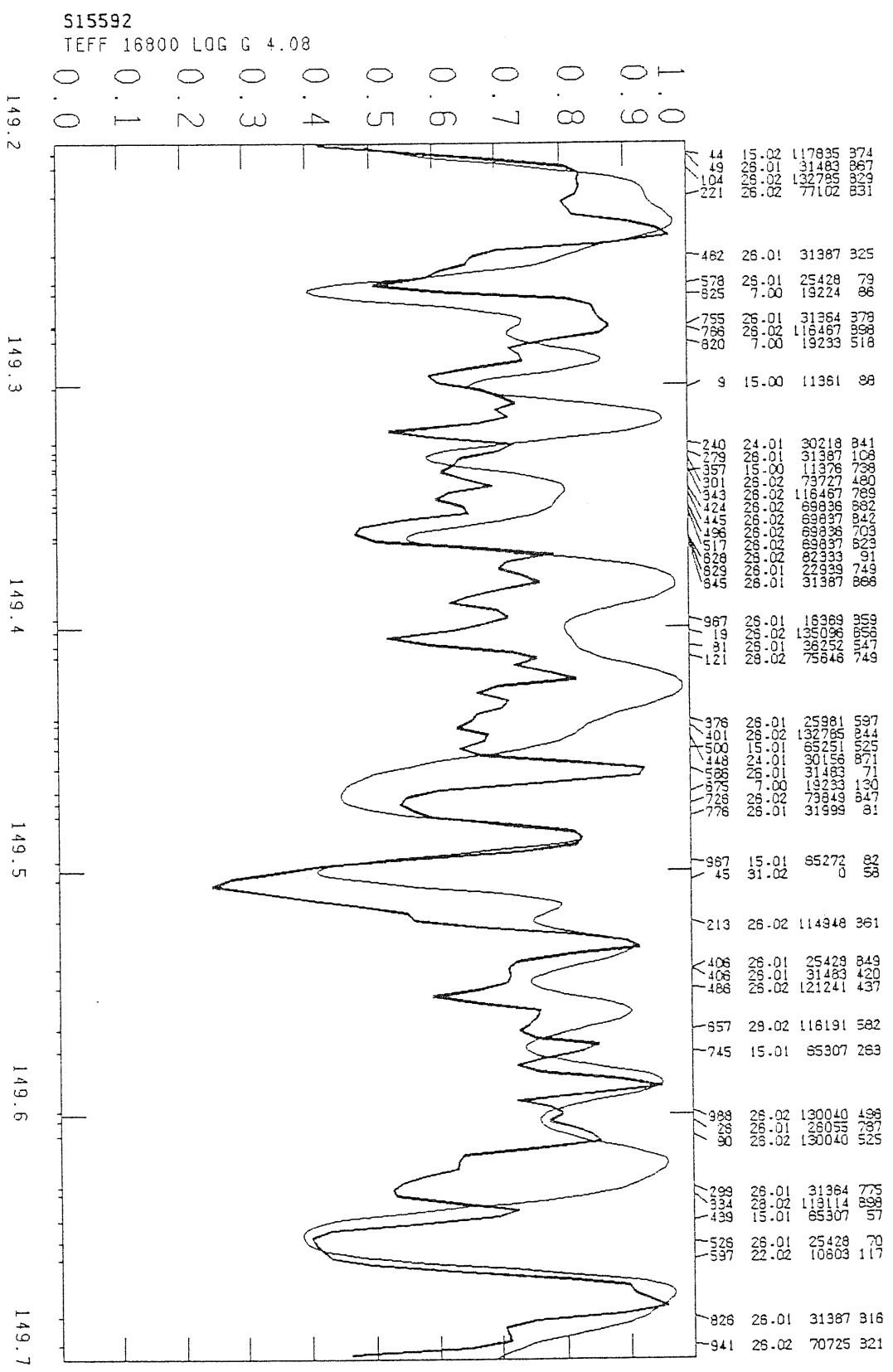
S15592
TEFF 16800 LOG G 4.08
0.0
0.1
0.2
0.3
0.4
0.5
0.6
0.7
0.8
0.9
1.0
149.2
149.3
149.4
149.5
149.6
149.7
44 15.02 117835 374
49 26.01 31483 867
104 26.02 132785 829
221 26.02 77102 831
462 26.01 31387 325
578 26.01 25428 79
825 7.00 19224 86
755 26.01 31364 378
786 26.02 116467 898
820 7.00 19233 518
9 15.00 11361 88
240 24.01 30218 841
279 26.01 31387 108
357 15.00 11376 738
301 26.02 73727 480
343 26.02 116467 789
424 26.02 69836 882
445 26.02 69837 842
496 26.02 69836 703
517 26.02 69837 823
628 26.02 82333 91
629 26.01 22939 749
845 26.01 31387 868
967 26.01 18369 959
19 26.02 135096 656
81 26.01 36252 547
121 26.02 75646 749
376 26.01 25981 597
401 26.02 132785 844
500 15.01 65251 525
448 24.01 30156 871
586 26.01 31483 71
675 7.00 19233 130
726 26.02 73849 847
778 26.01 31999 81
967 15.01 65272 82
45 31.02 0 58
213 26.02 114348 361
406 26.01 25428 849
406 26.01 31483 420
486 26.02 121241 437
657 28.02 116191 582
745 15.01 65307 263
988 26.02 130040 496
28 26.01 26055 787
90 26.02 130040 525
298 26.01 31364 775
334 28.02 119114 898
439 15.01 65307 57
526 26.01 25428 70
597 22.02 10803 117
826 26.01 31387 316
941 26.02 70725 321

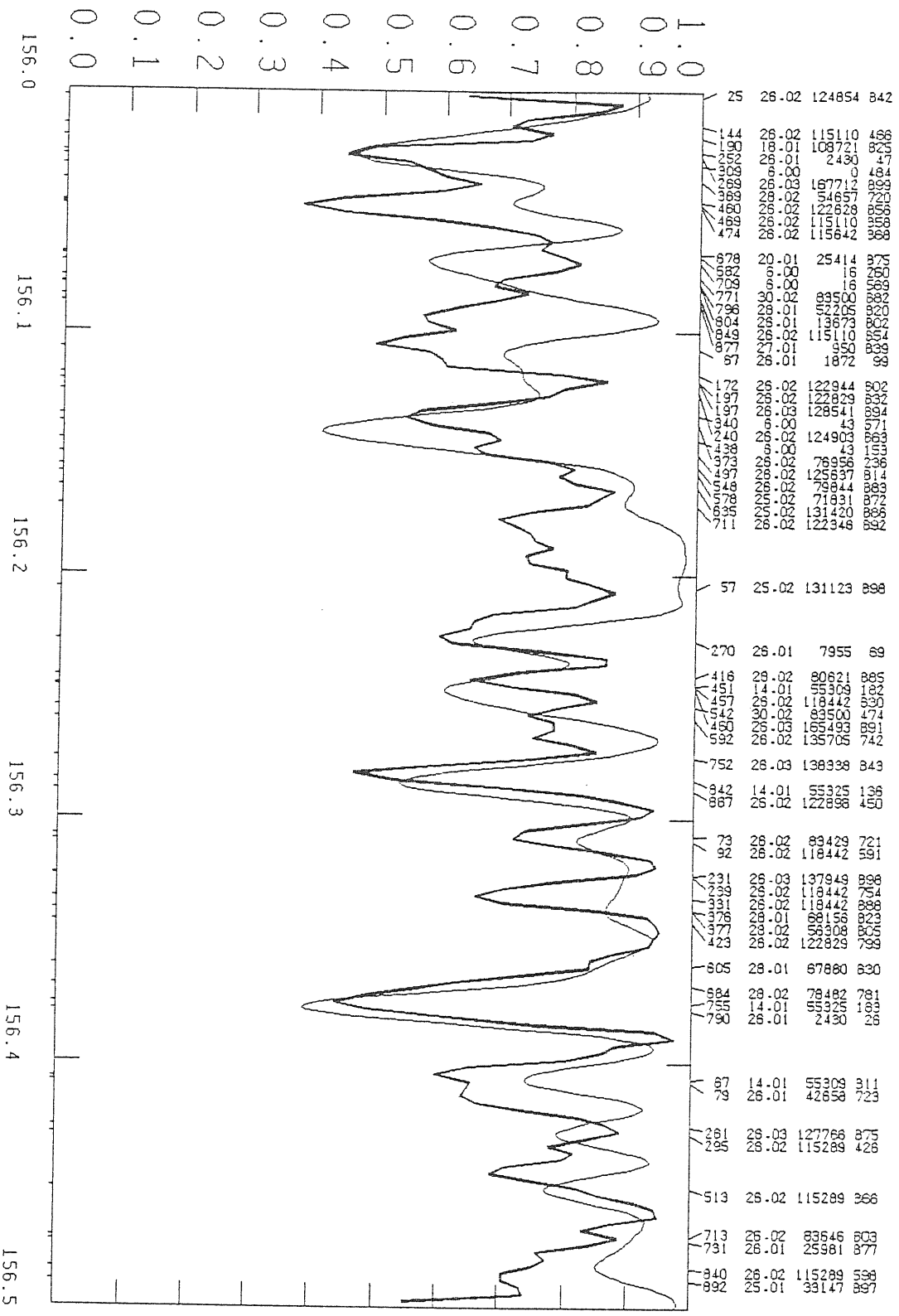
S15592
TEFF 16800 LOG G 4.08
0.0
0.1
0.2
0.3
0.4
0.5
0.6
0.7
0.8
0.9
1.0
156.0
156.1
156.2
156.3
156.4
156.5
25 26.02 124854 842
144 26.02 115110 466
190 18.01 108721 825
252 26.01 2430 47
309 6.00 0 484
269 26.03 167712 899
389 28.02 54657 720
480 26.02 122628 856
488 26.02 115110 858
474 26.02 115642 868
678 20.01 25414 875
582 6.00 16 260
709 6.00 16 569
771 30.02 83500 882
796 28.01 52205 820
804 28.01 13673 802
849 26.02 115110 854
877 27.01 950 839
67 28.01 1872 99
172 26.02 122944 802
197 26.02 122829 832
197 26.03 128541 894
340 6.00 43 571
240 26.02 124903 868
438 6.00 43 153
373 26.02 76956 236
497 26.02 125837 814
548 26.02 79844 883
578 25.02 71831 872
635 25.02 131420 886
711 26.02 122348 892
57 25.02 131123 898
270 26.01 7955 89
416 28.02 80621 885
451 14.01 55309 182
457 26.02 118442 830
542 30.02 83500 474
450 26.03 165493 891
592 26.02 135705 742
752 26.03 138338 843
842 14.01 55325 136
867 26.02 122898 450
73 26.02 83429 721
92 26.02 118442 591
231 26.03 137949 898
239 26.02 118442 754
331 26.02 118442 898
376 26.01 68156 823
377 26.02 56308 805
423 26.02 122829 799
805 26.01 67860 630
684 26.02 78482 781
755 14.01 55325 183
790 26.01 2430 26
67 14.01 55309 311
79 26.01 42658 723
281 26.03 127766 875
295 26.02 115289 426
513 26.02 115289 366
713 26.02 83646 803
731 26.01 25981 877
840 26.02 115289 538
892 25.01 33147 897

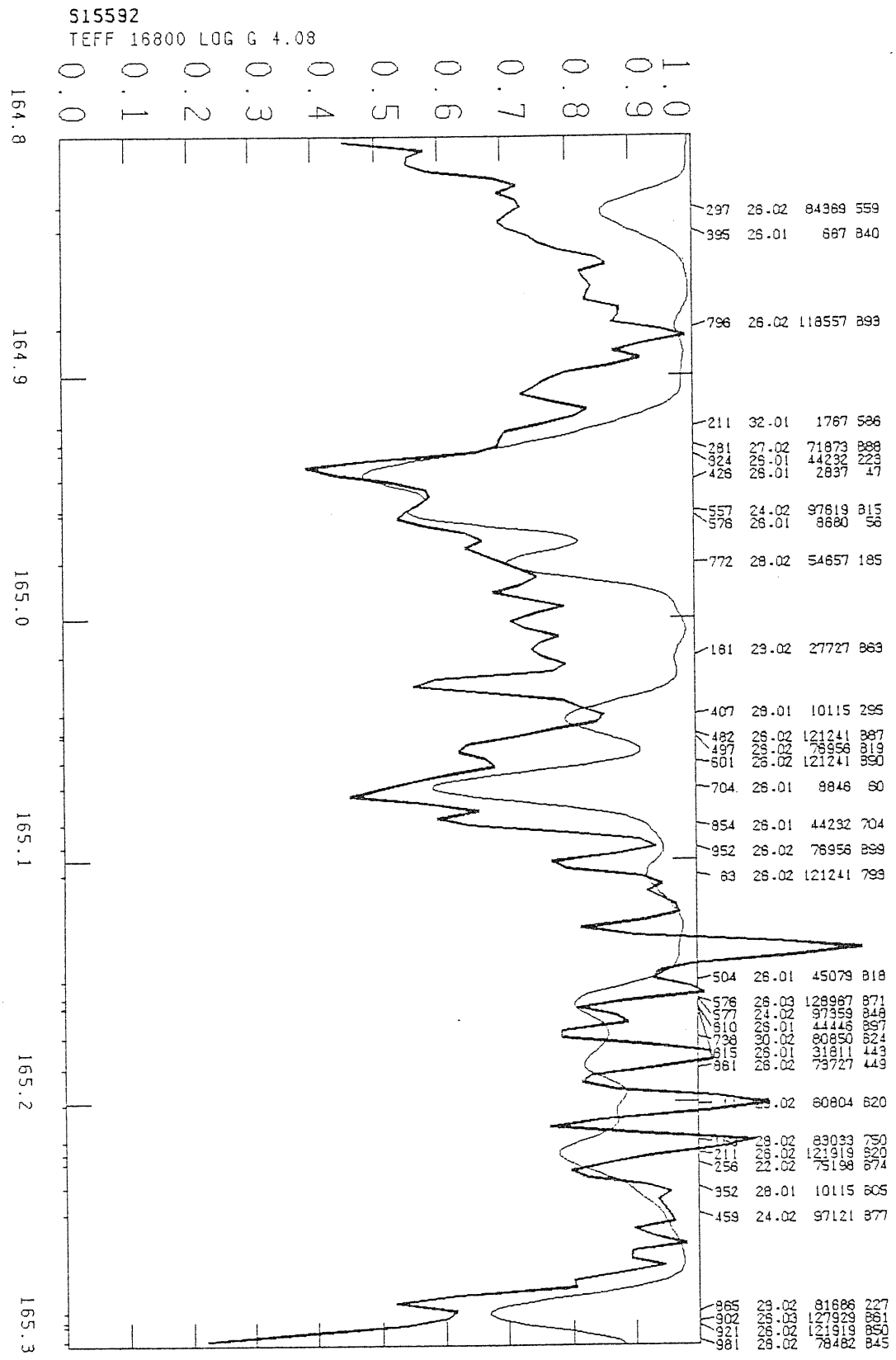
S15592
TEFF 16800 LOG G 4.08
0.0
0.1
0.2
0.3
0.4
0.5
0.6
0.7
0.8
0.9
1.0
164.8
164.9
165.0
165.1
165.2
165.3
297 26.02 84369 559
395 26.01 887 840
796 26.02 118557 893
211 32.01 1767 586
281 27.02 71873 888
924 26.01 44232 223
426 26.01 2837 47
557 24.02 97619 815
576 26.01 8680 56
772 28.02 54657 185
181 29.02 27727 863
407 29.01 10115 295
482 26.02 121241 887
497 26.02 78956 819
601 26.02 121241 890
704 26.01 8848 80
854 26.01 44232 704
952 26.02 78956 859
63 26.02 121241 799
504 26.01 45079 818
576 26.03 128967 871
877 24.02 97359 848
910 26.01 44446 897
738 30.02 80850 824
815 26.01 31811 443
881 26.02 79727 449
.02 60804 820
.02 83033 750
211 26.02 121919 820
256 22.02 75198 674
352 28.01 10115 805
459 24.02 97121 877
865 29.02 81686 227
902 26.03 127923 881
921 26.02 121919 850
981 28.02 78482 845

S15592

TEFF 16800 LOG G 4.08